High Efficiency Low Power Rectifiers and ZVS DC to DC Converters for RF Energy Harvesting

Najmehossadat Nourieh

A thesis submitted to the University of Hertfordshire in partial fulfilment of the requirements of the degree of Doctor of Philosophy

The program of research was carried out in the School of Physics, Engineering and Computer Science, University of Hertfordshire,

United Kingdom

September 2022

Najmehossadat Nourieh
School of Physics, Engineering and Computer Science, University of Hertfordshire

Najmehossadat Nourieh
School of Physics, Engineering and Computer Science, University of Hertfordshire

Abstract

In recent years, advancements in modern technologies have grown the demand for low-power wireless devices. Considering that enhancing the lifetime of the required battery to maintain the operation of these devices is still impractical, harvesting energy from ambient sources has become a promising solution to power portable low power electronic devices. Harvesting ambient energy from the electromagnetic wave (EM), which is referred to as radio frequency energy harvesting (RFEH), is one of the most popular power extracting methods. Scavenging energy can be used to fully supply the power required for wearable electronics devices, RFID, medical implantable devices, wireless sensors, internet of things (IoT) etc. RF energy is readily available in urban environments due to the abundant existence of HF and UHF technologies. Therefore, there is a great interest in studying systems working in UHF bands, including 300MHz to 3GHz frequencies.

Radio frequency energy harvesting is a method which converts the received signals into electricity. This technique offers various environmentally friendly alternative energy sources. Specifically, RFEH has interesting attributes that make it very practical for low-power electronics and wireless sensor networks (WSNs). Ambient RF energy can be provided by commercial RF broadcasting stations such as Wi-Fi, GSM, radar or TV. In this study, particular attention is given to design efficient low power circuits suitable to be applied for RFEH as a green technology, which is very suitable for overcoming problems such as powering wireless sensors located in inaccessible places or harsh environments, the possibility to power directly electronic devices, recharge batteries and etc. In RFEH, it is very important to enhance the efficiency of the circuits and systems to maximize the amount of harvested energy.

Najmehossadat Nourieh
School of Physics, Engineering and Computer Science, University of Hertfordshire

This thesis is mainly concerned with the design, simulation, and implementation of AC to DC circuits including phase shifter, rectifier, and DC to DC converter which is specifically designed for RFEH. It can be applied in various applications such as telecommunications, wireless sensors, medical devices, wireless charging, Internet of Things (IoT) and etc. In the designed system in this thesis, the signal must be passed through a phase shifter, rectifier, and voltage multiplier to reach the required level of output voltage. In another word, this system rectifies the sinusoidal AC waveform to DC and multiplies it to get higher voltages.

In this thesis, we propose 1 and 7-stage rectifiers, phase shifters and isolated/non-isolated DC to DC converters will be investigated individually in a general manner and integrated together to have the desired range of outputs for considered applications. This research methodology has three major phases: Phase 1: Theoretical analyses, Phase 2: Simulation investigations and Phase 3: Practical verification.

This thesis presents a review on the history of different circuits used to design a low power system for EH. Certain achievements in recent decades make power harvesting a reality, capable of providing alternative sources of energy for a wider range of applications. This review provides a summary of RFEH technologies to use as a guide for the design of RFEH units. Additionally, comprehensive analysis and discussions of various designs of rectifiers, isolated and non-isolated DC to DC converters and phase shifters in addition to their trade-offs for RF energy harvesting purposes are included.

In this thesis, novel designs of Dickson rectifiers with high voltage gain and efficiency operating with an input frequency of 915MHz is presented. The proposed circuits introduce a new method of deriving output characteristics of rectification circuit in terms of voltage. The design consists of different stages of the Dickson voltage multiplier. The rectifiers benefit from two input AC sources with 180° phase shift. This Dickson circuit is further discussed in two levels; the first one is a 1-stage rectifier operating with

Najmehossadat Nourieh
School of Physics, Engineering and Computer Science, University of Hertfordshire

Schottky diodes or diode-connected MOSFETs, and the second is a 7-stage rectifier discussed with both Schottky diodes and diode-connected MOSFETs producing higher output voltages.

Furthermore, the prototype of 1-stage rectifier is presented where the input voltage is between -10dBm and 2dBm and the output voltage gained is from 318mV to 1700mV, respectively. Also, the prototype of 7-stage rectifier is presented where the input voltage is -10dBm, -8dBm and -6dBm and the output voltage is gained 1220mV, 1330mV and 1550mV, respectively.

Additionally, a new non-isolated high voltage gain, high efficiency zero voltage switching (ZVS) resonant DC to DC converter working under ZVS condition is introduced, which can work in high frequencies with high power conversion rate as well as low losses. The proposed converter can provide 5V output from 350mV input voltage with efficiency of 72.8%. Furthermore, we proposed an isolated DC to DC converter which provides the output voltage of 6V with efficiency of 68%. Due to have an isolation transformer, this converter prevents electric shocks which makes it suitable for applications requiring more safety. All the theoretical analyses are verified by MATLAB and circuits are simulated in PSIM.

In addition, two combinations of high voltage gain circuits are introduced for low power applications such as RFEH. The first combination consists of a phase shifter, 1-stage rectifier and resonant ZVS DC to DC converter which has an output voltage of 6V with an efficiency of 71%. The second consists of a phase shifter, 1-stage rectifier and isolated resonant ZVS DC to DC converter with output voltage and efficiency of 5V and 65%, respectively.

In conclusion, this thesis is presented in 6 chapters discussing the designed high voltage gain high efficiency low power circuits to convert AC input with frequency of 915MHz to DC output. The circuits can be applied in different low power applications such as energy harvesting systems specifically RFEH.

Najmehossadat Nourieh
School of Physics, Engineering and Computer Science, University of Hertfordshire

Acknowledgement

I give thanks to Almighty God for His steadfast grace, love, guidance, protection, faithfulness and for providing me this opportunity and granting me the capability to proceed successfully.

I cannot express enough gratitude to my family and friends. I warmly thank and appreciate my parents and my sisters for the love, affection, and spiritual support they have shown me. They have stood by me all the way and have been there for me at all times.

I would like to express my sincere gratitude to my supervisor, Professor Yichuang Sun for his support and encouragement in preparation and development towards my research work and the completion of this thesis. I also want to thank my second supervisor, Dr Oluyomi Simpson, for his support and excellent advice during the whole PhD process.

I am grateful to my friends for their support, enthusiastic help, and cheerfulness.

Najmehossadat Nourieh
School of Physics, Engineering and Computer Science, University of Hertfordshire

Table of Contents

Najmehossadat Nourieh
School of Physics, Engineering and Computer Science, University of Hertfordshire

Najmehossadat Nourieh
School of Physics, Engineering and Computer Science, University of Hertfordshire

Najmehossadat Nourieh
School of Physics, Engineering and Computer Science, University of Hertfordshire

Table of Figures

Najmehossadat Nourieh
School of Physics, Engineering and Computer Science, University of Hertfordshire

Najmehossadat Nourieh
School of Physics, Engineering and Computer Science, University of Hertfordshire

Najmehossadat Nourieh
School of Physics, Engineering and Computer Science, University of Hertfordshire

Najmehossadat Nourieh
School of Physics, Engineering and Computer Science, University of Hertfordshire

Najmehossadat Nourieh
School of Physics, Engineering and Computer Science, University of Hertfordshire

Najmehossadat Nourieh
School of Physics, Engineering and Computer Science, University of Hertfordshire

Najmehossadat Nourieh
School of Physics, Engineering and Computer Science, University of Hertfordshire

Table of Tables

Najmehossadat Nourieh
School of Physics, Engineering and Computer Science, University of Hertfordshire

List of Publications

Declaration: The following papers have been published and parts of their material are included in this thesis:

Relevant Journal Publication

1. N. Nourieh, Y. Sun, O. Simpson, "A Novel Resonant ZVS Converter with Self-Driven Synchronous Rectifier for Low-Voltage High-Current Applications", IET Power Electronics, Vol. 14, Issue 8, pp. 1397-1408, March 2021.

Relevant Conference Publication

2. N. Nourieh, Y. Sun, O. Simpson, " A Step-Down ZVS Power Converter with Self-Driven Synchronous Rectifier", IEEE International Symposium on Circuits and Systems, April 2021.
3. N. Nourieh, Y. Sun, O. Simpson, "An Isolated ZVS DC/DC Converter with Diode-connected MOSFET in Rectifier", IEEE Asia Pacific Conference on Circuits and Systems, September 2021.

Relevant Journal Submission

4. N. Nourieh, Y. Sun, O. Simpson, "A Novel ZVS DC/DC Converter for Low Power Applications", Analog Integrated Circuit and Signal Processing, May 2022.

Najmehossadat Nourieh
School of Physics, Engineering and Computer Science, University of Hertfordshire

List of Acronyms

RF	Radio Frequency
IoT	Internet of Things
WSN	Wireless Sensor Network
UHF	Ultra High Frequency
RFEH	Radio Frequency Energy Harvesting
DC	Direct Current
PCE	Power conversion Efficiency
RFID	Radio Frequency Identification
MOSFET	Metal Oxide Silicon Field Effect Transistor
NMOS	N-Channel MOSFET
PMOS	P-Channel MOSFET
CMOS	Complementary metal-oxide-semiconductor
MHZ	Megahertz
ITU	International Telecommunication Union
LNA	Low Noise Amplifier

Najmehossadat Nourieh
School of Physics, Engineering and Computer Science, University of Hertfordshire

DCPO	DC to DC power optimizer
ZVS	Zero Voltage Switching
IC	Integrated Circuit
PV	Photovoltaic
LED	Light Emitting Diode
PCB	Printed Circuit Board
BNC	Bayonet Neill-Concelman
SMA	SubMiniature version A
ISI	Inter-Symbol Interference
e.m.f	electromotive force
LPF	Low Pass Filter
HPF	High Pass Filter

Najmehossadat Nourieh
School of Physics, Engineering and Computer Science, University of Hertfordshire

1 Introduction

This chapter provides a brief introduction of the thesis. This includes the motivation of the research, the research scope and objectives, the original contributions, and the thesis structure.

1.1 Motivation

The promise of the Internet of Things (IoT) pervasively connecting many devices that can sense and communicate, is particularly attractive in today's world, which provides unlimited applications [1, 2]. The scaling of the (IoT) devices to thousands or millions of nodes is currently impractical if the energy required for the operation of these sensors is supplied by batteries (because of their limited lifetime and energy storage capacity) [3, 4]. However, powering a range of low-power electronic devices capable of sensing, computing, and communicating by energy harvesting is now feasible, enabled by recent advances in energy harvesting systems [5, 6].

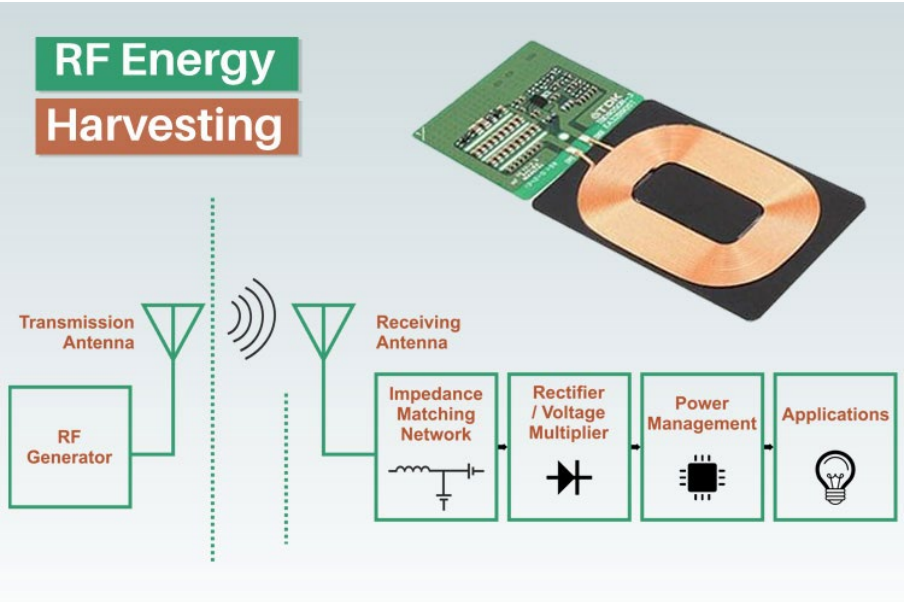

Figure 1.1 Radio frequency energy harvesting [7]

Najmehossadat Nourieh
School of Physics, Engineering and Computer Science, University of Hertfordshire

Wireless power transmission system is a unit that emits electrical power from one place and captures it at another place in the atmosphere of the earth without any wire or other supporting mediums. The history of radio frequency (RF) power harvesting in our ambient environment began in the period between 1950 to 1960 when the microwave-powered helicopter system was invented [7]. Later, the concept of power scavenging was defined as a technique to get energy from the environment using different techniques such as vibrational excitation, thermoelectric conversion, pressure gradient and solar energy conversion. This method promises great opportunity to replace small batteries in low power electrical appliances. Figure 1.1 presents the structure of an RF energy harvesting (RFEH) system. It shows different parts of the whole RFEH system from the transmission antenna to the load [7]. RF wireless power harvesting (WPH) gives great potential to replace batteries or increasing their lifetime. Now, batteries power most of the low-power remote sensors and embedded devices. In fact, batteries have limited lifespans and require regular replacements. By applying power harvesting methods, devices become self-sustaining concerning the energy required for their operation, thus obtaining an unlimited operating lifespan. Therefore, the demand for power maintenance is negligible.

The energy required for the operation of low-power (microwatt) IoT devices can be harvested from any of these or a multitude of these sources: RF [8], kinetic or vibration [9], thermal [10], and solar power [11]. RFEH, the process of scavenging energy from ambient electromagnetic waves has been considered as one of the most viable options because of the available RF energy (wireless networks required for wireless data transmission). It is very important to enhance the efficiency of the RFEH to maximize the amount of energy harvested which enables the development of self-powered wireless sensors with enhanced performance.

As illustrated in Figure 1.1 an RFEH circuit consists of an antenna or coil for converting electromagnetic energy of wireless waves to electrical energy, a matching network to maximize power transfer to the next stage, an RF to DC power converter (also known as RF rectifier or rectifier), and an energy storage

Najmehossadat Nourieh
School of Physics, Engineering and Computer Science, University of Hertfordshire

element along with required power management circuitry capable of powering downstream electronic circuits.

Furthermore, RF energy harvesting is becoming a viable solution for powering the wireless IoT sensors eliminating the need for a battery and associated storage, plus lifetime limitation [12-14]. The power harvester unit, consisting of a multi-stage rectifier, is a key component in an RFEH system that converts the incoming weak RF signal into a DC voltage. The performance of the rectifier unit can be evaluated based on its power conversion efficiency (PCE), sensitivity i.e., the minimum required input power to produce a DC voltage at the output section, and finally, the output DC voltage range. To increase the rectifier's PCE, the energy losses introduced by the non-zero ON resistance of rectifying devices must be reduced. To increase sensitivity and output voltage level, rectification components with lower threshold voltage are required, since the performance of the power harvester is strongly affected by the threshold voltage of the rectifying devices [15].

Further research has shown that there are innovative solutions for the reduction of the threshold voltage using both technologies and circuit-level techniques. For the technology-based approach, the rectifier circuit can be implemented using Schottky diodes [16, 17] or low forward-voltage transistors [18, 19]. The drawback of using a technology-based approach is higher production costs due to the use of CMOS technology. As an alternative for using specialized semiconductor technologies, circuit-based approaches can be used to enhance the performance of RFEH. These circuit techniques can be classified into active and passive. The active technique requires an external power source (secondary battery) and is generally used in active sensors or active radio frequency identifications RFIDs [6]. This enables more sophisticated applications at the price of higher cost and maintenance. The passive technique does not require an additional source of energy but may require an additional circuit as discussed in [20], where an auxiliary rectification chain is used to generate the compensating threshold voltage for the main RF to DC power conversion circuit. The auxiliary chain requires an additional power source and occupies a

Najmehossadat Nourieh
School of Physics, Engineering and Computer Science, University of Hertfordshire

larger area. An internal cancellation circuit is used in [21] where a capacitor stores the threshold voltage that is applied at the gate-source terminal of the MOS transistor. This technique uses high capacitance and resistance value which leads to a relatively large silicon area on the chip. Similarly, a self-biasing technique consisting of an off-chip high impedance resistive network is used in [22] to provide DC biasing voltage. Instead of generating a passive threshold voltage through additional circuitry, the work presented in [23] utilizes floating gate transistors as rectifying diodes. In fact, the floating gate transistors are able to store pre-charged voltage, thus effectively lowering the threshold voltage, this technique requires an additional pre-charge phase making it unsuitable for fully battery-less applications. The RF to DC power conversion circuit consisting of N-channel MOSFET (NMOS) transistors with a grounded body terminal leads to an increase in threshold voltage with the number of stages due to the body effect which degrades the efficiency of the power conversion circuit [24]. For this scenario, the body terminal of transistors can be dynamically controlled using additional circuits [25] or floating well devices [26]. This can minimize the undesired body effect. However, the floating well technique generates undesirable substrate current. Also, the parasitic capacitance at each node is increased in triple-well source-body connected devices leading to reduced efficiency. In this thesis, the diode-connected MOSFET which functions as a diode is applied (floating gate transistor).

1.2 Research Aims and Objectives

This research aims to design a novel energy-efficient circuit including a phase shifter, RF to DC rectifier, and DC to DC converter to maximize the energy harvested and transferred from the RF sources to the desired range of DC signals with the highest possible efficiency.

Considering all the summarized solutions in the section 1.1, in this PhD thesis, the focus is on researching novel circuits to amplify and convert a very low power with low voltage level harvested from RF sources to practical voltages used for different applications such as battery-less devices, IoTs, mobile

communications, medical devices, etc. In this regard, three main circuit blocks were designed. Initially, we designed a phase shift circuit to produce two separate signals with a 180° phase difference. Then, we designed efficient rectifier to amplify and convert the harvested energy from RF sources for different output levels. After that, two isolated and non-isolated DC to DC converters were designed to be combined with a 1-stage rectifier and produce greater output voltage levels. For validating the whole concept as the fourth phase, after undertaking theoretical analysis and simulation investigation, we discussed the experimental process including the design of PCB boards using the DesignSparks environment, implementation of components on the boards, preparation of all tools and devices needed to test the circuits and finally testing the circuits.

The proposed novel techniques in RFEH have properties such as low losses, high efficiency, low cost, flexibility in output voltage range, high reliability, environment friendly and compatibility to harvest energy from radio frequencies ranges.

The research is verified by simulation investigations in PSIM software, while equations are validated by MATLAB (where equations are complicated). The progression of this thesis is explained in Figure 1.2. Mainly, four circuit blocks are proposed in this thesis including 1-stage rectifier, 7-stage rectifier, isolated resonant DC to DC converter and non-isolated resonant DC to DC converter. For the Dickson rectifiers, a phase shifter was needed to produce two input signals with 180° phase difference which is also presented in this thesis. All the circuits were analysed theoretically. The simulation results were also investigated to verify the theoretical analyses. Finally, the PCB board of three circuits including phase shifter, 1 and 7-stage rectifiers were designed with DesignSpark software, and the proposed circuits were tested in the laboratory.

Najmehossadat Nourieh
School of Physics, Engineering and Computer Science, University of Hertfordshire

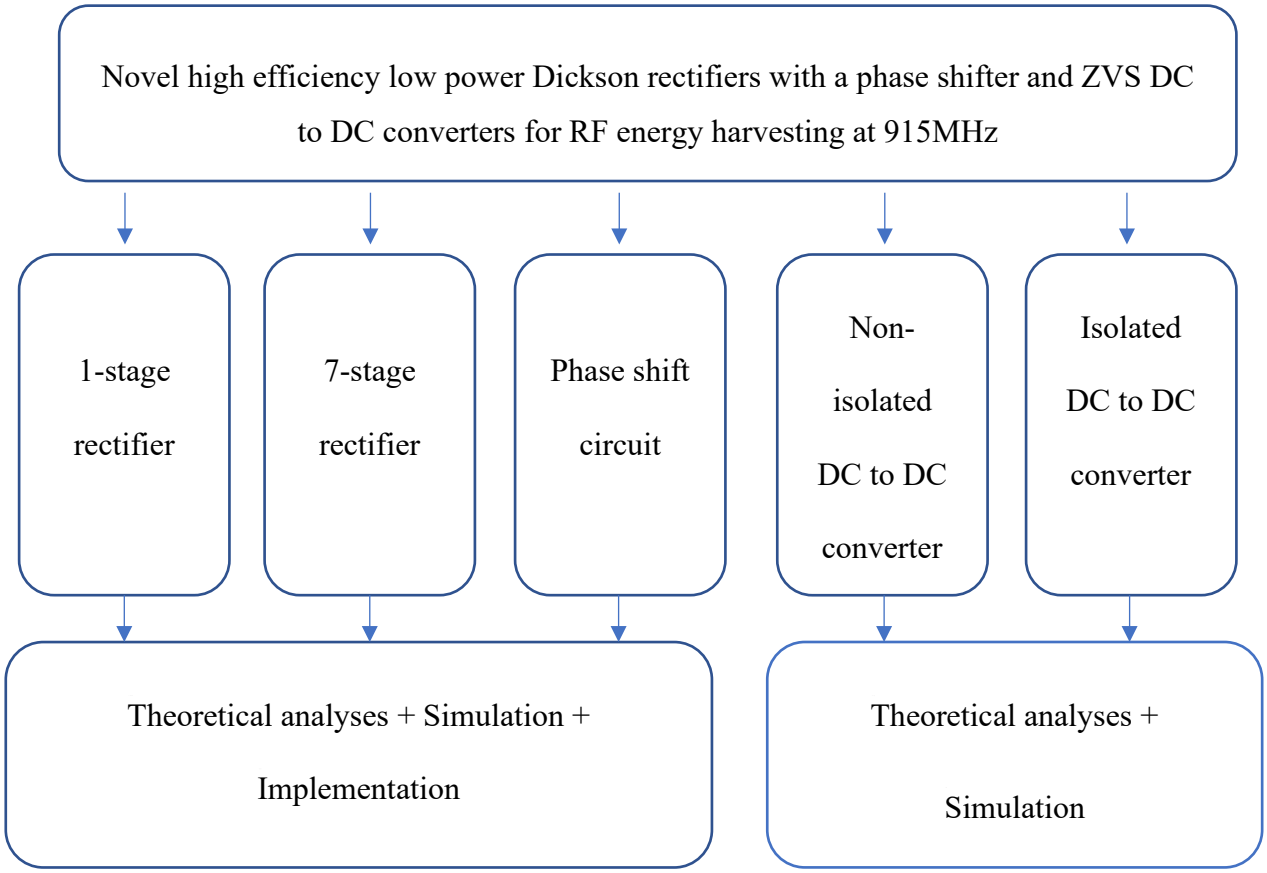

Figure 1.2 The diagram of how this thesis is prepared

1.2.1 Methodology

The methodology of this research is circuit design based on the theories and assumptions, different system models and application scenarios verified by simulations using PSIM and MATLAB tools. Furthermore, the software DesignSpark was used to design the PCB boards. Then, the prototype of one complete system, from low power/low voltage AC signal (-10dBm, 100mV and 915MHz) to DC output with desired voltage level, was tested in the laboratory to prove the accuracy of the designed circuit's operation in a practical environment.

Najmehossadat Nourieh
School of Physics, Engineering and Computer Science, University of Hertfordshire

For this research, related articles were assessed to gain knowledge of existing low power energy conversion circuits, specifically in RFEH application. The majority of these related articles were sourced from e-Journals, conference proceedings, tutorials and overview publications. Such sources were the IEEE Xplore® website, related research databases and other online technical publications. Other sources include the exchange of emails, suggestions and notes from expert researchers and institutions working on related projects that contribute to the development of low power energy conversion technologies. This facilitated both general and in-depth knowledge of the desired areas.

Furthermore, using the University's library resources, academic database and different software were also useful for the research process. Also, regular meetings and discussions with my first and second supervisors contribute immensely to this research, as my supervisors facilitated the conduction of this PhD research in the right direction.

1.3 Thesis Contribution

The major contributions of this thesis are summarized as follows:

Chapter 3

The design of a novel Dickson rectifier with two inputs of 180° phase shift is discussed in one and seven repetitive levels followed by the simulation results and practical investigations. First, we explained 1-stage rectifier with two input sources with 180° phase difference. Second, a 7-stage rectifier with two input sources with 180° phase difference is presented. Third, the design of 180° phase shifter including analysis of phase errors on the performance of rectifiers is given. Then, the simulation results of both one and seven stage rectifier with 180° phase shifter is discussed. After discussions about the theory and simulation the implementation and practical tests of one and seven stage rectifiers with 180° phase shifter are presented. Finally, the performance comparison of the proposed 7-stage rectifier and other works is investigated.

Chapter 4

The design process includes theoretical analyses and simulation investigations of two isolated and non-isolated resonant zero-voltage switching DC to DC converters. The key contributions of chapter 4 are isolated DC to DC converter, simulation of isolated DC to DC converter, LC resonant DC to DC converter, simulation of LC resonant DC to DC converter, performance comparison of the two converters and performance comparison with other converters in the literature.

Chapter 5

The complimentary discussion of two combinations of the proposed circuits with further comparison of their performance is presented in this chapter. The main contributions of chapter 3 are the proposed combination of phase shifter, one stage rectifier and isolated DC to DC converter, the proposed combination of phase shifter, one stage rectifier and non-isolated resonant converter and comparisons of all proposed circuits.

1.4 Structure of Thesis

The reminder of this thesis is structured as follows:

In chapter 2, an overview on energy conversion circuits for RF energy harvesting is presented. The rest of chapter 2 is organized as follows: In section 2.2, a general description of phase shift circuits is presented. Brief overviews are presented on rectifiers and DC to DC converters are presented in section 2.3 and section 2.4, respectively. In section 2.4, an overview of DC to DC converters is discussed in two major subjects: isolated and non-isolated converters. A review of the performance criteria of some most related published circuits is also investigated in section 2.5 by simulating these rectifiers in PSIM

Najmehossadat Nourieh
School of Physics, Engineering and Computer Science, University of Hertfordshire

software. Then, section 2.6 gives information about the potential applications of the designed circuits in this thesis. Finally, conclusions are drawn in section 2.7.

In chapter 3, The different designs of the novel modified 1 and 7-stage Dickson rectifier is presented. The rest of chapter 3 is organized as follows: The theoretical analyses of a 1-stage Dickson rectifier is presented in section 3.2. In section 3.3, the analyses of the 7-stage Dickson rectifier with dual input sources are discussed in detail. In section 3.4, the design of a phase shifter producing a phase difference of 180° is presented. Then, the simulation results of 1 and 7-stage modified Dickson rectifier along with phase shifter are discussed in section 3.5. Consequently, the effects of phase shift errors are investigated in section 3.6. Furthermore, the implementation and practical results of the tested prototype of the combination of 1 and 7-stage modified rectifier with dual inputs made by phase shifter are presented in section 3.7. Finally, conclusions are drawn in section 3.8.

In chapter 4, the proposed high voltage gain resonant zero voltage switching DC to DC isolated and non-isolated converters are presented. The rest of chapter 4 is organized as follows: The proposed step-up DC to DC converter working under ZVS condition is discussed in section 4.2. In section 4.3, the simulation results of this converter and the comparisons with other works are presented. Then, the proposed isolated DC to DC converter working under ZVS condition is introduced in section 4.4 while in section 4.5 the simulation results of this converter are investigated. Section 4.6 discusses the comparisons of two proposed converters and other works. Finally, conclusions are drawn in section 4.7.

In chapter 5, the combination of phase shifter, rectifier and DC to DC converters are introduced. In section 5.2, the combination of phase shifter, 1-stage rectifier and non-isolated boost DC to DC converter is presented theoretically and by simulation in PSIM. Following that, in section 5.3, the combination of phase shifter, 1-stage rectifier and isolated resonant ZVS DC to DC converter is discussed in detail. The conclusions are drawn in section 5.5.

Finally, chapter 6 summarizes the thesis and states possible future research. Section 6.1 conclude the presented thesis and a comparison of all proposed circuits and combinations is given. In section 6.2, the future works to improve the suggested circuits are given.

Najmehossadat Nourieh
School of Physics, Engineering and Computer Science, University of Hertfordshire

2 An Overview of High Voltage Gain Energy Conversion Circuits

In recent decades, energy harvesting (EH) systems have attracted attention as this technology takes into considered available resources. RFEH, the process of scavenging energy from ambient electromagnetic waves has been considered as one of the most viable options because of the available RF energy. It is very important to enhance the efficiency of the RFEH circuits and systems to maximize the amount of harvested energy.

This chapter presents a review on the history of different circuits used to design a low power system for EH. Certain achievements in recent decades make power harvesting a reality capable of providing alternative sources of energy for a wider range of applications. This review provides a summary of RFEH technologies to use as a guide for the design of RF energy harvesting units. Energy harvesting circuits are designed to operate relatively with small voltages and currents; hence they rely on specific technologies for obtaining high efficiency. Thus, comprehensive analysis and discussions of various designs of rectifiers, isolated and non-isolated DC to DC converters and phase shifters in addition to their trade-offs for RF energy harvesting purposes are included. After discussions, simulation results and analysis are presented.

2.1 Introduction

Energy harvesting can be applied in different applications such as passive RFID, medical implantations, internet of things (IoT), sensors, etc [27- 30]. Conventionally, electrical means are powered by battery or direct connection of electricity; however, these techniques are being substituted by energy harvesting

Najmehossadat Nourieh
School of Physics, Engineering and Computer Science, University of Hertfordshire

systems for many purposes including the fact that battery has a limited lifetime, and it must be replaced frequently. Therefore, they are not efficient for some applications such as medical implants where battery replacement is not practical. Hence, EH is a technique that enables us to have long life energy consumption [31]. Also, with RF energy it is possible to use the same source for powering many systems. In this system, RF to DC rectifier plays the most critical role in producing DC voltage from the received RF signals via the antenna [32- 33].

In this chapter, we discussed the different recent proposed structures of rectifiers, isolated and non-isolated converters, and phase shifters for low power applications with specifically focus on RF energy harvesting using radio waves since radio waves are ubiquitous here and there and easy to gather recently.

2.2 Phase Shift Circuit

Lately, due to the quickly growing trend of multifunctional and highly integrated devices, different high-performance phase shift circuit designs attract excessive attention [34- 37].

Currently, many techniques are applied to attain desired phase shift with the least phase error by using different topologies in circuit design. Generally, phase shift circuits are classified into two main categories: digital and analogue. First, in digital phase shifters, the phase shifts are separated by discrete steps. That means the considered steps are defined by the bit formation of phase shifter. Second, in analogue circuits, phase shifts are incessant, and any level of phase shift can be directly gained without steps [38- 41].

In digital phase shifter, the performance of the 180º considerably affects the overall bandwidth. A larger bandwidth for the 180º phase bit is achievable by increasing the order of the topologies [42]. Nevertheless, when the order increases, the phase error and the insertion loss are affected by the parasitic

Najmehossadat Nourieh
School of Physics, Engineering and Computer Science, University of Hertfordshire

characteristics of the circuit. Thus, for larger phase shifts, hybrid and distributed networks are applied to provide small phase errors.

Analogue phase shifters are common components in microwave communication circuits. We need to achieve small size lumped elements in low/high-pass or all-pass topologies. For large phase shifts, such as 180º, it is found that the performance of circuit is significantly worse than smaller phase shifts when the bandwidth rises. Typically, phase errors reported for the 180º phase, are between ±2º and ±5º while the return loss is above 14dB without the effect of switches [43].

The simplest phase shifter consists of two transmission line sections of different lengths (Figure. 2.1); however, this only provides the required phase difference over a very narrow bandwidth. In [44], a broadband phase shifter which employs loaded transmission line is presented together with detailed theoretical analysis. Based on a systematic analytical procedure, various design parameters for typical phase shifts are given, resulting in a simple design procedure. Based on the design formulas, trade-offs between phase deviation, desired phase shift and bandwidth are more apparent.

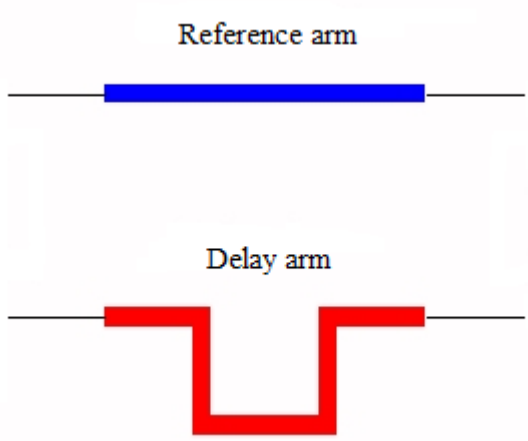

Figure 2.1 Transmission line phase shifter

Najmehossadat Nourieh
School of Physics, Engineering and Computer Science, University of Hertfordshire

Phase shift method is based on the measurement of the phase shift of a sinusoidal signal that propagates along the transmission line. Phase shift is defined by frequency and velocity of the propagating signal as well as physical specifications of the transmission line [45].

2.3 Rectification

Energy harvesting is the process of collecting weak energy from the surrounding environment, such as vibration, heat, light, radio waves, etc., to use as a power source. This concept can be applied to realize battery-less sensors. When using sensors to make wireless sensor networks (WSNs), lifetime of the batteries is a serious problem because it is troublesome and expensive to replace sensor batteries regularly.

In this thesis, we focused on RF energy harvesting using radio waves among energy sources since radio waves are ubiquitous here and there and easy to gather recently. For this purpose, rectifier is a key part that converts AC radio waves into a DC signal. In the following paragraph, we discuss the different recent proposed structures of rectifiers for RF energy harvesting circuits and systems.

Diodes are mainly used for their rectification application to convert the AC signal to DC. In power harvesting applications, antenna retrieves RF signals with sinusoidal waveforms. The harvested signal will be boosted and rectified to meet the current/voltage requirements of defined applications, after transformation through a phase shifter. One of the conventional topologies of rectification, is half-wave rectifier which has capacitors and a single diode called D_1 as shown in Figure 2.2(a). By conducting diode D_1, the positive cycle of AC signal is transferred to output and the negative cycle is removed; hence, half of the AC signal is wasted. Furthermore, the gained output V_{out} is remained discontinuous, as the negative cycle is cut off. Even though it is very simple, a half-wave rectifier is not efficient for most of applications [46]. Thus, a full-wave rectifier is more preferred. The structure of full-wave rectifier is presented in Figure 2.2(b). When input signal is in negative cycle, it passes through diode D_1, and charges capacitor

Najmehossadat Nourieh
School of Physics, Engineering and Computer Science, University of Hertfordshire

C_1 to the corresponding energy cycle. When C_1 is charged , diode D_2 transfers the energy and diode D_1 is blocked, so capacitor C_2 starts to be charged. Consequently, at the output stage, there are two capacitors in series (each one stores a voltage of V_{peak}) to send their stored energy to output stage. Hence, V_{out} will be equal to $2V_{peak}$ [47, 48]. Considering explanation of how full-wave rectifier works, this topology is more efficient and stable comparing to the half-wave type. Another topology of rectification that transfers both positive and negative cycles of the AC signal is a bridge rectifier. This topology gives equal output voltage to input peak voltage ($V_{out} = V_{peak}$). In this structure, pairs of diodes D_1, D_4 and D_2, D_3 are

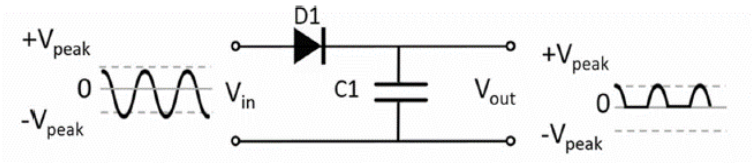

(a)

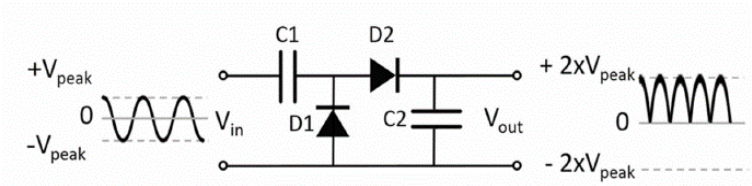

(b)

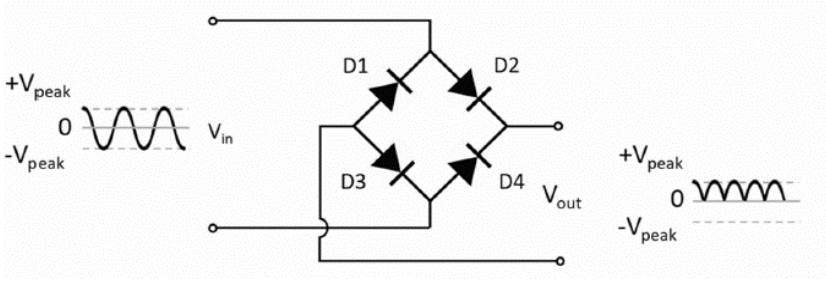

(c)

Figure 2.2 Some common topologies of rectifiers: (a) Half wave, (b) Full wave, (c) Bridge [49]

alternatively blocked (Figure 2.2(c)) [47, 48]. Another rectification topology that converts and boosts AC input signal to DC output is called voltage multiplier. In some cases, where the voltage of rectified signal

Najmehossadat Nourieh
School of Physics, Engineering and Computer Science, University of Hertfordshire

is not enough for specific application, we can increase voltage gain by adding series of stacked single rectifiers, forming voltage multiplier. Some configurations of the voltage multiplier are shown in Figure 2.3 [49].

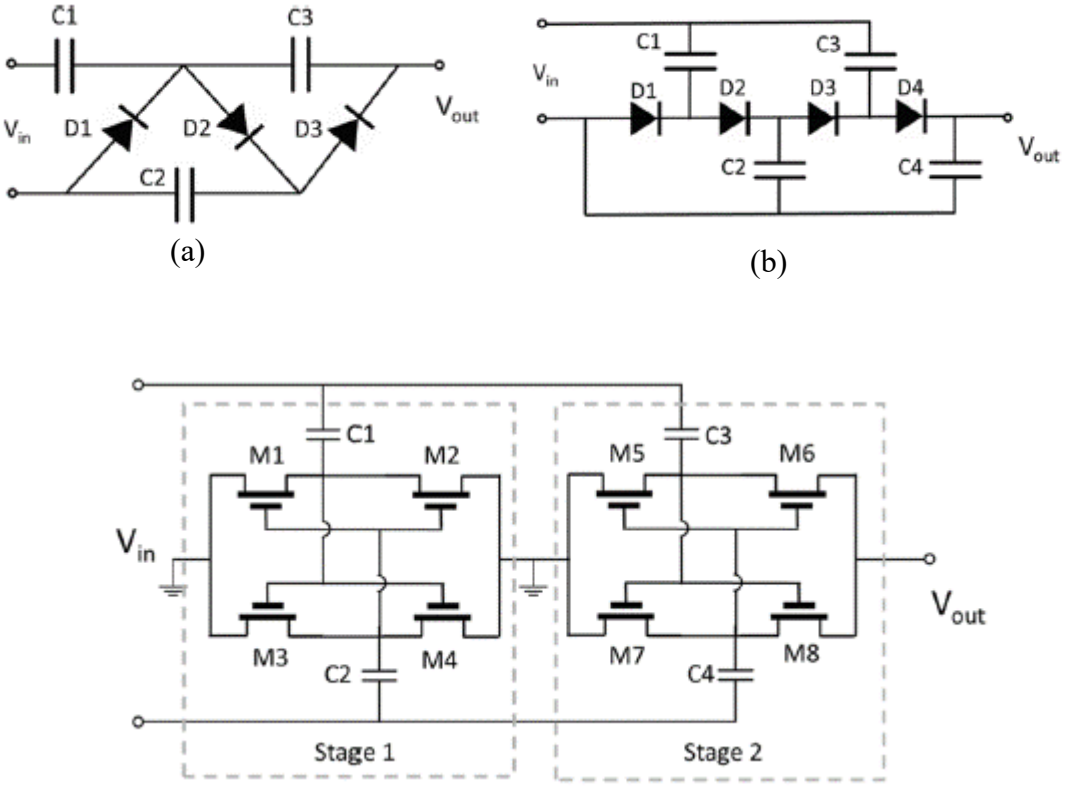

Figure 2.3 Common voltage multiplier configurations: (a) Three stages Cockcroft–Walton voltage multiplier, (b) Four stages Dickson voltage multiplier, (c). Two stages voltage multiplier comprised of differential drive unit [49]

One of the most fundamental configurations of multipliers, is the Cockcroft–Walton configuration (Figure 2.3(a)). The operational principles of this circuit are very similar to a full-wave rectifier but has more stages to gain higher voltages at the output stage. A modification of this topology is called Dickson multiplier which is shown in Figure 2.3(b). This configuration has capacitors in each stage, which are

Najmehossadat Nourieh
School of Physics, Engineering and Computer Science, University of Hertfordshire

shunted for reducing parasitic effects. Considering simplicity and high efficiency, the Dickson multiplier gains attention for small voltage applications. To increase the efficiency of these circuits, MOSFET (metal-oxide-semiconductor field-effect transistor) technology can be a proper replacement for diodes to overcome the limitations of diode. By replacing diodes with NMOS as shown in Figure 2.3(c), the Dickson multiplier can be integrated into integrated circuits (ICs). Relatively, high PCE and low threshold voltage are main features of this topology. Moreover, the differential drive voltage multiplier (Figure 2.3(d)) is widely used as it has low leakage current and potential for further modification for specific applications [49].

2.3.1 Dickson Rectifier

To convert the received AC signal, a basic rectifier of Dickson voltage doubler shown in Figure 2.4 is often used [50, 51]. The operation of the circuit shown in Figure 2.4 is as follows:

1. For ($-Vs$) negative peak: Capacitor C_1 is charged to Vs through diode D_1.
2. For ($+Vs$) positive peak: Voltage of capacitor C_1 is added to that of the source, therefore it charges C_2 to $2Vs$ through D_2.
3. Negative peak: Voltage of C_1 decreased to 0V allowing capacitor C_3 to be charged through D_3 *to* $2Vs$.

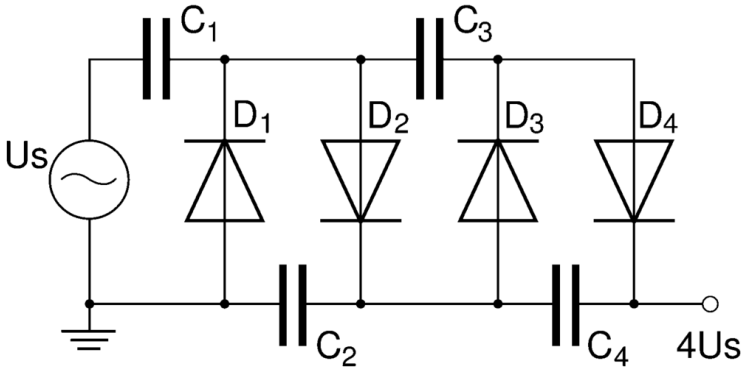

Figure 2.4 Basic schematic of Villard voltage doubler [50]

Najmehossadat Nourieh
School of Physics, Engineering and Computer Science, University of Hertfordshire

4. Positive peak: Potential of C_2 rises to $2Vs$ (similar to step 2), also charging capacitor C_4 to $2Vs$. The output voltage (the sum of voltages for C_2 and C_4) rises until $4Vs$ is achieved.

This Dickson multiplier is intended to have low output voltage for low power applications. To ameliorate the function of the basic Dickson model, the new circuit was introduced to have higher efficiency as illustrated in Figure 2.5 [52, 53].

To describe the ideal operation of the circuit, we numbered the diodes D_1, D_2, etc. from left to right and the capacitors C_1, C_2 etc. When the clock ϕ_1 is low, D_1 will charge C_1 to V_{in}. When ϕ_1 goes high the top plate of C_1 is pushed up to $2V_{in}$. Diode D_1 is then turned off and D_2 is turned on and C_2 begins to charge to $2V_{in}$. On the next clock cycle, ϕ_1 again goes low and now ϕ_2 goes high, pushing the top plate of C_2 to $3V_{in}$. D_2 turned off and D_3 turned on, charging C_3 to $3V_{in}$ and so on with charge passing up the chain. The final diode-capacitor cell in the cascade is connected to the ground rather than a clock phase and hence is not a multiplier; it is a peak detector that merely provides smoothing. In fact, there are several factors which reduce the output from the ideal case of nV_{in}. One of these parameters is the threshold voltage, V_T of the switching devices, which is the voltage required to turn the component on. The output will be reduced by at least nV_T due to the voltage drop across the switches. To solve this issue, Schottky diodes are commonly used in Dickson multipliers because of their low forward voltage drop, which leads to achieve an output voltage closer to the ideal one. Another critical issue in these circuits is that there are parasitic capacitance to the ground at each node.

To enhance this circuit, other works [53, 54] have been done to reach a higher clock frequency which is beneficial to reduce the ripple and the high frequency makes the remaining ripple easier to filter. Also, the size of needed capacitors is reduced since less charge needs to be stored per cycle. However, the loss through stray capacitance is increased in coordinate with an increment of clock frequency with practical limitation of around a few hundred kilohertz.

Najmehossadat Nourieh
School of Physics, Engineering and Computer Science, University of Hertfordshire

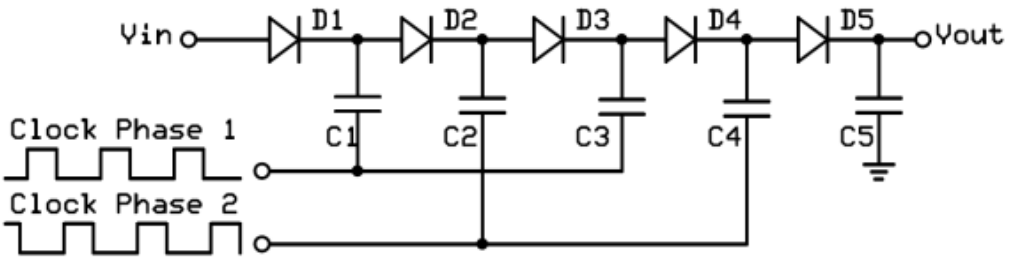

Figure 2.5 The enhanced Dickson multiplier [52]

Thus, as it is demonstrated in Figure 2.6, the diodes in the Dickson multiplier are often replaced by diode-connected MOSFETs to operate as rectifying devices instead of Schottky diodes [54- 56]. The operation of this rectifier is same as the one shown in Figure 2.5.

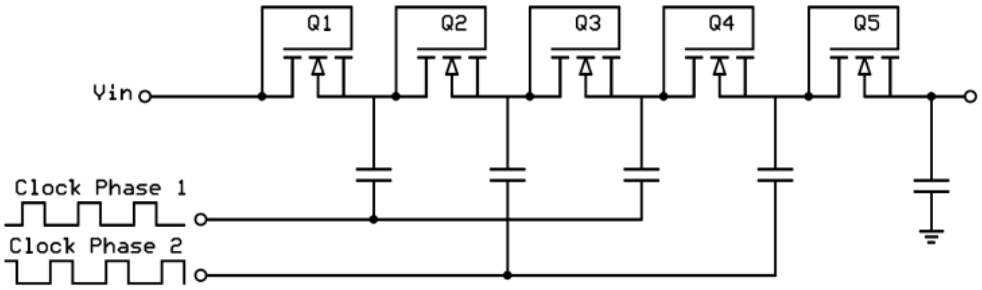

Figure 2.6 The diode connected Dickson multiplier [54]

The diode-connected MOSFET version of the Dickson multiplier does not work very well at very low voltages because of the large drain-source voltage drop of the MOSFETs. To overcome this issue, a more complex circuit is used. One solution is to connect another MOSFET in parallel with the switching MOSFET, biased into its linear region as illustrated in Figure 2.7. This paralleled combination of MOSFETs has a lower drain-source voltage than the switching MOSFET on its own because the switching MOSFET is driven hard. Consequently, the output voltage is increased. The gate of linear biased MOSFET is connected to the output of the next stage so that, it is turned off while the next stage is charging from the previous stage capacitor. That means, the linear-biased transistor is turned off at the

Najmehossadat Nourieh
School of Physics, Engineering and Computer Science, University of Hertfordshire

same time as the switching transistor. An ideal 4-stage Dickson multiplier with an input of 1.5V would have an output of 7.5V. However, a diode-wired MOSFET 4-stage multiplier might only have an output

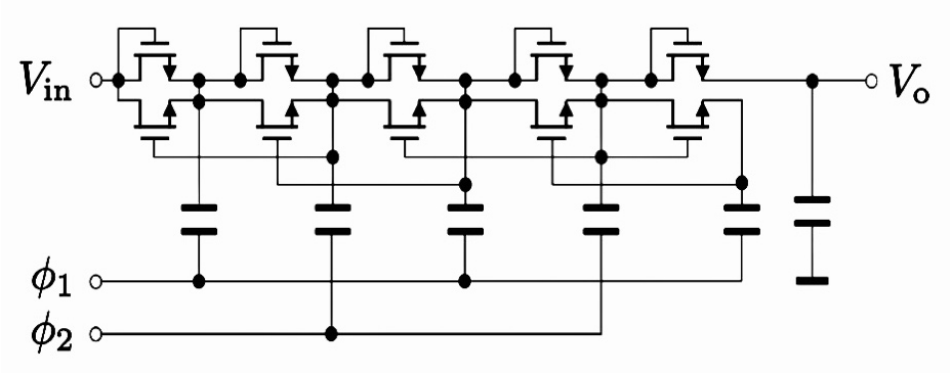

Figure 2.7 Dickson rectifier with paralleled MOSFETS [54]

of 2V. Adding parallel MOSFETs in the linear region improves the voltage to around 4V [54].

2.3.2 Cross-Coupled Switched Capacitor

A voltage multiplier can be formed from cross-coupled switched capacitor cascade voltage doublers (Figure 2.8). This circuit is typically used instead of a Dickson multiplier when the source voltage is less than 1.2V.

In [55, 56], the improvement of the conventional Dickson multiplier is discussed as shown in Figure 2.9. In Figure 2.9(a), each MOSFET gate is connected to the drain of the following switch which means each switch runs the gate of the switch before. In Figure 2.9(b), the first and last switches are diode-connected, but for others, the gate of each switch is connected to the source of previous MOSFET. As illustrated in

Najmehossadat Nourieh
School of Physics, Engineering and Computer Science, University of Hertfordshire

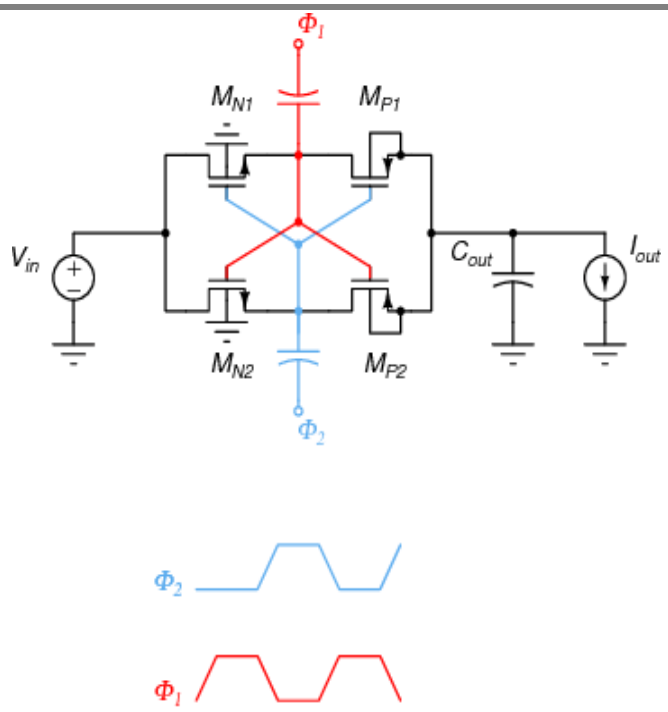

Figure 2.8 Dickson multiplier with cross-coupled switch capacitors [55]

Figure 2.9(c), the gates of MOSFETs with odd numbers are connected to the drain of the following switches while the gates of MOSFETs with even numbers are connected to the source of previous switches. In Figure 2.9(d), the gates of the first three switches are connected to the drains of the three following MOSFETs, while the last switch is diode-connected and the gates of the rest are connected to the source of the three MOSFETs before.

The threshold voltage reduction techniques which require additional circuits are not suitable for low power energy harvesting applications as these circuits occupy a large area leading to additional power dissipation [57, 58]. Passive threshold voltage reduction techniques such as the self-compensation method, can reduce the threshold voltage without additional circuits [59].

Improving the efficiency of the previously studied circuits, the latest version of the Dickson multiplier is introduced as shown in Figure 2.10, where all MOSFETs are directly connected to the power source to operate as a switch [60].

Najmehossadat Nourieh
School of Physics, Engineering and Computer Science, University of Hertfordshire

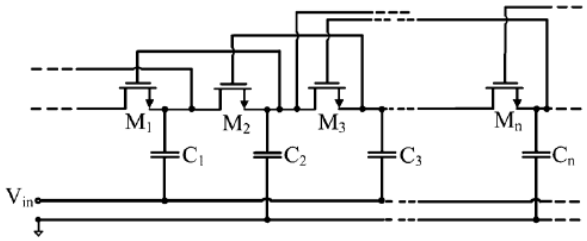

(a)

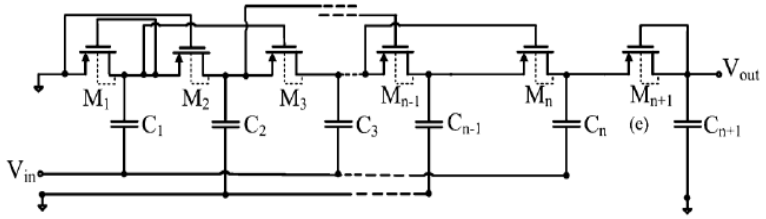

(b)

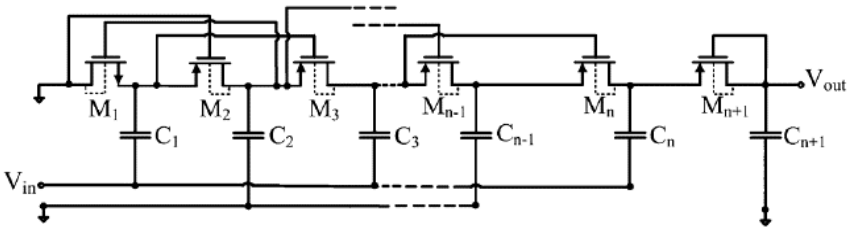

(c)

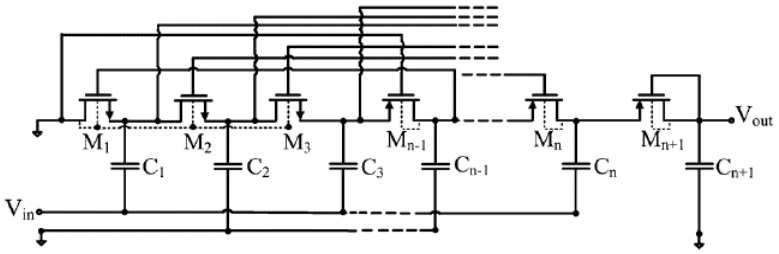

(d)

Figure 2.9 Modified Dickson rectifier (a) Forward-compensated NMOS [55]. (b) Proposed level-1 back-compensated using PMOS [55]. (c) Proposed level-1 hybrid forward and back-compensated using NMOS and PMOS [56] (d) Proposed level-3 hybrid forward and back-compensated using NMOS and PMOS [56]

Najmehossadat Nourieh
School of Physics, Engineering and Computer Science, University of Hertfordshire

Considering all the reviewed rectifiers, the best performance belongs to the Dickson rectifier with diode-connected MOSFETs, as it does not need any external battery and the efficiency for this circuit is higher than others.

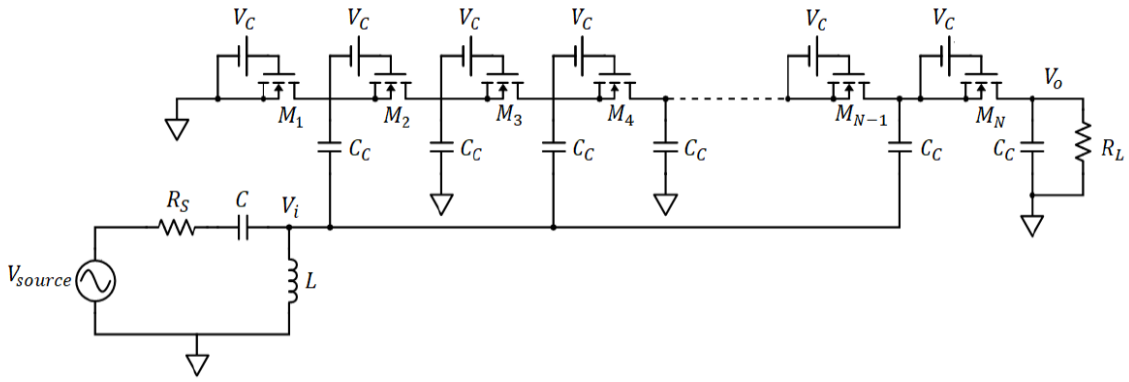

Figure 2.10 Dickson multiplier working with operating MOSFETs [60]

2.4 DC to DC Converters

A DC to DC converter is a power electronic circuit that converts a source of direct current from one voltage level to another. Power levels range from very low (small batteries) to very high (high-voltage power transmission) [60].

DC to DC converters are used in portable electronic devices such as cellular phones and laptop computers, which are supplied by batteries primarily. Such devices often contain several sub-circuits, each with its own voltage level requirement, different from the one supplied by the battery or an external source (higher or lower than the supply voltage). Additionally, the battery voltage declines as its stored energy is drained. Switched DC to DC converters offer a method to increase voltage from a partially lowered battery voltage, thereby saving space instead of using multiple batteries to accomplish the same function [61- 63]. Most DC to DC converters regulate the output voltage. Two exceptions to be noticed

Najmehossadat Nourieh
School of Physics, Engineering and Computer Science, University of Hertfordshire

are a high-efficiency LED power source, which is a kind of DC to DC converter that regulates the current through the LED, and a simple charge pump which doubles or triples the output voltage [64- 66]. Furthermore, DC to DC converters which are developed to maximize the harvested energy for photovoltaic systems and wind turbines are called power optimizers presented in [65, 66]. A DC to DC power optimizer (DCPO), which is a converter with an input connected to the photovoltaic (PV) panel and an output connected to more DCPOs in series, has been proposed and widely studied in [67, 68]. In the subsequent sections, we will discuss some of the recent proposed boost converters for low power applications of isolated and non-isolated DC to DC converters.

2.4.1 Non-Isolated DC to DC Boost Converters

In general, a non-isolated DC to DC converter is a circuit that uses power switches, inductors, diodes, and capacitors to transfer the energy of the input stage to the output. This circuit can be arranged in different topologies to realize the buck, boost or buck-boost types. Some of the the recent proposed non-isolated high voltage gain boost converters are presented in the sub sections 2.4.1.1 to 2.4.1.4. In section 2.4.2 the isolated high gain converters are discussed.

2.4.1.1 Step-up/Boost Converter

In [69], a minimum-phase response non-isolated fourth-order boost DC to DC converter (FBDC) exhibiting continuous input and output current is proposed. A voltage-mode controller is adopted to this converter to perform bus voltage regulation in a low voltage low power distribution system (LVPDS). FBDC supports additional load demand by interconnecting a second power source/battery (Figure 2.11).

As shown in Figure 2.11, this converter constitutes two switching MOSFETs, two capacitors and inductors to provide the voltage gain of maximum 3.7.

Najmehossadat Nourieh
School of Physics, Engineering and Computer Science, University of Hertfordshire

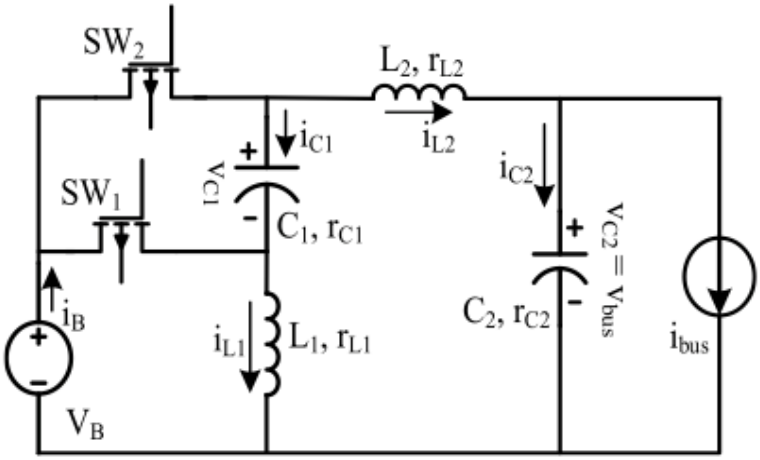

Figure 2.11 Fourth-order boost converter [69]

2.4.1.2 An Improved Three-level DC-DC Boost Converter

A fundamental boost DC to DC converter uses single switch, diode, capacitor and inductor which are arranged to step-up the input voltage, so that output voltage level is higher than input, proportional to duty cycle. In three-level boost converter, two blocks of simple boost converter are combined to provide higher voltage gain as shown in Figure 2.12.

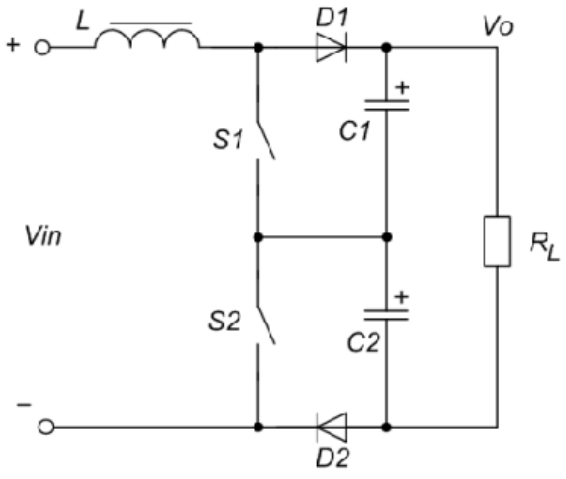

Figure 2.12 Three-level boost converter [70]

Najmehossadat Nourieh
School of Physics, Engineering and Computer Science, University of Hertfordshire

In [71], a simple non-isolated high gain three-level boost (TLB) converter is developed by the addition of two power switches and two diodes to the standard TLB converter (Figure 2.13). The voltage boosting and balancing is achieved by regulating the phase shift between the main switches.

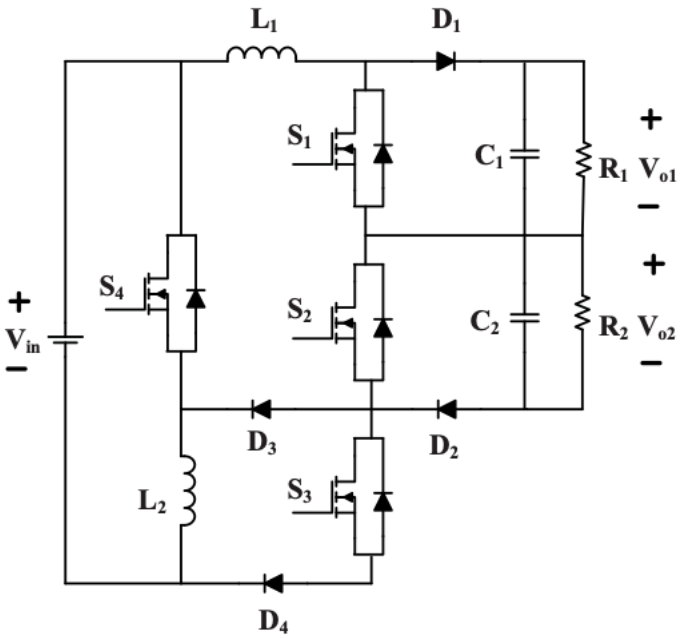

Figure 2.13 Three-level boost converter [71]

2.4.1.3 Multi-level Boost Converter

In Figure 2.14, a multi-level resonant DC-DC converter with high voltage gain, low number of switches, low voltage stress on transistors, ZVS and ZCS operation and high efficiency is presented. The converter uses resonant switched-capacitors (SC) circuits with five switches which allows it to reach a six-fold voltage gain. By the application of adequate switching patterns, seven levels of voltage adjustment can be achieved [72].

Najmehossadat Nourieh
School of Physics, Engineering and Computer Science, University of Hertfordshire

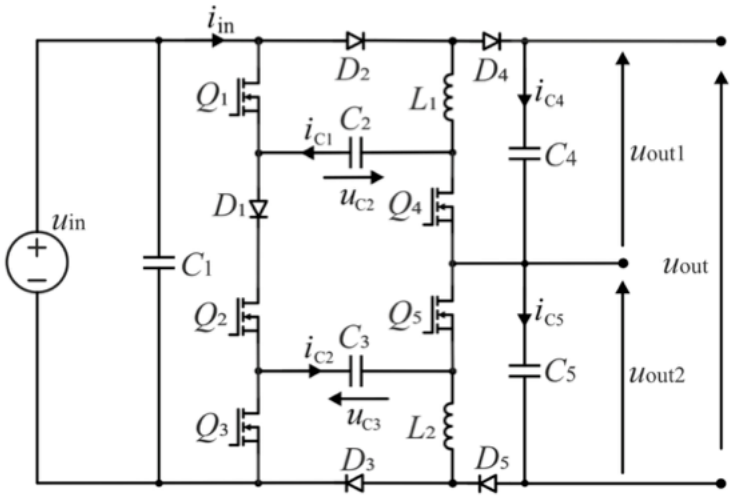

Figure 2.14 Multi-level high gain boost converter [72]

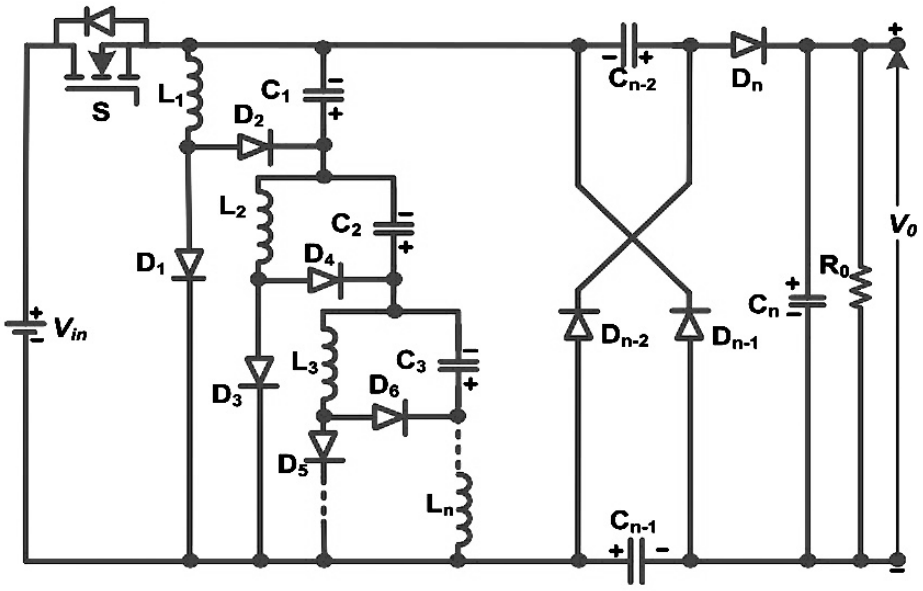

Figure 2.15 Reduced switch voltage stress ultra-gain multi-stage DC to DC converter for low power application [73]

2.4.1.4 Reduced Switch Voltage Stress Ultra-gain Multi-stage Boost Converter

Najmehossadat Nourieh
School of Physics, Engineering and Computer Science, University of Hertfordshire

An ultra-voltage gain DC to DC converter is proposed which is composed of an active impedance network with a single MOSFET switch. The proposed converter utilizes minimum components and achieves the ultra-gain with lower switch voltage stress. The general structure of an n-stage active switched impedance topology is presented in Figure 2.15 [73].

2.4.2 Isolated DC to DC Converters

Many methods have been proposed for achieving high voltage gain in DC-DC converters. In most cases, high voltage gain DC-DC converters are divided into isolated and non-isolated [74-75]. In the following sub section, two isolated high voltage gain converters are studied.

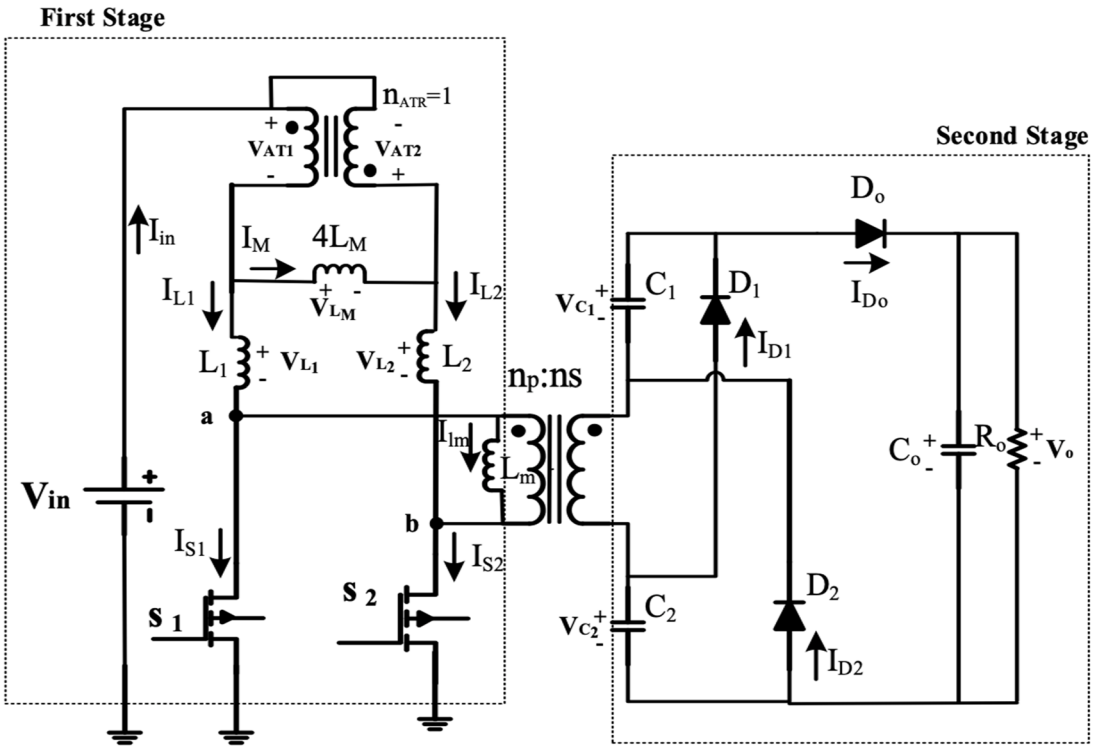

Figure 2.16 Dual switch/inductor isolated DC-DC converter configuration [76]

Najmehossadat Nourieh
School of Physics, Engineering and Computer Science, University of Hertfordshire

2.4.2.1 Dual Switch/Inductor Isolated Hight Voltage Gain Converter

In this section, a dual switch/inductor isolated DC-DC converter configuration for high voltage gain applications is presented. The high voltage gain regulation of the proposed converters is achieved in a wide voltage range by employing an auxiliary transformer and voltage lift circuit. The auxiliary transformer couples the current paths of the two boost inductors, and the used voltage lift circuit led to the increased voltage gain. The presented converter is developed using the interleaving technique to achieve low-size filter components (Figure 2.16) [76].

2.4.2.2 Self Balanced High Gain Multi-Port Converter

In this section, a high-voltage gain multi-port DC- DC converter for Photovoltaic (PV) and Fuel cell (FC) power generation systems is proposed. The traditional three-level boost converter and forward converter are integrated together for obtaining the proposed converter. Voltage gain across each port is equivalent to the gain of the conventional boost converter. Moreover, the proposed topology can produce four output

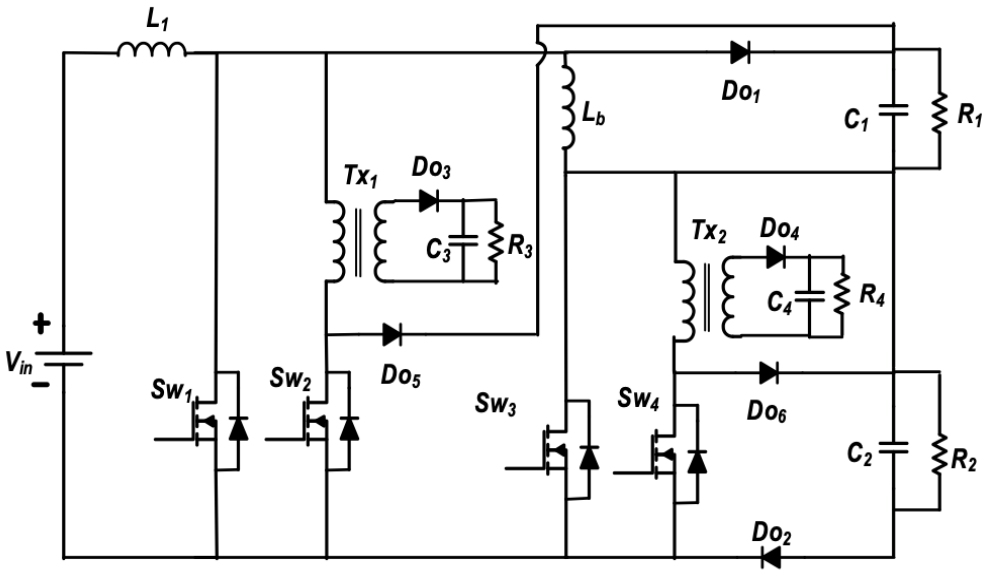

Figure 2.17 A high-voltage gain multi-port DC- DC converter [77]

Najmehossadat Nourieh
School of Physics, Engineering and Computer Science, University of Hertfordshire

ports in which two are isolated type and the other are non-isolated type. The voltage gain and asymmetrical outputs across isolated port can be further adjusted by increasing/decreasing the transformer turns ratio (Figure 2.17) [77].

2.5 The Simulation of Recent Proposed Dickson Rectifiers

In this section, the simulation results of the recently proposed circuits will be presented. All the discussed simulation results are obtained using the PSIM simulator. The PSIM environment is used where all the components can operate by defining all parameters and specifications individually.

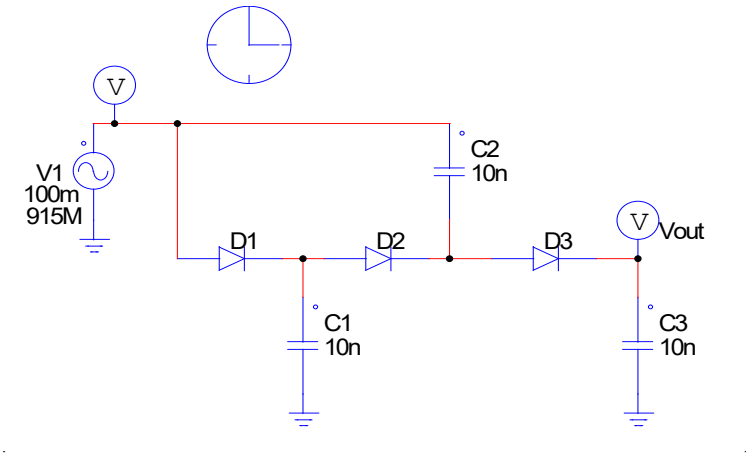

(a)

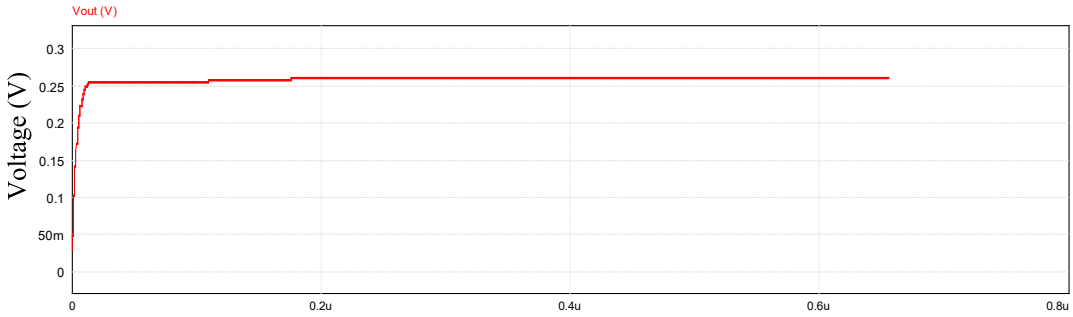

(b)

Figure 2.18 A conventional Dickson rectifier with Schottky diode, (a) The schematic, (b) The output voltage

Najmehossadat Nourieh
School of Physics, Engineering and Computer Science, University of Hertfordshire

First, the simple Dickson rectifier with Schottky diode illustrated in Figure 2.18(a) is simulated. The frequency of all switches is set at 915MHz, the input voltage is 100mV$_{p-p}$, and the output load is 3kΩ. The simulated output voltage is approximately 260mV as shown in Figure 2.18(b).

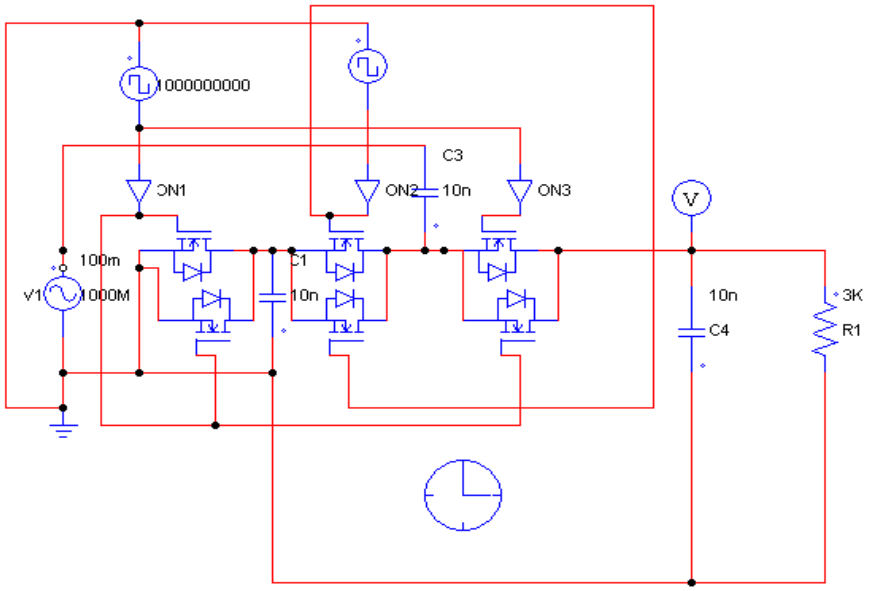

(a)

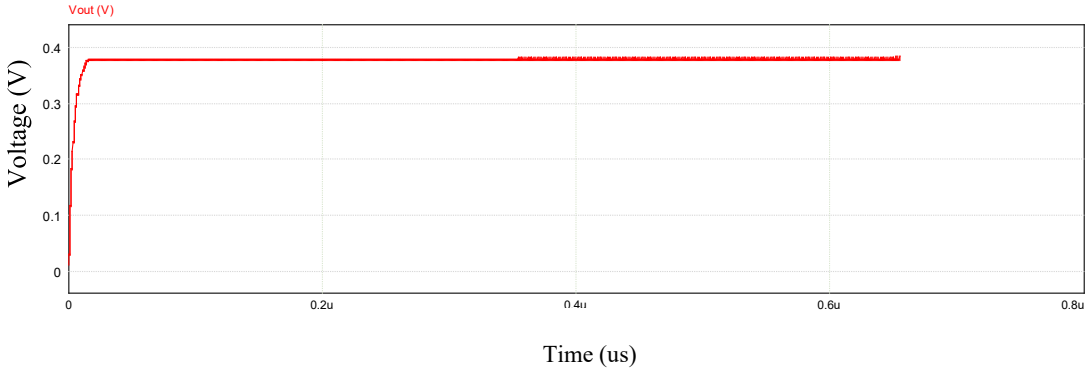

(b)

Figure 2.19 An improved Dickson rectifier with paralleled MOSFETs, (a) The schematic, (b) The output voltage

Najmehossadat Nourieh
School of Physics, Engineering and Computer Science, University of Hertfordshire

In Figure 2.19(a), the PSIM designed schematic of an improved Dickson rectifier with paralleled MOSFETs is presented where the output voltage of this circuit is 380mV for the input voltage of 100mV and frequency of 915MHz as illustrated in Figure 2.19(b).

2.6 Application Wireless Energy Harvesting

In this thesis, we proposed three combinations of circuits to be applied for low power energy harvesting systems. All the designed parameters were considered to be matched with RFEH applications. Energy is an essential requirement of any active system to operate. At every moment, RF energy is transmitted from millions of devices and transmitters all over the world. There are many advantages if we are able to harvest this energy from sources around us, as we have been depending on many energy sources for centuries. Since the modern science and electronic industry have grown rapidly, there is a great demand for more energy-efficient sources. In RF energy harvesting, any radio transmitting device can be considered as a source of energy. The most common radio wave sources are mobile base and radio broadcasting station, satellite, TV broadcasting and wireless LAN transmitter (Wi-Fi).

2.6.1 Applications of Wireless Energy Harvesting [49], [78, 79]

As it is discussed in Ref. [49] and Ref. [78, 79], there are several applications for wireless energy harvesting which includes battery-less power source, charging RFID tags, smart lighting applications, smart switches for home automation, Internet of Things (IoT) applications, recharging of devices, power source for smart sensors, wireless charging of portable devices, biomedical applications, LEDs, implantable devices, environment monitoring and microcontrollers.

Najmehossadat Nourieh
School of Physics, Engineering and Computer Science, University of Hertfordshire

2.6.2 Advantages of Wireless Energy Harvesting [80]

The advantages of wireless energy harvesting are considered as availability, unlimited spectrum of sources, efficient source of energy, no wastage, green energy, eco friendly, no need for periodic replacement of battery, extended life for devices due to recharging of storage battery during sleep mode, simple design and cost-effective and externally resettable for microprocessor control.

2.6.2 Disadvantages Wireless Energy Harvesting [78- 80]

Some of disadvantages of wireless energy harvesting are low density, efficiency inversely proportional to the distance, design of RF energy harvesting receiver is complex for wide frequency range specification and it requires longer charge-time.

There is a great potential capacity of wireless energy harvesting for applications such as home automation projects and the Internet of Things (IoT). Smart sensor technology can produce low-power tools with advanced embedded technology capable of operating at microwatt input power. Furthermore, wireless sensors for humidity, proximity and temperature are widely used in industry, home automation and automobile application. In recent years, wearable devices and medical sensors were capable of using wireless energy as a power source. Enhanced security devices with smart sensor technology can make use of power from wireless energy harvesting.

2.7 Novelties

In this thesis, we have designed very low power circuits which can be applied for RF energy harvesting applications which can have all the mentioned advantages of RFEH applications including availability, unlimited spectrum of sources, efficient source of energy, no wastage, green energy, eco-friendly, no need for periodic replacement of battery, extended life for devices due to recharging of storage battery

during sleep mode and simple design. The novelties of the proposed circuits are separately discussed in chapter 3, 4 and 5 which is briefly about improving the voltage level of rectifier by using a phase shifter to produce an additional signal with 180° phase difference (comparing to the first original signal). The proposed 7-stage rectifier can provide 1.2V at the output stage for the input power level of -10dBm. Furthermore, two DC to DC converters are introduced to boost the voltage level to the desired output. The first, ZVS DC to DC converter is capable of operating in high switching frequencies to provide the highest efficiency. As the input power level is weak, all the parameters are carefully designed to produce very low losses. In this circuit, by adding the series of inductor and capacitor we provide the ZVS condition for the main switch. Also, the diode-connected MOSFET is used instead of Shottkey diode in order to decrease the conduction loss of diode.

In addition, this thesis also proposes an isolated ZVS DC to DC converter which can be applied to the output of the proposed 1-stage rectifier to produce high output voltages more than 1.2V. This circuit also benefits from a paralleled diode-connected MOSFET with resonant capacitor to bypass the capacitor in some discharging operation modes which means the energy of primary side of transformer can be linearly transfer to secondary. Another advantage of this converter is to use the leakage inductance of transformer instead of the resonant inductor. Moreover, this converter benefits from diode-connected MOSFETs at the secondary side which considerably reduce conduction loss of diode. The combination of this converter with dual input rectifier and phase shifter makes a unique system for low power applications.

2.8 Conclusion

The energy sources for wireless energy harvesting (WEH) are available in many forms, such as solar power, wind energy, thermal energy, electromagnetic energy, kinetic energy, etc. Among them, electromagnetic energy is abundant in space and can be retrieved without limitation. Electromagnetic waves come from a variety of sources such as satellite station, wireless internet, radio station, and digital

multimedia broadcasting. A radio frequency power harvesting system can capture and convert electromagnetic energy into a usable direct current (DC) voltage. The key units of an RF power harvesting system are the antenna and rectifier circuit that allows the RF power or alternating current (AC) to be converted into DC energy. The processing of battery wastes is a critical problem. Most batteries end up in landfills, leading to the pollution of the land and water underneath. The most effective solution for reducing battery wastes is to replace them with possible alternatives. Applying WPH technology will help to reduce the dependency on batteries, which will ultimately have a positive impact on the environment. Moreover, the process of harnessing electromagnetic energy will not generate waste as it is a clean energy source.

Najmehossadat Nourieh
School of Physics, Engineering and Computer Science, University of Hertfordshire

3 The High Voltage Gain Multi-stage Dickson RF Rectifier

Radio frequency energy harvesting (RFEH) is currently experiencing fast development because of the increasing number of transmitter sources. This chapter presents novel designs of Dickson rectifier with high voltage gain and efficiency at frequency of 915MHz. The proposed circuits introduce new method of deriving output characteristics of rectification circuit in terms of voltage. The design consists of different stages of the Dickson voltage multiplier. Specifically, we introduced two novel modified Dickson rectifiers, with one and seven stages for different purposes.

The rectifiers benefit from two input AC sources with 180° phase shift. This Dickson circuit is further discussed in two levels; the first one is a 1-stage rectifier operating with Schottky diodes or diode-connected MOSFETs, and the second is a 7-stage rectifier producing a higher output voltage.

3.1 Introduction

Figures 3.1 and 3.2 introduce the Villard voltage multiplier and Dickson charge pump topologies, which work with diodes [81, 82]. Villard multiplier has the most similar configuration to Dickson rectifier. The main difference is that the Villard voltage multiplier connects the voltage doubler in series form while Dickson rectifier/multiplier connects the voltage doubler in parallel form. To enhance the operation of these circuits, diodes (Schottky diodes) are replaced by diode-connected MOSFETs. The diode-connected MOSFET operates as a diode. When this transistor is turned on, it is in forward-biased mode.

Najmehossadat Nourieh
School of Physics, Engineering and Computer Science, University of Hertfordshire

When it is off, it operates in reverse-biased mode. In this structure, the gate of the diode-connected transistor is connected to its drain.

Furthermore, with the increasingly high-performance requirements of high-efficiency/high-voltage gain circuits, the power division and phase shifting concepts are considered to increase the performance quality of the systems. Most attention is paid to the phase shift networks providing a wide range of phase differences between 90º to 180º to enhance the efficiency [82- 87].

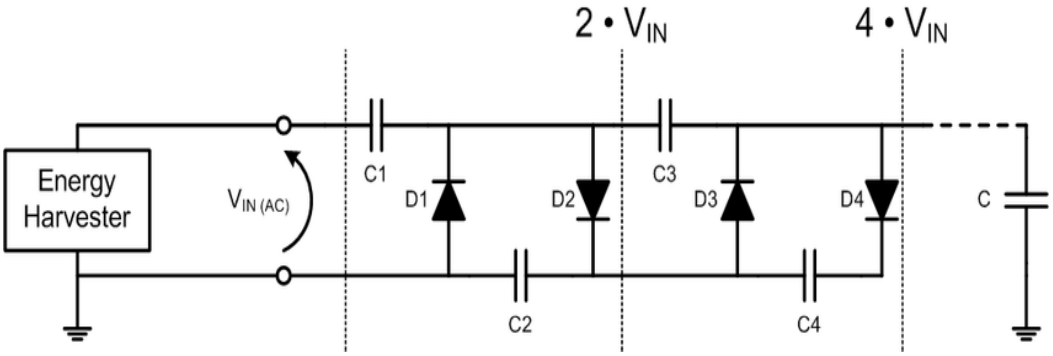

Figure 3.1 Villard voltage multiplier [81]

3.2 Proposed 1-stage Dickson Rectifier

Rectification of radio (microwave) signals to direct current (DC) power has been the subject of various research for nearly half a century. This is achieved by rectifying the RF signals obtained from each antenna element before combining them in the DC output. More energy can be collected because each antenna element provides a broader pattern, which potentially grows the amount of energy received by the antenna. However, the important point that should be considered is the non-linearity of the rectifier's impedance with respect to input power and frequency [82], [88- 89]. Also, the impedance matching network is sometimes applied to match the impedance from main circuits and antenna. Hence, an

Najmehossadat Nourieh
School of Physics, Engineering and Computer Science, University of Hertfordshire

alternative method is designing an individual antenna combined with a single band voltage rectifier/multiplier [90- 94].

3.2.1 Dickson Rectifier with One Input Signal

Generally, a multiplier circuit requires an AC power supply to function correctly. One side of the power supply is grounded, and remains at zero potential level, and the other side varies between plus and minus V_S [95]. As shown in Figure 3.2, capacitor C_1 is charged through diode D_1 to the voltage of Vs, which is the value of the negative peak. This positively charges the capacitor at the right side and negatively at its left. On the left side of the diagram, there is a $+Vs$ voltage at the top side of the power supply shown in Figure 3.3, which charges capacitor C_1 (the capacitor was also charged in the previous operation mode). Accordingly, capacitor C_2 is charged through diode D_2 to $2Vs$. Note that the stored charge in capacitor C_1 was used in the last cycle to charge capacitor C_2; thus, C_1 is now being charged by diode D_1. Similarly, capacitor C_3 is charged through diode D_3 up to $2Vs$. Then the power supply is again at its positive peak and capacitor C_2 is now being recharged. At the same time, capacitor C_4 is charged up to $2Vs$. Capacitors do not charge spontaneously; hence they do not attain the full voltage until a certain number of cycles have passed. That number of cycles depends on the charging current [95].

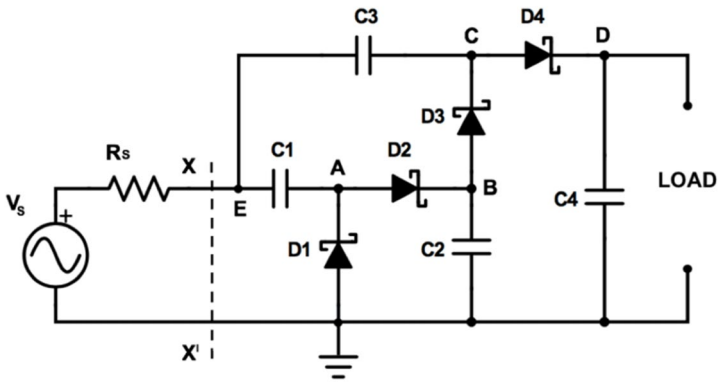

Figure 3.2 Dickson charge pump

Najmehossadat Nourieh
School of Physics, Engineering and Computer Science, University of Hertfordshire

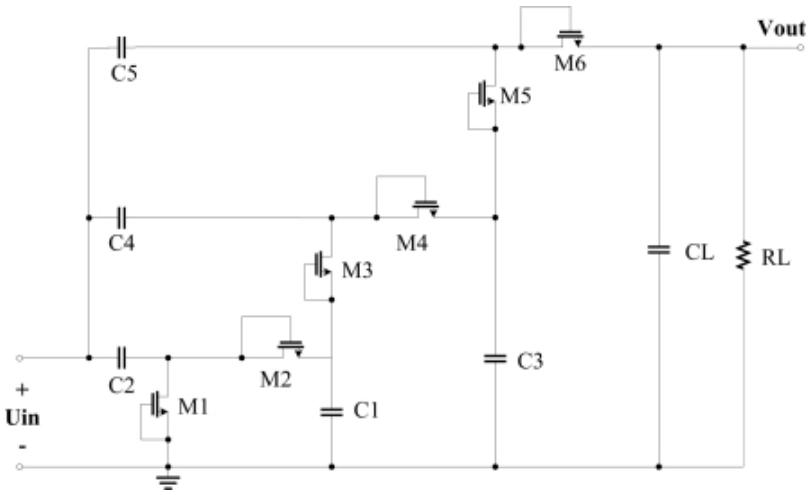

Figure 3.3 Dickson rectifier [95]

To design the proper rectifier for RF energy harvesting, the rectifying elements play a very important role. Rectifying components such as diodes and transistors are essential elements of rectifier/multiplier circuits, which can determine the operating frequency and power-conversion efficiency. Conventionally, Schottky diodes were used because of their low threshold voltage. Besides, there are also tunnel (Esaki) diodes, spin diodes and metal– insulator–metal (MIM) diodes with recent technology improvements making them more suitable for low power circuits. Notably, the tunnel diodes can function at very high frequencies with rapid responses because of their low parasitic features. Furthermore, the MIM diode technology can be integrated with the CMOS process, but the Schottky diodes cannot. In addition, spin diodes have lower threshold voltage than Schottky diodes. Shottkey diodes are the perfect combination of being fast in high frequencies, low threshold voltage and low parasitic features.

Figure 3.4 presents the simulation results of a single input Dickson rectifier where input voltage is $100mV_{p-p}$, frequency is 915MHz, capacitors are 10nF, output resistor is 3kΩ, diode model is SMS7630-079LF and the output voltage is 260mV. The efficiency of this circuit is 19%. The result of this simulation will be compared with the proposed two-input configuration in the following sub-section. As we need to keep the output ripple as low as possible, we chose 10nF to keep ΔVo/Vo lower than 1%. Also, we chose the value for output resistor to get appropriate output power $(V_{out})^2/R_{out}=P_{out}$.

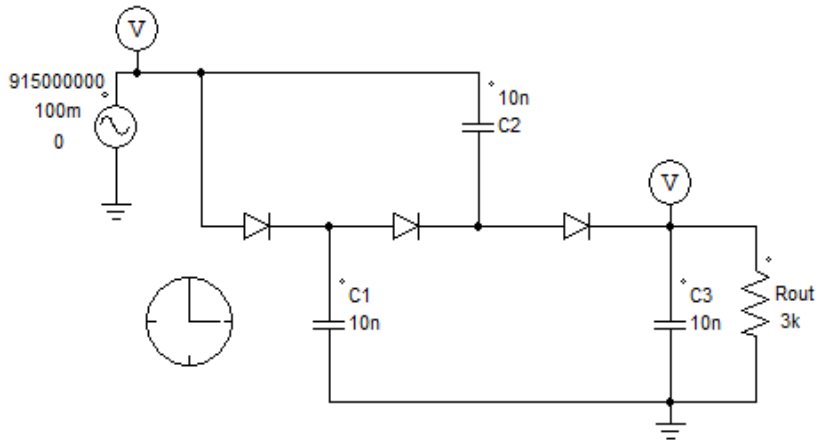

(a)

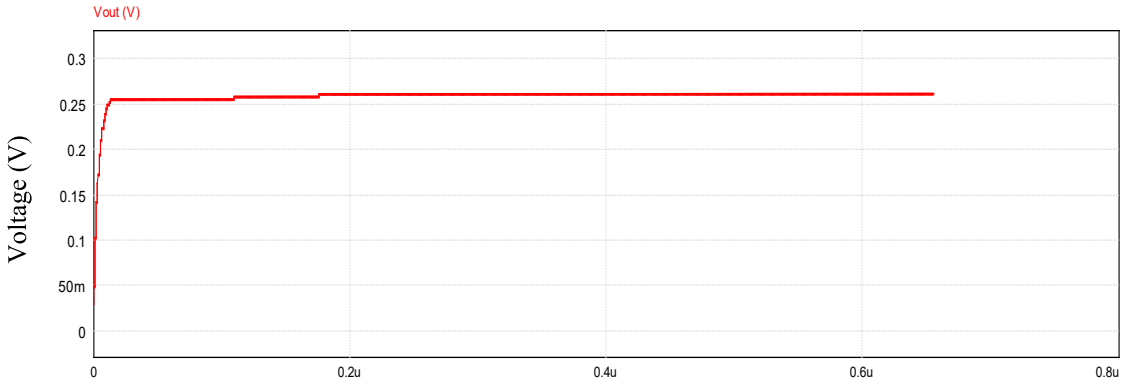

(b)

Figure 3.4 Single input rectifier, (a) The schematic, (b) The diagram of the output voltage

Najmehossadat Nourieh
School of Physics, Engineering and Computer Science, University of Hertfordshire

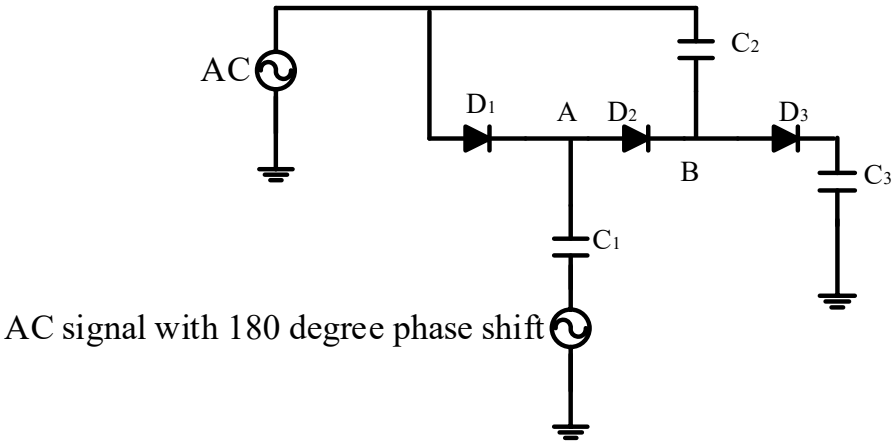

Figure 3.5 The schematic of the proposed dual input rectifier

3.2.2 Proposed Dickson Rectifier with Two Input Sources

The proposed Dickson rectifier with two input signals with a 180° phase difference, can have approximately 50% more voltage gain compared to the same Dickson rectifier with a single input. In Figure 3.5 the schematic is presented, where three diodes and three capacitors are employed to increase the voltage. For better efficiency, we replaced diodes with diode-connected MOSFETs. This provides the advantages of simple operation of diode without any need for drivers and more efficient structure of MOSFETs for low power circuits.

In Figure 3.6, the circuit of the proposed rectifier with diode-connected MOSFETs has been presented. In this figure MOSFETs and capacitors are called from Q_1 to Q_3 and C_1 to C_3 respectively. The amplitude of the input signal is Vs for the conventional (single input) circuit, but in the proposed circuit, the amplitude is $2Vs$. This is achieved by the introduction of the second input signal with a 180° phase difference. One side of the two input signals with 180° phase difference, is grounded and remains at zero potential, and the other side varies between plus and minus Vs.

Najmehossadat Nourieh
School of Physics, Engineering and Computer Science, University of Hertfordshire

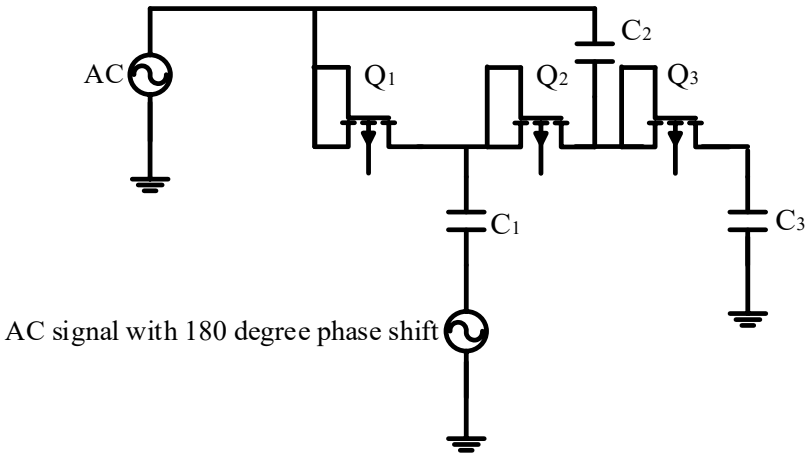

Figure 3.6 The schematic of the proposed rectifier working by diode-connected MOSFETs with two input sources with 180° phase shift.

In Figure 3.5, capacitors and diodes are labelled in numbers from 1 to 3. In the positive cycle of the first input source (which is the negative cycle of the second source), the diode D_1 conducts and capacitor C_1 is charged to $2Vs$. (one side of C_1 is $-Vs$ and the other side is $+Vs$, which means the magnitude of the voltage is $2Vs$). In the same mode, C_2 and C_3 are charged through D_3. In the next mode, the capacitor C_2 will be charged through D_2 and C_1, also the energy stored in C_1 is transferred to C_2 and the voltage of C_2 reaches more than $4Vs$. In the next cycle, when D_3 conducts, the energy stored in C_2 transfers to C_3 (which is the output capacitor).

In order to analyse this proposed rectifier, we need to model the diode-connected MOSFET with its characteristics shown in Figure 3.7, where each diode-connected MOSFET or simple diode has been modelled by R_D and jX_D while capacitors are modelled by jX_C [96]. The equivalent impedance of diode is called Z_D, the input current is I_s and the input voltage is $V_S = V_a\cos(\omega t)$ where V_a is the peak voltage of AC source and ωt is the angular frequency. Therefore, to calculate the output voltage of 1-stage

Najmehossadat Nourieh
School of Physics, Engineering and Computer Science, University of Hertfordshire

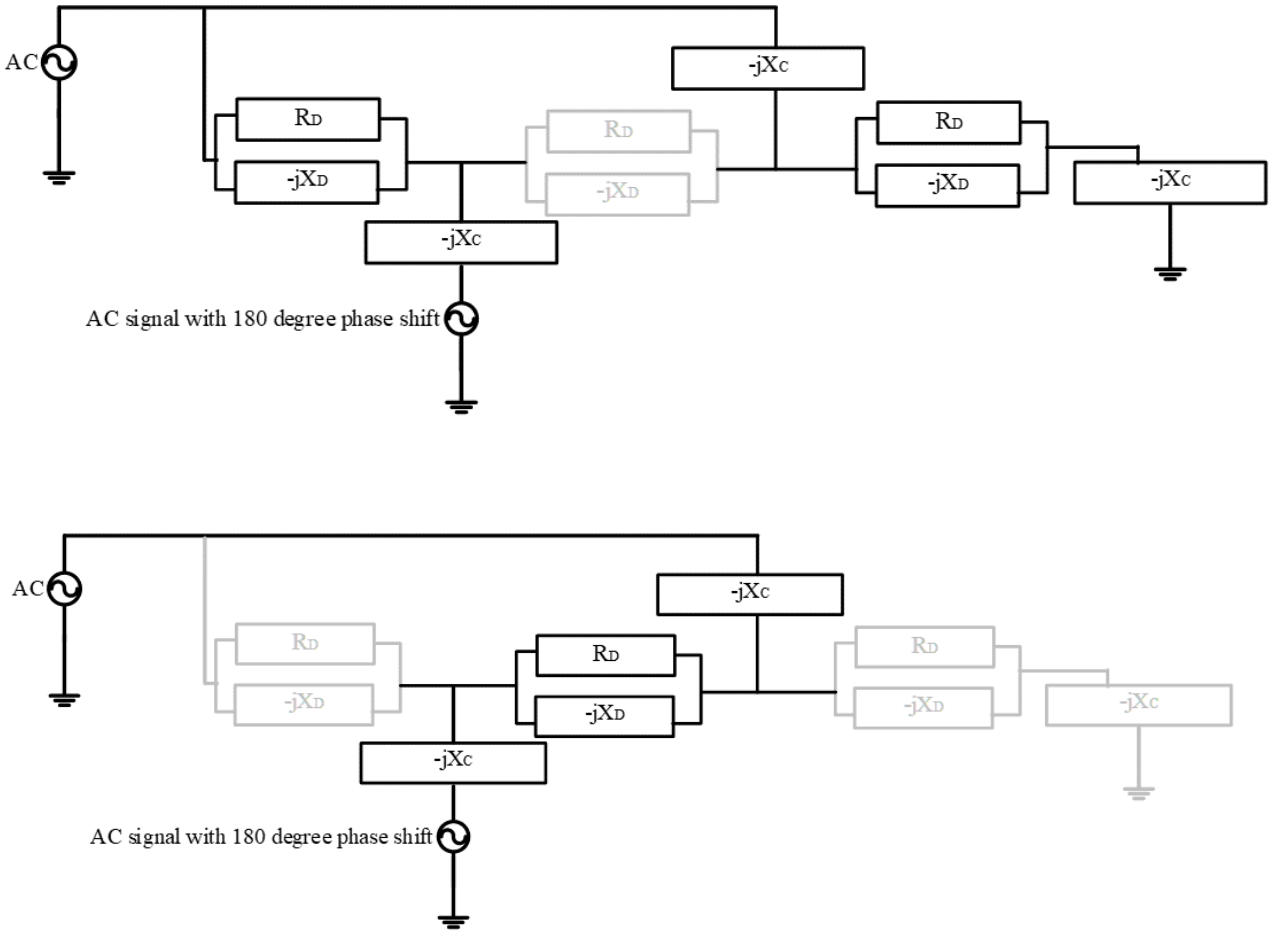

Figure 3.7 Analytical model of Dickson voltage multiplier circuit

rectifier, the Eq. (3.1) is used. For n-stage of the modified Dickson rectifier working with two input sources with 180° phase difference, the Eq. (3.2) is used.

In the proposed rectifier with one stage of voltage multiplier, the output voltage is presented in Eq. (3.1). Moreover, the Eq. (3.3) was considered to calculate the rectifier current. The voltage of V_2 means the output voltage after second period.

$$V_2=2V_a\cos(\omega t)+I_s(-jX_C+Z_D) \tag{3.1}$$

$$V_n=2V_a\cos(\omega t)+\left(\frac{n}{2}-1\right)\left(\frac{-jX_C+Z_D}{-2jX_C+Z_D}\right).2V_a\cos(\omega t)+I_S(-jX_C+Z_D) \tag{3.2}$$

Najmehossadat Nourieh
School of Physics, Engineering and Computer Science, University of Hertfordshire

$$I_n = \frac{V_n}{R_n} \tag{3.3}$$

3.2.3 The Simulation Results of The Proposed 1-Stage Rectifier with Dual Inputs

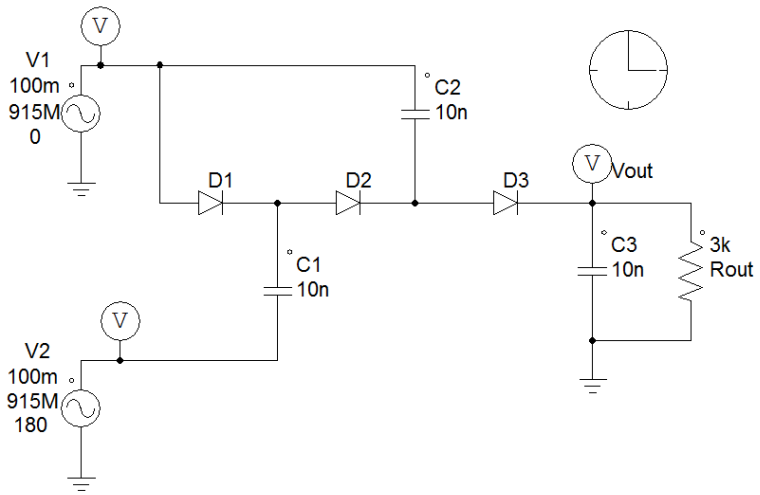

Figure 3.8 The simulated circuit of the proposed Dickson voltage multiplier with diode

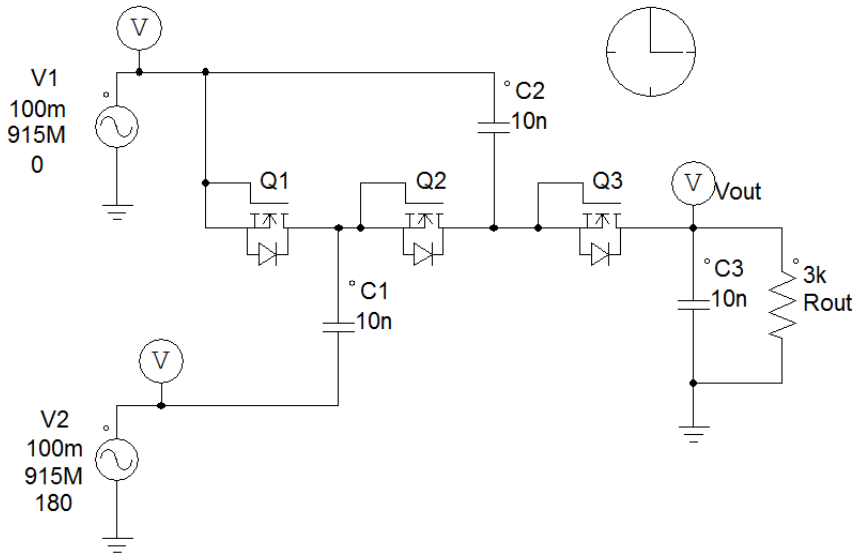

Figure 3.9 The simulated circuit of the proposed Dickson voltage multiplier with diode-connected MOSFET

The proposed circuit is simulated in the PSIM environment, where the characteristics of all elements were defined using their datasheets (note: all the characteristics are considered to be in the worst-case

Najmehossadat Nourieh
School of Physics, Engineering and Computer Science, University of Hertfordshire

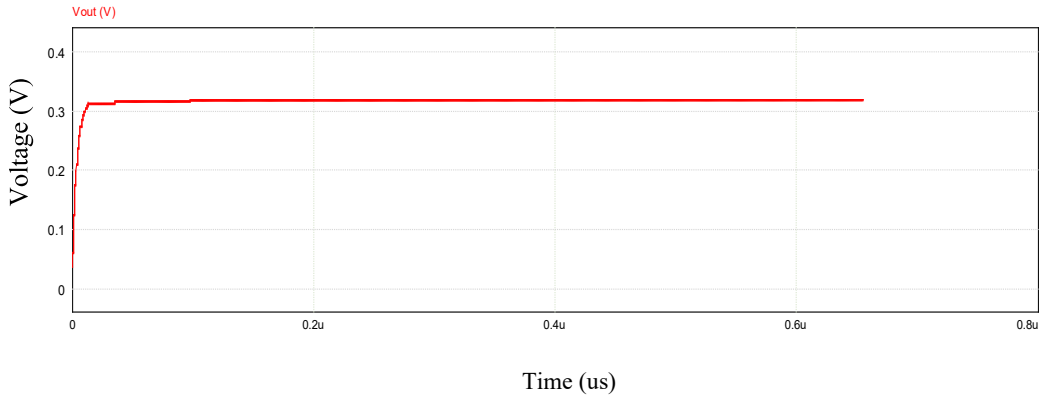

Figure 3.10 The output voltage of the proposed Dickson multiplier with Schottky diode

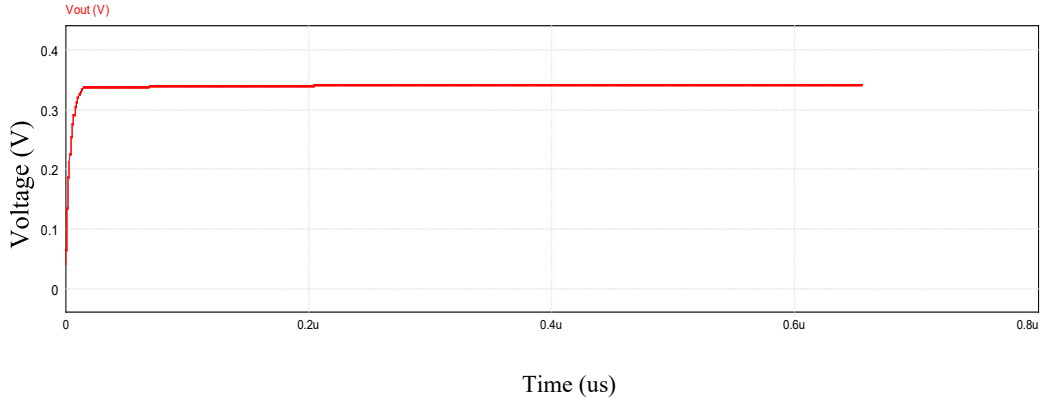

Figure 3.11 The output voltage of the proposed Dickson multiplier with diode-connected MOSFET

scenario). The diode-type proposed rectifier is presented in Figure 3.8, then the same circuit with diode-connected MOSFET is shown in Figure 3.9. Respectively, in Figure 3.10 and Figure 3.11, the difference between the output voltages using these two rectifiers, is shown. The output voltage of the diode rectifier is 320mV, while it is 340mV for the diode-connected MOSFET. The input voltage is $100mV_{p-p}$, frequency is 915MHz, capacitors are 10nF, output resistor is 3kΩ, diode are modelled by specifications of SMS7630-079LF, MOSFETs are modelled by specifications of EPC8008ENGR. The efficiency of this rectifier with diode is 34.13% while it is 38.5% for diode-connected type.

Najmehossadat Nourieh
School of Physics, Engineering and Computer Science, University of Hertfordshire

3.3 The Proposed 7-Stage Dickson Rectifier

In Figure 3.12, the modified diode-base 7-stage Dickson rectifier with dual input signals is introduced. A modified multi-stage Dickson rectifier in seven stages is shown in Figure 3.13. The objective of this section is to find the output voltage for the available power delivered from the antenna. This converter has seven levels which will be discussed in the following sections. In Figure 3.14, the input signals with 180° phase difference for this circuit is shown where the peak voltage is 100mV.

Dickson rectifiers are intrinsically nonlinear because of the switching behaviour of rectifier elements.

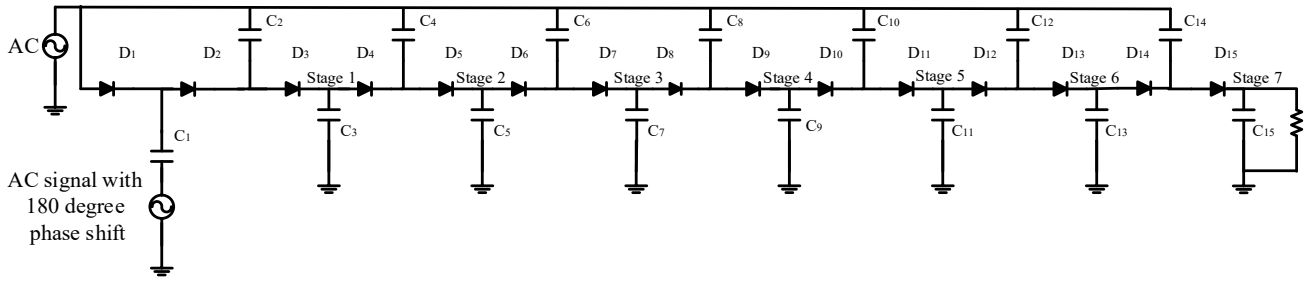

Figure 3.12 7-stage Dickson rectifier with diodes

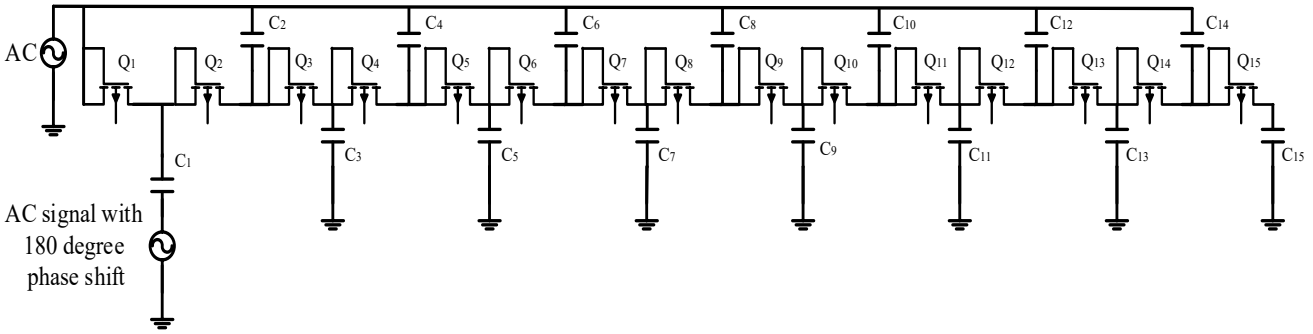

Figure 3.13 7- stage Dickson rectifier with diode-connected MOSFETs

Nevertheless, in steady-state mode, we can assume that the input voltage of rectifier is sinusoidal

Najmehossadat Nourieh
School of Physics, Engineering and Computer Science, University of Hertfordshire

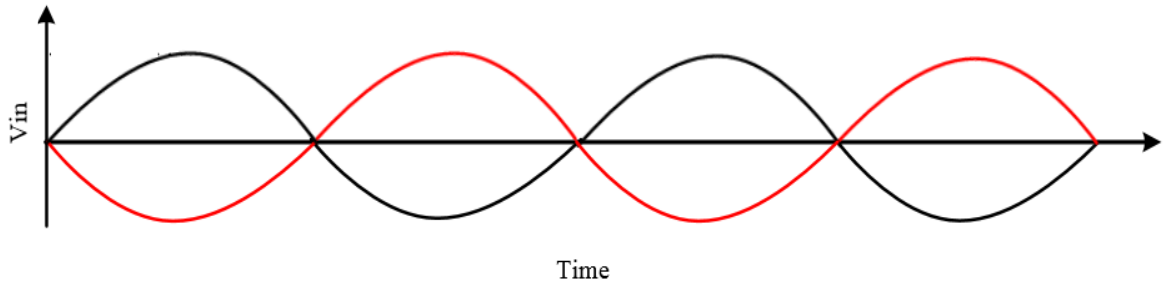

Figure 3.14 The input signal of the first and second input signals with 180° phase difference

($V_S = V_a\cos(\omega t)$), *Va* is the maximum voltage of V_S and $V_{in}=2V_S$, as we applied dual input sources with 180° phase shift for input power of $P_{in} < -10$ dBm. The energy harvesting circuit has a sinusoidal input source assumed as a $V_S = V_a\cos(\omega t)$. In this case, the input impedance of the rectifier is modelled with a resistor R_{in} in parallel with a capacitor. The power delivered to the rectifier and the power consumed by R_{in} are given in Eq. (3.4).

$$P_{in}=\frac{(V_a\cos(\omega t))^2}{R_{in}} \tag{3.4}$$

The level of the output voltage of an energy harvesting system is defined based on the AC to AC power transmission of the impedance matching network (IMN), AC to DC voltage multiplication and rectification of multistage Dickson rectifier. For the proposed novel rectifier with dual inputs, the output voltage has been calculated as presented in Eq. (3.5). By seven stages of the designed rectifier, we reached the desired voltage of 1.2V.

$$V_7=2V_a\cos(\omega t)+\left(\frac{7}{2}-1\right)\left(\frac{-jX_C+Z_D}{-2jX_C+Z_D}\right)2V_a\cos(\omega t)+I_S(-jX_C+Z_D) \tag{3.5}$$

In conclusion, we need to do a trade-off between the number of amplification stages, efficiency and the delivered input power to load. Although this multi-stage rectifier has advantages such as being well fitted for CMOS technology usage, small size and simple analyse process, we are not able to have voltages of more than around 1.2V with high efficiency in the RFEH as the input power is too weak. Therefore, for

Najmehossadat Nourieh
School of Physics, Engineering and Computer Science, University of Hertfordshire

applications with higher required output voltages, we proposed to use the two presented methods in chapter 5 (1-stage Dickson rectifier and resonant ZVS DC to DC converter as well as 1-stage Dickson rectifier and isolated resonant ZVS DC to DC converter).

3.3.1 The Simulation Results of The Proposed 7-Stage Rectifier in PSIM

The simulation schematic of the diode-base Dickson rectifier with seven stages (PSIM environment) is presented in Figure 3.15, while the output voltage is shown in Figure 3.16, where it is shown that the output voltage of 7-stage rectifier is about 1.2V, which is suitable for IoT applications. The frequency is

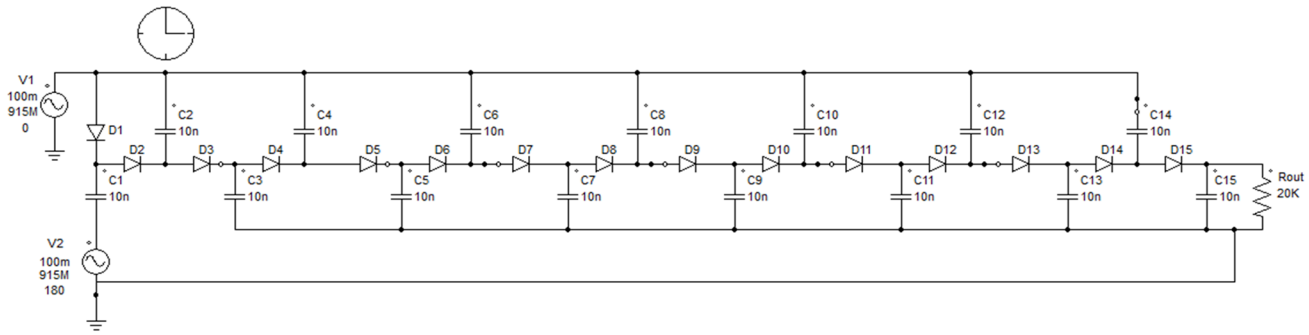

Figure 3.15 The PSIM model of 7-stage diode-base Dickson rectifier

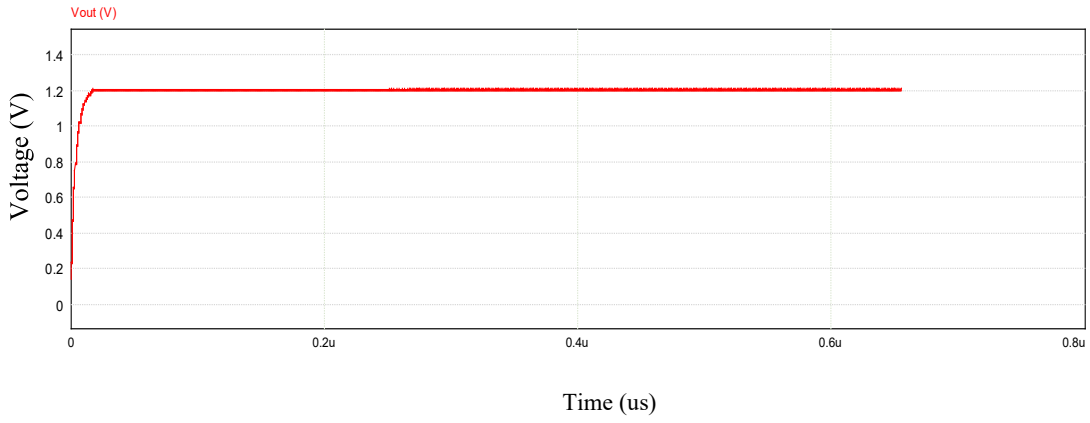

Figure 3.16 The output voltage of the 7-stage diode-base proposed rectifier

915MHz and the time to reach steady state is about 35ns. In Figure 3.17 the schematic of diode-connected

Najmehossadat Nourieh
School of Physics, Engineering and Computer Science, University of Hertfordshire

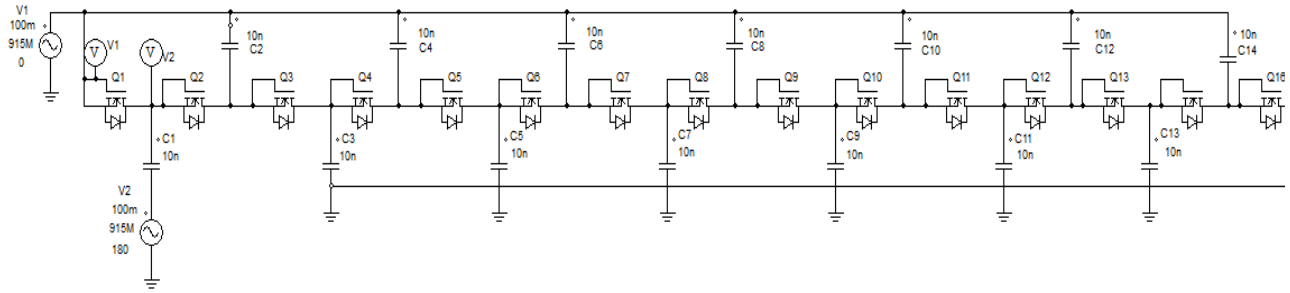

Figure 3.17 The PSIM model of 7-stage rectifier with diode-connected MOSFET

MOSFET Dickson rectifier with dual input signal is presented while in Figure 3.18, two input signals with 180° phase difference are shown. In the same condition for this MOSFET rectifier, the output

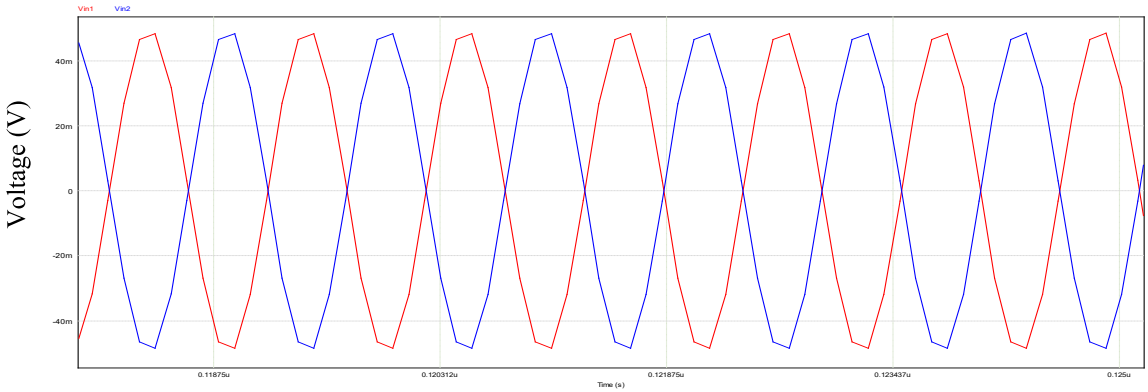

Time (s)

Figure 3.18 The input signals with 180° phase difference

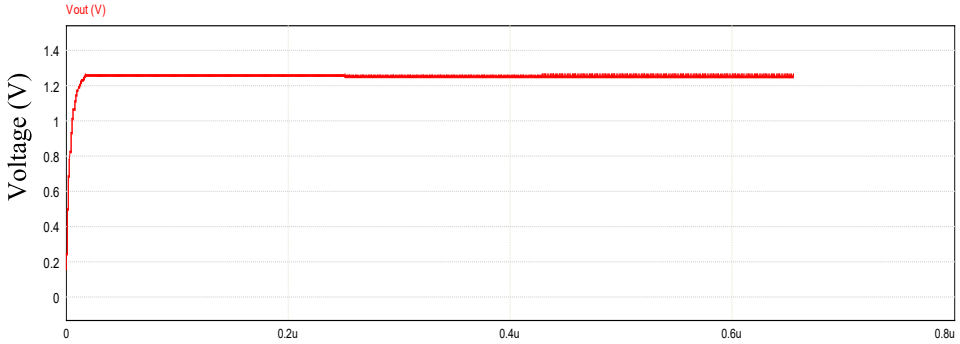

Figure 3.19 The output voltage of the proposed seven-stage Dickson rectifier/multiplier with diode-connected MOSFET

Najmehossadat Nourieh
School of Physics, Engineering and Computer Science, University of Hertfordshire

voltage is around 1260mV which shows better voltage gain for the designed circuit (Figure 3.19). For this circuit, the calculated efficiency is 79.38%.

3.4 Design of Phase Shift Circuit

Today, phase shift circuits are a common part of microwave communication systems and phased array antennas. To attain smaller size, the lumped elements in a low-pass/high-pass or an all-pass topology are often used [8, 42, 98]. It has been found that for large phase shifts, such as 180º, the performance of the circuit is considerably worse than smaller phase shifts when the frequency increases [99]. However, when the order increases, the phase errors and the insertion losses are affected by parasitic elements [100]. The general phase errors are presented in [101- 103] which for 180º phase shifters are between ±2º to ±5º, when the return losses are above 14dB, excluding the effect of the switches. However, one drawback of the distributed networks is the significant area required [42, 104].

3.4.1 180° Phase Shift

In this section, two methods to provide 180°phase difference is presented. In 3.4.1.1, a circuit is designed to produce a signal with phase difference of 180°. In 3.4.1.2, we used transmission lines to make the phase shifter.

3.4.1.1 Phase Shift Circuit of 180° Phase Difference

In this section, a phase shifter based on lumped elements providing 180° phase shift is proposed. At low frequencies, the proposed circuit in [105, 106] is smaller compared to the distributed networks. The series and paralleled *LC* networks are applied to control the phase angle of the insertion phase. Additionally, by linking the series *LC* resonator with shunted parallel *LC* resonators, a bandpass response can be gained. A prototype example with a specific frequency of 915MHz is designed and measured. The measured

Najmehossadat Nourieh
School of Physics, Engineering and Computer Science, University of Hertfordshire

phase shift is around 173° in practical tests (discussed in section 3.8.1) while it is 180° in theory and simulation analyses.

The high pass (HP)/low pass (LP) phase shifter has one arm as a high pass filter (HPF) section and another arm as a low pass filter (LPF) section. These HPF and LPF sections can be implemented as either Pi or T networks [107, 108].

The phase shift is due to the different phase response provided by the high pass and low pass filters. The design of the HPF and LPF networks involves determination of values for the lumped components (the inductor *L* and capacitor *C*). The design was started with the aim to find the ideal component values and later focused on determining the practical component values. This section shows the calculation of ideal values and implementation of these values in the schematic [109- 113].

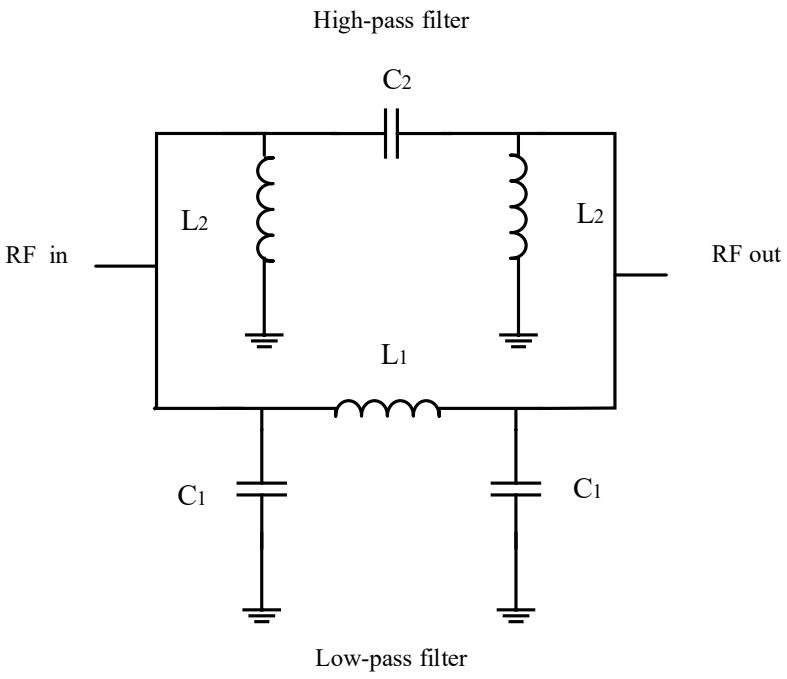

Figure 3.20 The phase shift circuit

Najmehossadat Nourieh
School of Physics, Engineering and Computer Science, University of Hertfordshire

Figure 3.20 shows the low-pass and high-pass circuit schematics. The formulas used for the calculation of *L* and *C* values in this circuit are presented. To calculate the value of capacitors and inductors in the low-pass filter, Eq. (3.7) and Eq. (3.8) must be considered. Here, φ is the desired phase shift in radians, ω is the angular centre frequency in radians/sec and Z_0 is the characteristic impedance of the network (here Z_0 is 50Ω) [114].

$$L_1=\frac{Z_0 \sin\varphi}{\omega} \tag{3.7}$$

$$C_1=\frac{1-\cos\varphi}{\omega Z_0 \sin\varphi} \tag{3.8}$$

It is assumed that if φ is the required phase shift in HPF/LPF phase shift circuits, then HPF needs to provide $\varphi/2$ phase shift and LPF should provide the remained $\varphi/2$ phase shift. Therefore, by shifting the signal from one arm to another (for example HPF to LPF), the signal will have a net phase shift of φ radians.

Considering Eq. (3.7), Eq. (3.8), f=915MHz, $\varphi=\pi/2$ and $Z_0=50\Omega$, in the low pass filter the value of the inductor is L_1=8.6nH and capacitor is C_1= 3.47pF.

A high pass (HP) filter in this network has two inductors and one capacitor connected as shown in Figure 3.19. To calculate the value of components in the low pass filter, Eq. (3.9) and Eq. (3.10) must be considered.

$$L_2=\frac{Z_0 \sin\varphi}{\omega(1-\cos\varphi)} \tag{3.9}$$

$$C_2=\frac{1}{\omega Z_0 \sin\varphi} \tag{3.10}$$

Considering these equations f=915MHz, $\varphi=\pi/2$ and $Z_0=50\Omega$ in a high pass filter, the value estimated for inductor is L_2=8.6nH, while it is C_2=3.47pF for capacitor.

Najmehossadat Nourieh
School of Physics, Engineering and Computer Science, University of Hertfordshire

3.4.1.2 Transmission line

For RF, transmission lines can be used in circuit elements instead of discrete lumped components; For example, the coaxial cable can actually be a circuit element itself. The phase shift is achieved by enhancing the length of the transmission line which induces a delay in the input signal. The length of the transmission line phase shifter is governed by the equation given in Eq. (3.11), where v is velocity of propagation, f (frequency), l (cable length), c (speed of light) and ε (permeability of material). For the coaxial cables that we use, the velocity factor is $2.61*10^8$ and frequency is 915MHz, which gives us the length of 28.5cm. Although, we now know that we need the cable with length of 28.5cm, but we need to consider the connectors as well [44]. Hence, for the exact length of the cable, we need to use VNA (Vector Network Analyser), which will be discussed in section 3.7.

$$v = f.l = c/(\varepsilon)^{-1/2} \tag{3.11}$$

In theory, if we choose the second cable with twice the length of the first cable, we will have 180° phase difference.

By sending the signal in two pre-determined lengths of transmission lines, it is possible to define a specific phase shift of $\Delta\varphi$ at a considered frequency.

$$\Delta\varphi = 2\pi\,(\Delta L/\lambda) \tag{3.12}$$

where ΔL is the difference between the physical lengths of the delay line (L_2) and the reference line (L_1), λ is the wavelength and $\Delta\varphi$ is the phase shift. Phase shifters made by transmission lines are generally used for 90° and 180° phase shifts. Considering Eq. (3.12), when path L_2 is a half wavelength ($\lambda/2$) longer than path L_1, the phase of signal coming through L_2 introduces a phase difference of 180°. So, to get a 180° phase shift the required physical length difference should be $\Delta L = \lambda/2$ [45].

Najmehossadat Nourieh
School of Physics, Engineering and Computer Science, University of Hertfordshire

3.5 Simulation Analyses of 1-Stage and 7-Stage Rectifier with Phase Shifter

In this section, the analyses of the two rectifiers with one and seven stages in simulation are presented. In Figure 3.20 the schematic of simulated 1-stage Dickson rectifier (with diode-connected MOSFET)

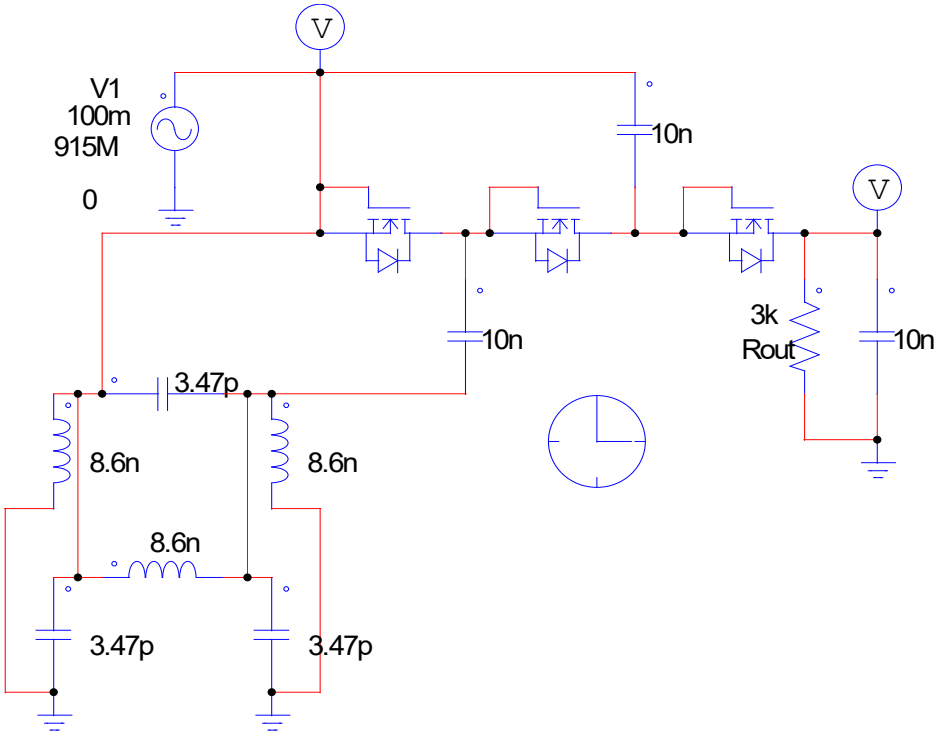

Figure 3.20 Schematic of the combination of phase shift circuit and 1-stage rectifier in PSIM

with phase shifter is shown, while in Figure 3.21 the gained output voltage of 340mV is illustrated. The input voltage is 100mV$_{p\text{-}p}$, frequency is 915MHz, capacitors are 10nF, output resistor is 3kΩ and MOSFETs are modelled by specifications of EPC8008ENGR. The efficiency of this rectifier is 38.5%. In phase shift circuit, the capacitors are 3.47pF and the value of inductors are 8.6nH. In Figure 3.22, the simulated schematic of a 7-stage rectifier with 180° phase shift circuit is presented. For this circuit, the

Najmehossadat Nourieh
School of Physics, Engineering and Computer Science, University of Hertfordshire

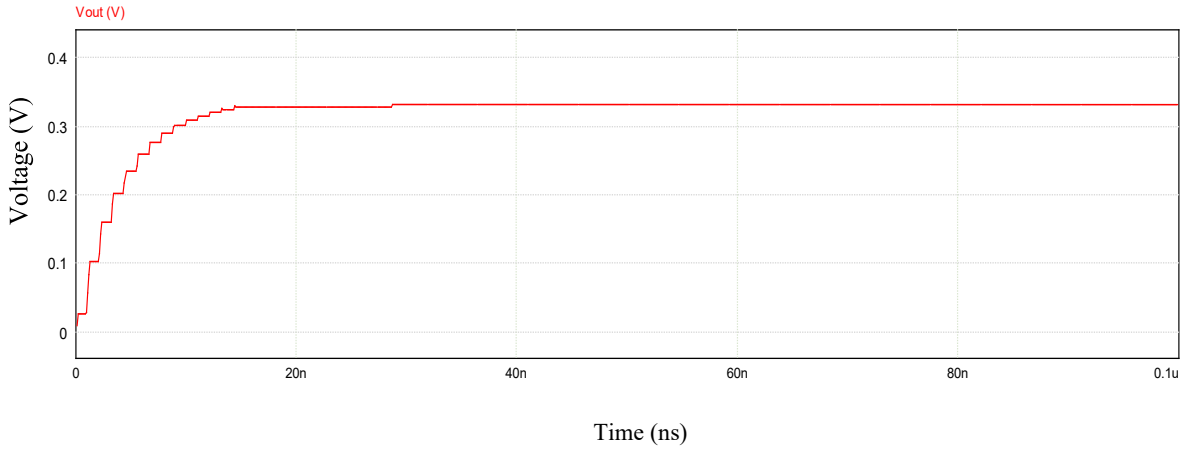

Figure 3.21 The output voltage of combination of phase shift and 1-stage rectifier in PSIM

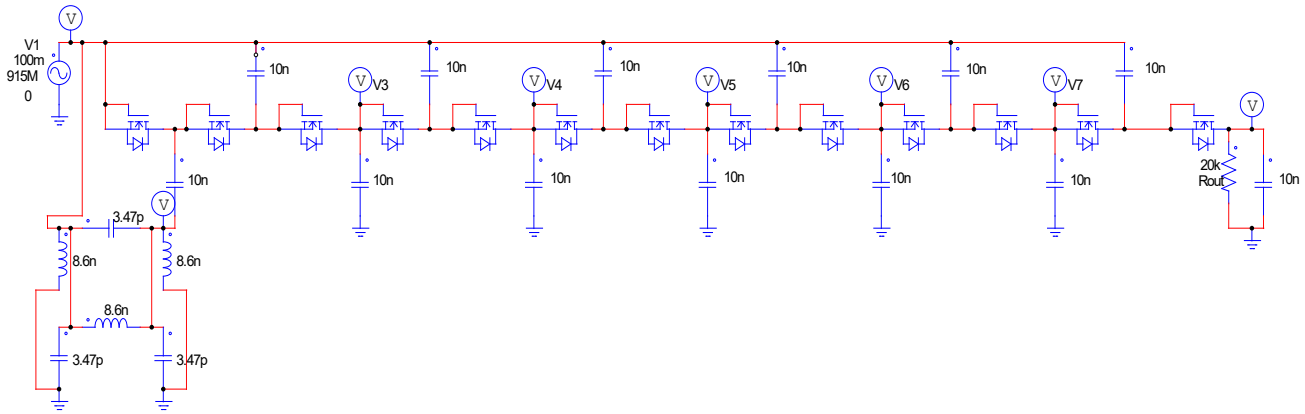

Figure 3.22 The schematic of phase shifter and 7-stage rectifier in PSIM

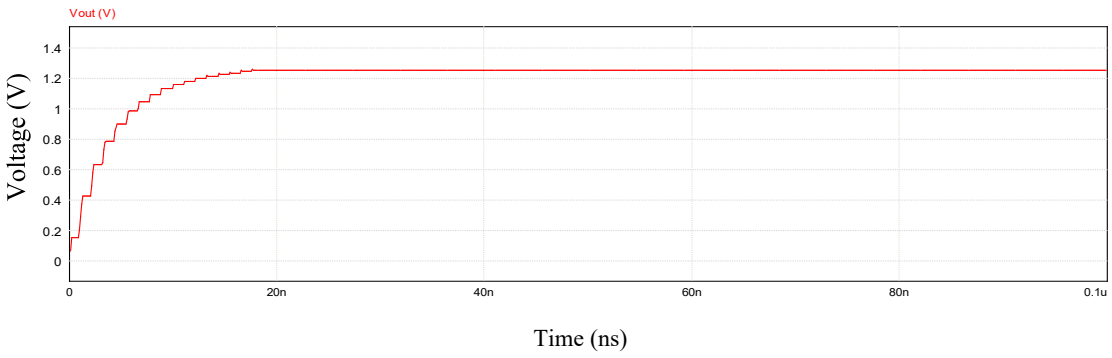

Figure 3.23 The output voltage of phase shifter and 7-stage rectifier in PSIM

output voltage gained in PSIM environment is around 1260mV as shown in Figure .23. For this circuit,

the calculated efficiency is 79.38%, while input voltage is 100mV$_{p-p}$, frequency is 915MHz, capacitors are 10nF, output resistor is 20kΩ and MOSFETs are modelled by specifications of EPC8008ENGR.

3.6 The Effect of Phase Shift Errors on Rectifier Performance

In the simulation process, we also considered the phase shift error effects on the output voltage. Assuming that we use the 1-stage and 7-stage Dickson rectifiers with diodes, the effect of phase error is presented in Figure 3.24, where phase errors between 1% and 11% are simulated.

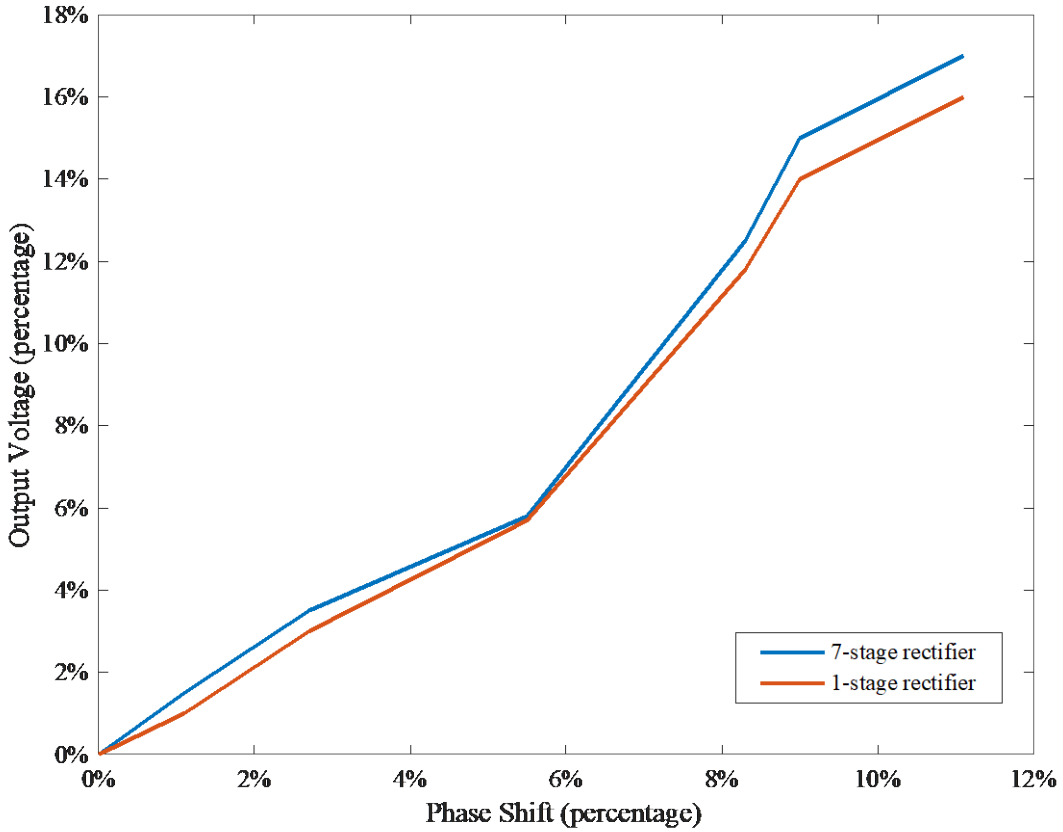

Figure 3.24 The effect of phase shift error on the output voltage of both 1 and 7-stage rectifier with diode for every 2% (in percentage)

In Figure 3.25, the effect of phase shift errors in degrees on output voltage (mV) is shown. As illustrated on the graph, the phase shift errors affect the 7-stage rectifier slightly more when compared to the 1-stage

Najmehossadat Nourieh
School of Physics, Engineering and Computer Science, University of Hertfordshire

circuit. For a 1% phase error, the one stage rectifier experienced a 1% difference in output voltage, while it is around 1.3% for 7-stage rectifier. The larger phase errors considered the more deviation in output voltage we experienced. For phase error of 11%, the 1-stage rectifier shows a 16% error in output voltage, while it is nearly 17.1% for the 7-stage circuit. Considering Figure 3.25, for phase difference of 178°, 175° and 170°, in 1/7-stage rectifiers, the output voltage is 316.8mV/1182mV, 310.4mV/1158mV and 298.3mV/1134mV respectively. For phase difference of 165°, 162° and 160°, the output voltage of 1/7-stage is 282.3mV/1050mV, 275.2mV/1020mV and 268.8mV/996mV respectively.

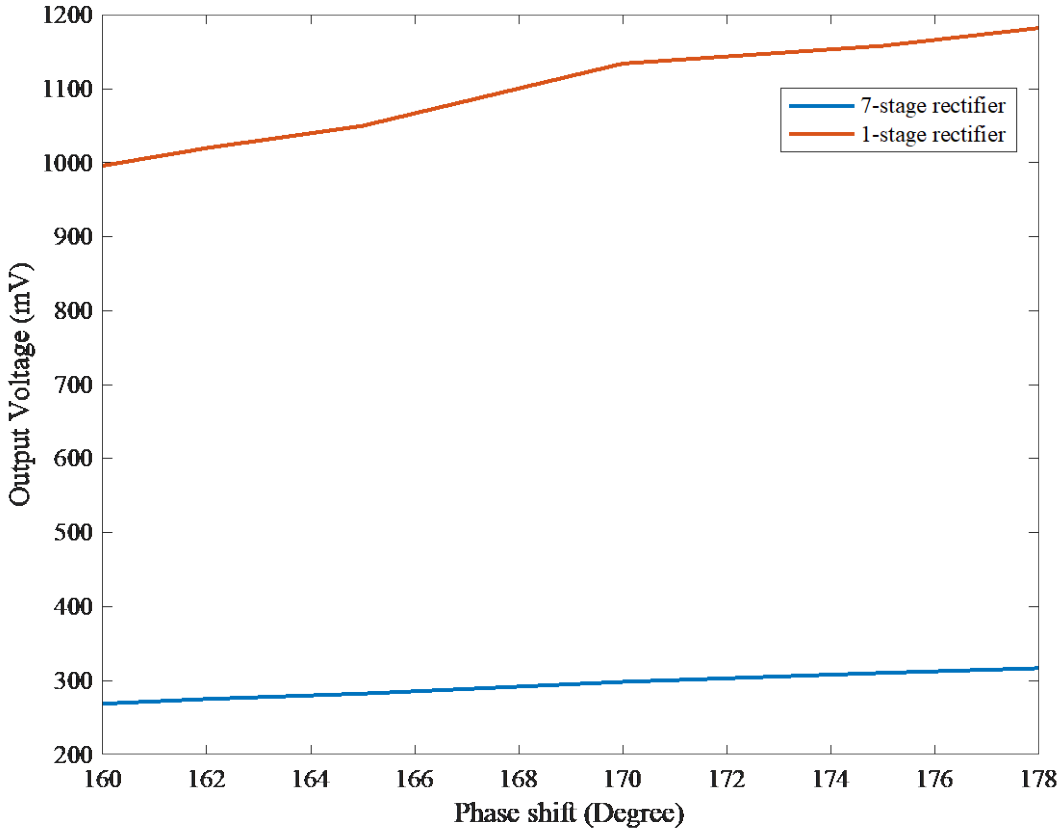

Figure 3.25 The effect of phase shift error (in degree) on output voltage (mV)

Najmehossadat Nourieh
School of Physics, Engineering and Computer Science, University of Hertfordshire

3.7 Implementation and Practical Results of 1-Stage and 7-Stage Rectifier with Phase Shifter

In this section, the process of testing both the 1-stage and 7-stage rectifiers, the difference between phase shifters, and the practical results of the combination of chosen circuits are presented.

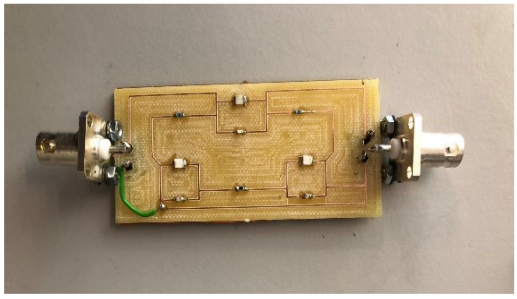

Figure 3.26 The phase shift circuit with BNC connector

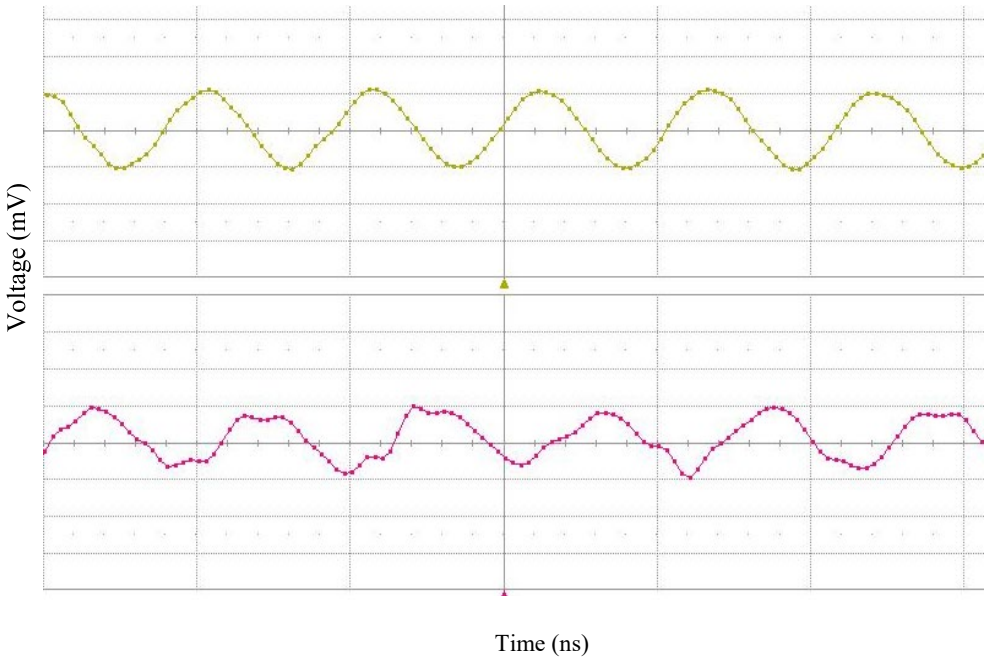

Figure 3.27 The waveform generated by signal generator (first waveform), the output of the phase shift circuit (second waveform), 50mV/div and 1ns/div

Najmehossadat Nourieh
School of Physics, Engineering and Computer Science, University of Hertfordshire

3.7.1 Choose the Best Phase Shifter

To test the phase shift circuit, connectors and cables play key roles to gain the proper output of 180° from the circuit. In this subsection, we will compare the different outputs attained from the same phase shifter with different cables and connectors.

In Figure 3.26, the phase shift circuit with BNC terminals are shown which gives us the output signals given in Figure 3.27 (The frequency is considered to be 915MHz). As it is illustrated in Figure 3.27, the output signal is shifted 180° compared to the input signal, but there is a significant disturbance in the

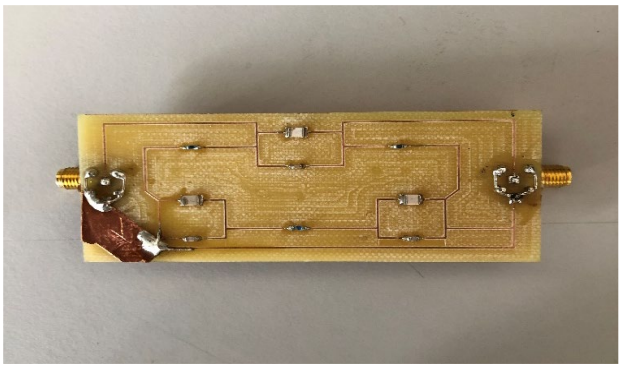

(a)

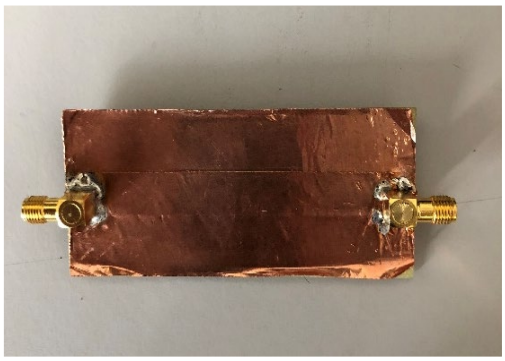

(b)

Figure 3.28 The phase shift circuit with SMA connector, a. Front side and b. Back side

Najmehossadat Nourieh
School of Physics, Engineering and Computer Science, University of Hertfordshire

output waveform (These signals are shown in the oscilloscope). Furthermore, the gained loss is also considerable as the input signal has a *Vp-p* of 100mV while it is nearly about 30mV for the output of phase shifter, showing great loss within cables, circuits and connectors (All of the output signals from the signal generator came from a T- junction).

To reduce the loss and obtain proper signals, we replaced the BNC connectors with SMA ones (Figure 3.28).

In Figure 3.29, the output signal produced by the phase shifter with SMA connectors illustrated in Figure 3.28 is shown which clearly gives a smoother output signal with notably less losses (a T-junction has been used to gives us two outputs from the signal generator). Although the output signal is smoother, the phase shift is about 165°, measured by oscilloscope. This result encouraged us to consider changing the cable to obtain better performance. By testing the designed phase shift circuit using an SMA connector on the VNA device, we see that the measured phase shift is 168.78° at 915MHz illustrated in Figure 3.30.

To obtain closer practical results to simulation, we made another phase shifter PCB board with shorter and thicker tracks which can improve the performance of the phase shift circuit as shown in Figure 3.31. The result of testing this board is presented in Figure 3.32, where the approximate phase shifting at 915MHz, as VNA shows, is improved to be around 173° .

Najmehossadat Nourieh
School of Physics, Engineering and Computer Science, University of Hertfordshire

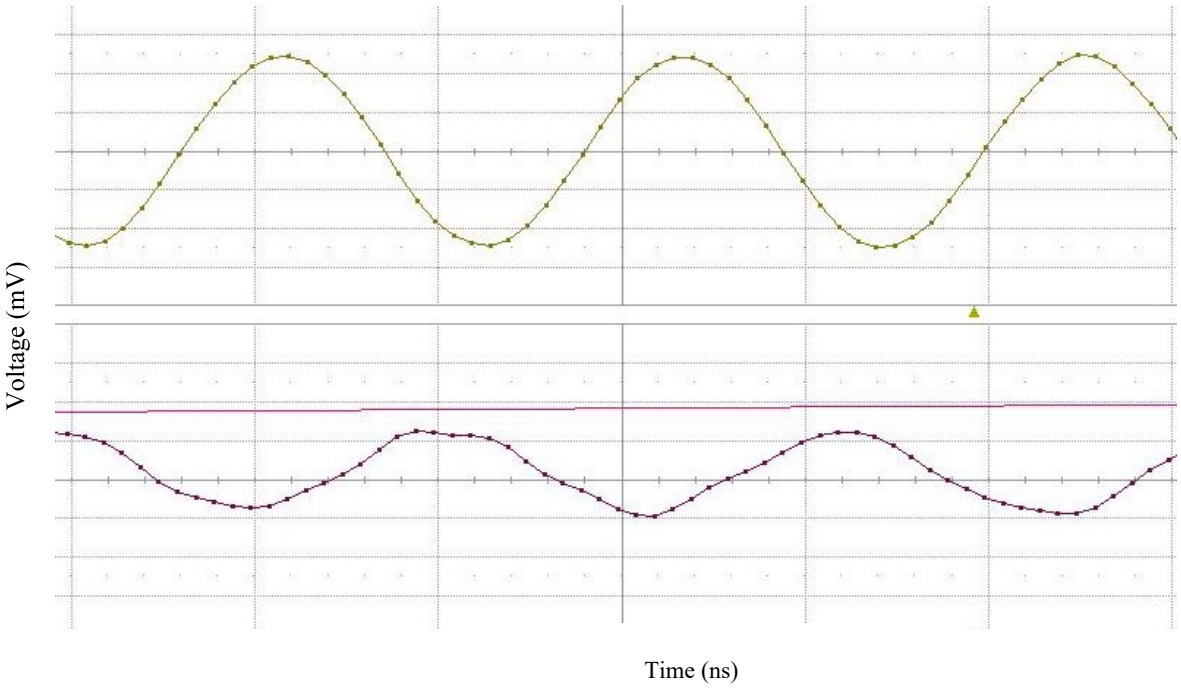

Figure 3.29 The output voltage (V_1) of signal generator (first waveform), the output voltage (V_2) of the phase shift circuit with SMA connector (secone waveform), V_1: 20mV/div, V_2: 50mV/div, Time: 1ns/div

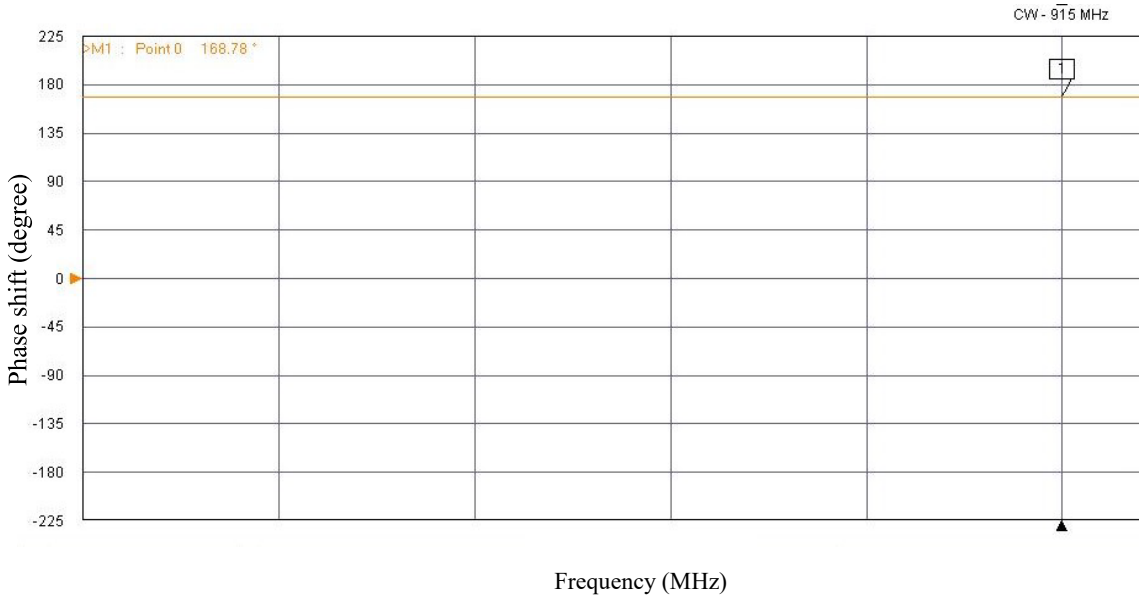

Figure 3.30 The output phase of the phase shift circuit with SMA connector measured by VNA

Najmehossadat Nourieh
School of Physics, Engineering and Computer Science, University of Hertfordshire

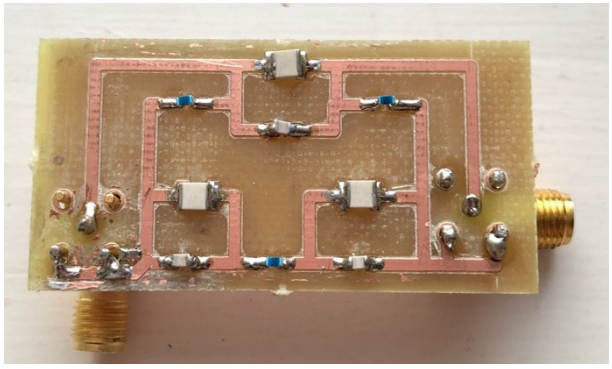

(a)

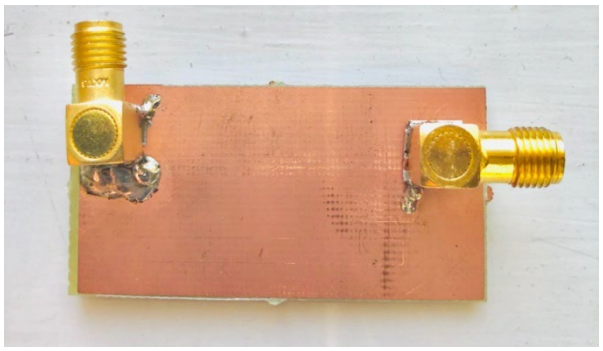

(b)

Figure 3.31 The PCB board of phase shifter with smaller package, (a) Front, (b) Back

The laboratory environment to test the PCB board of the phase shifter is also shown in Figure 3.33. As different parameters affect the phase shift process, including the length and thickness of tracks on the PCB board, we decided to also prepare cables that can provide 180° phase shift. The series of a cable with the size of 12.6cm with two other 14.8cm cables, provide the phase shift of 29.05°, measured by the VNA, as shown in Figure 3.34. Also, in Figure 3.35, the laboratory environment for measuring the phase shift of these cables is illustrated.

Najmehossadat Nourieh
School of Physics, Engineering and Computer Science, University of Hertfordshire

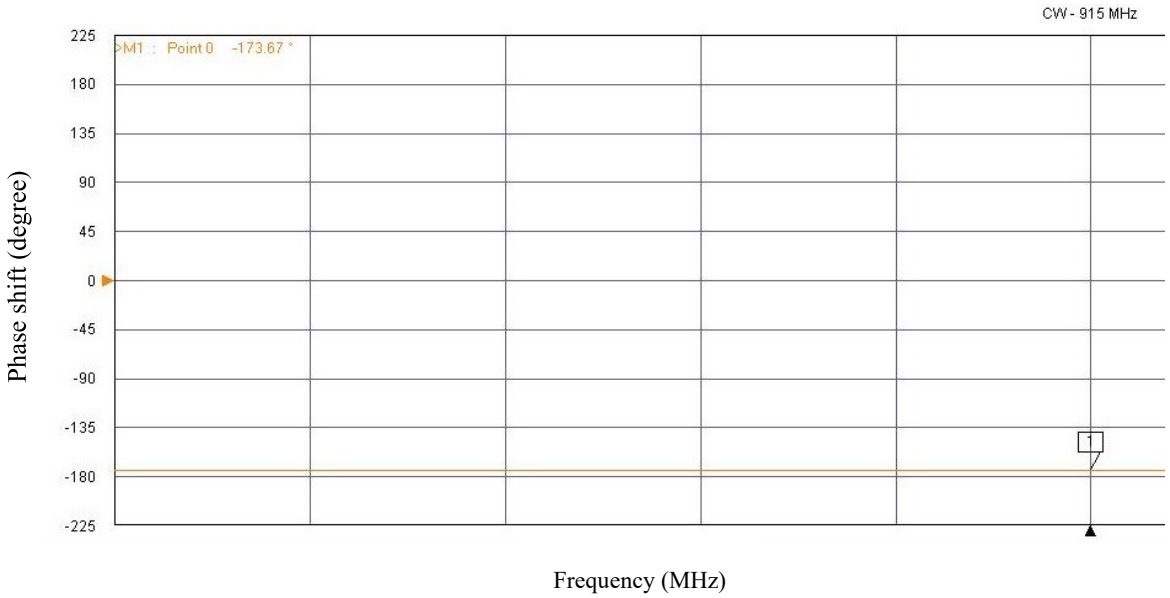

Figure 3.32 The output phase of the new phase shifter PCB board on VNA

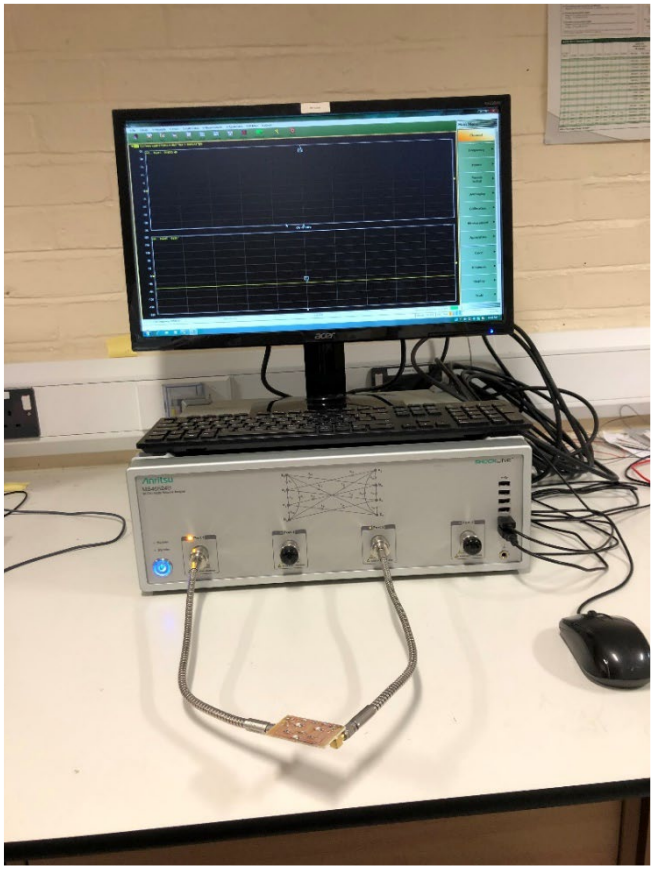

Figure 3.33 The laboratory environment to test phase shifter PCBs with VNA.

Najmehossadat Nourieh
School of Physics, Engineering and Computer Science, University of Hertfordshire

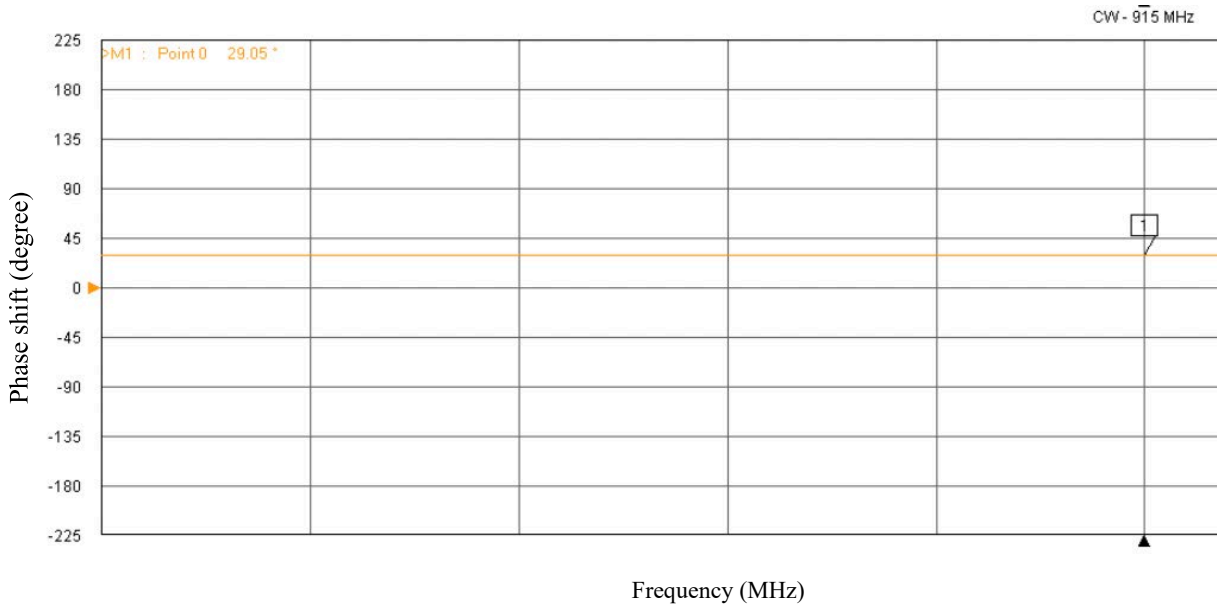

Figure 3.34 The phase shift of 29.05° of three cables of one 12.6cm and two 14.8cm.

We prepared another cable of 29.8cm which provides -151.76° phase shift (Figure 3.36) which together with the combination of three cables, shows 179.81° phase shift (very close to the desired phase shift of 180°). For better understanding, the measurement of the 14.8cm cable on VNA is illustrated in Figure 3.36, while in Figure 3.37, the laboratory environment for testing the cables is presented. Then, as shown in Figure 3.38, at the output of the signal generator, we used a splitter to produce two signals with the same amplitude. One of the outputs of the splitter is connected to the 29.8cm cable and the other one is linked with the integration of three cables.

3.7.2 Implementation and Measurement Results of Proposed Rectifiers

In previous sections, we have proposed new methods to gain the desired voltage in the output stage of the RF to DC system. One of the main blocks of this system is the rectifier which is tested practically in the laboratory. At the first stage, we tested the proposed 1-stage rectifier with two input signals (with 180 ° phase difference) composed of Schottky diodes and 10nF capacitors. The rectifier is tested with

Najmehossadat Nourieh
School of Physics, Engineering and Computer Science, University of Hertfordshire

different input power ranges between -10dBm and 2dBm, which is the available range on signal

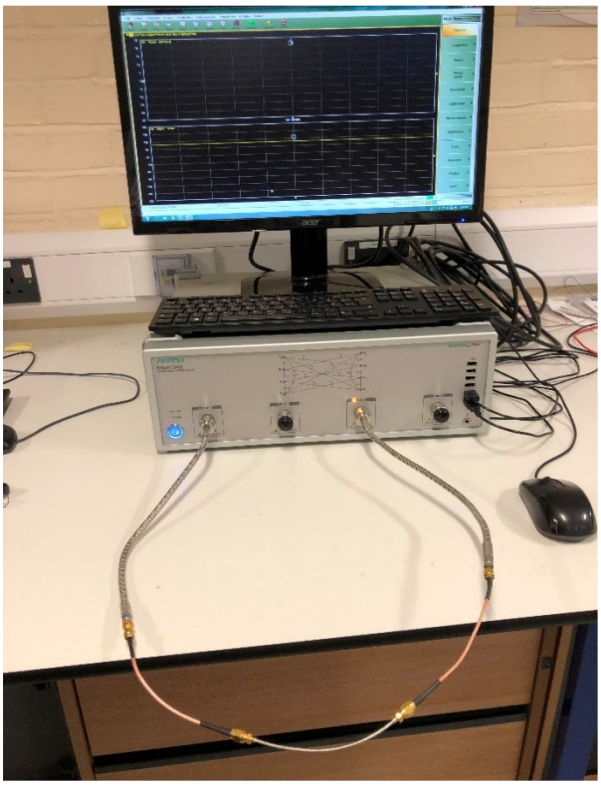

Figure 3.35 The testing equipment for the integration of three cables.

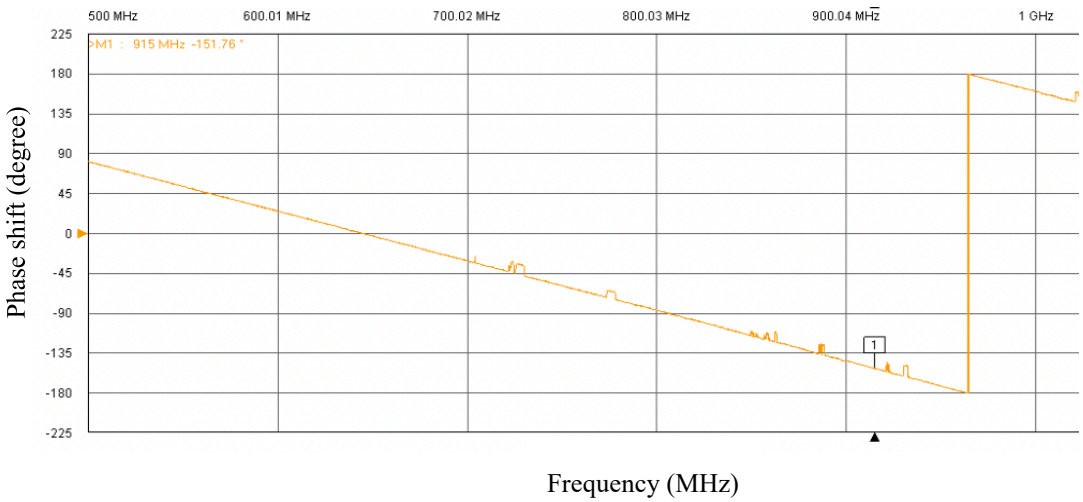

Figure 3.36 The phase shift of -151.76° of cable 29.8cm.

Najmehossadat Nourieh
School of Physics, Engineering and Computer Science, University of Hertfordshire

generator.

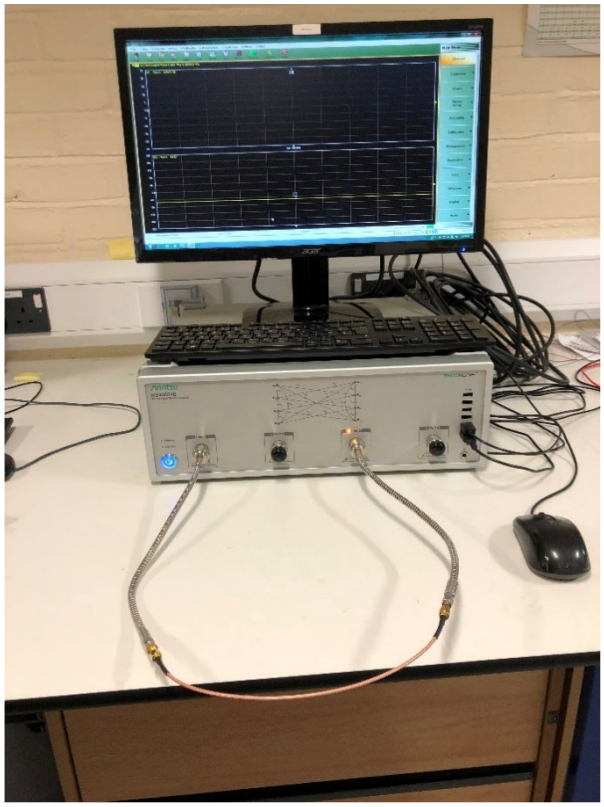

Figure 3.37 The testing equipment for the 29.8 cm cable.

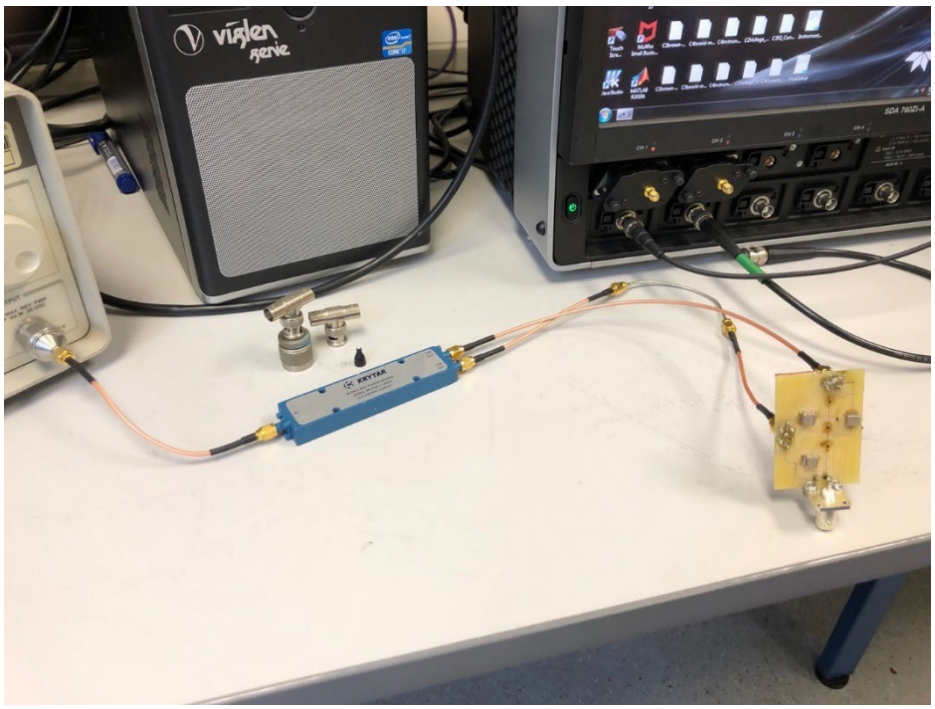

Figure 3.38 The picture of splitter with two outputs connected to the signal generator.

Najmehossadat Nourieh
School of Physics, Engineering and Computer Science, University of Hertfordshire

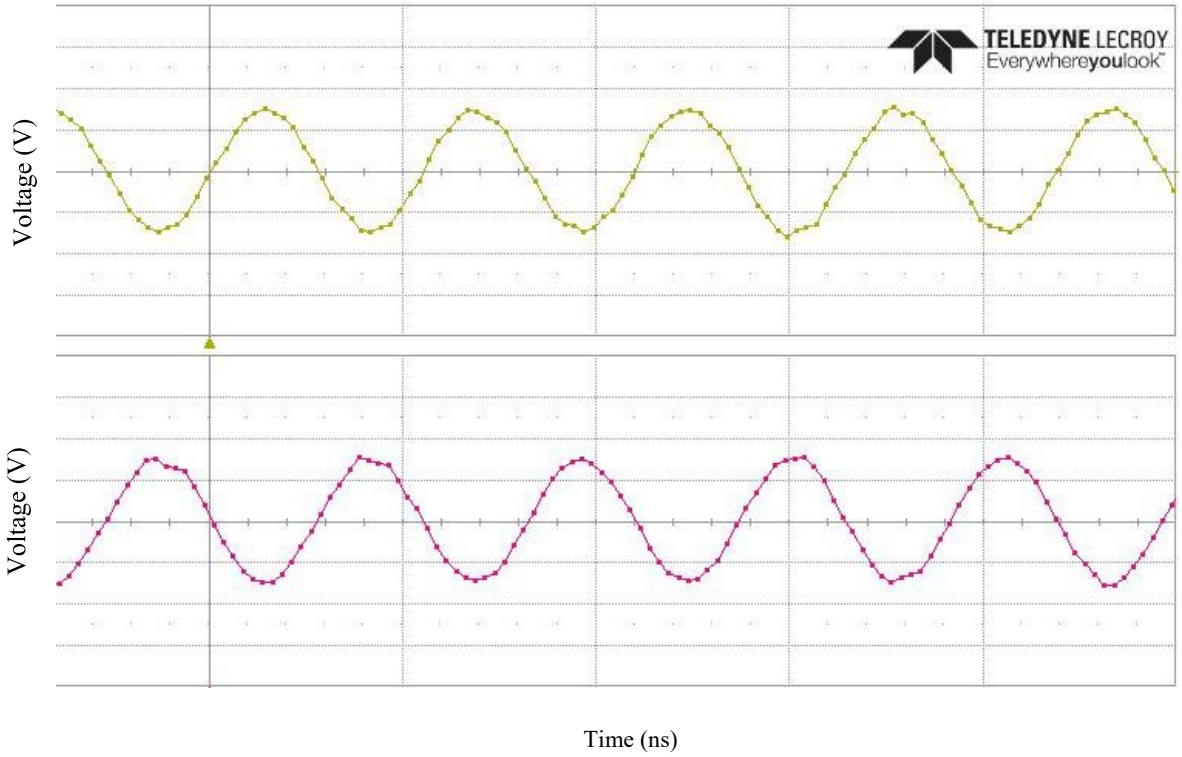

Figure 3.39 The two inputs of rectifier with 179.8 degrees phase shift (50mV/div and 1ns/div).

In Figure 3.39, two input signals of rectifier are measured by the oscilloscope, as it is clear from this figure, the phase difference between two inputs is 179.8° . The output of the rectifier for the input of -10dBm is shown in Figure 3.40, which is about 320mV. The components that we used in this circuit are Schottky diodes (SMS7630-079LF), 10nF capacitors, 200nH inductor (which is in parallel with the input source to make DC path) and output resistor of 3kΩ. In Figure 3.41, the schematic of the 1-stage rectifier is shown, where point A is defined, which we further use to show the voltage of this point compared with the output voltage for the range of input powers ranging from -10dBm to 2dBm. In Figure 3.42, the PCB

Najmehossadat Nourieh
School of Physics, Engineering and Computer Science, University of Hertfordshire

board of 1-stage rectifier used to test in the laboratory is presented, where a SMA connector is used to see the DC output signal on the oscilloscope.

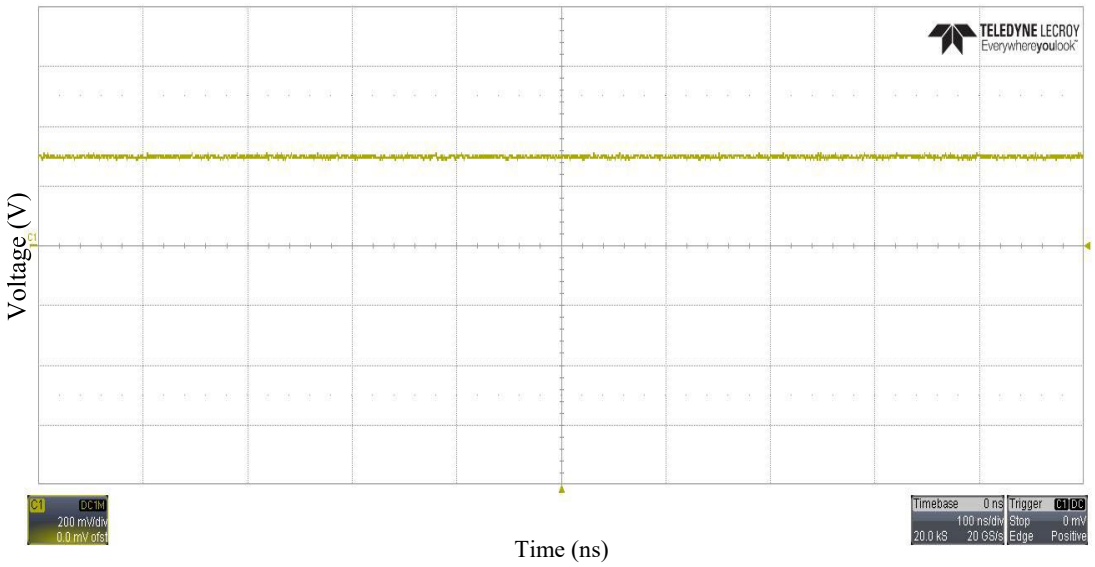

Figure 3.40 The output voltage of rectifier (with phase shifter) shown 320mV (200mV/div and 100ns/div).

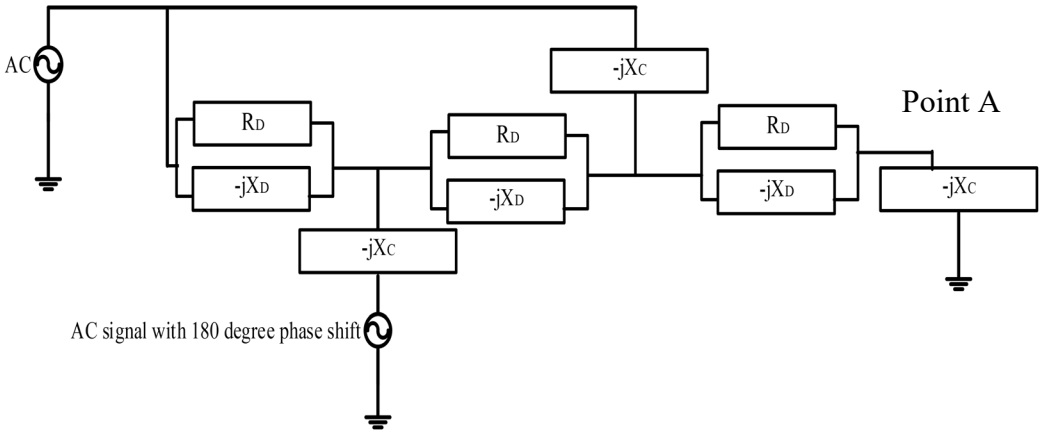

Figure 3.41 The schematic of the rectifier where point A is defined.

Najmehossadat Nourieh
School of Physics, Engineering and Computer Science, University of Hertfordshire

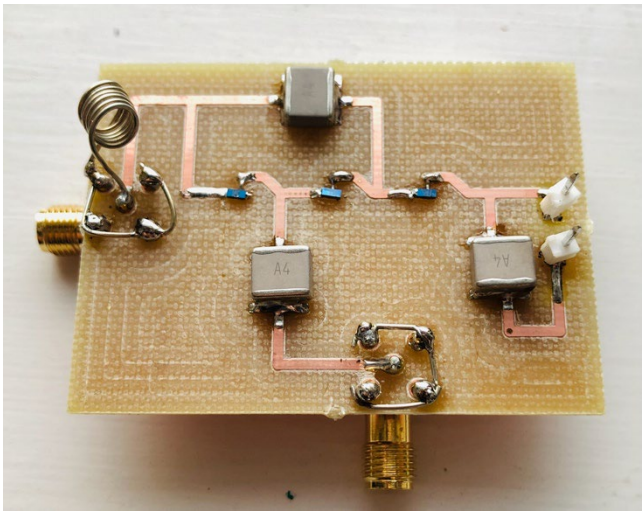

Figure 3.42 The PCB board of the designed 1-stage rectifier.

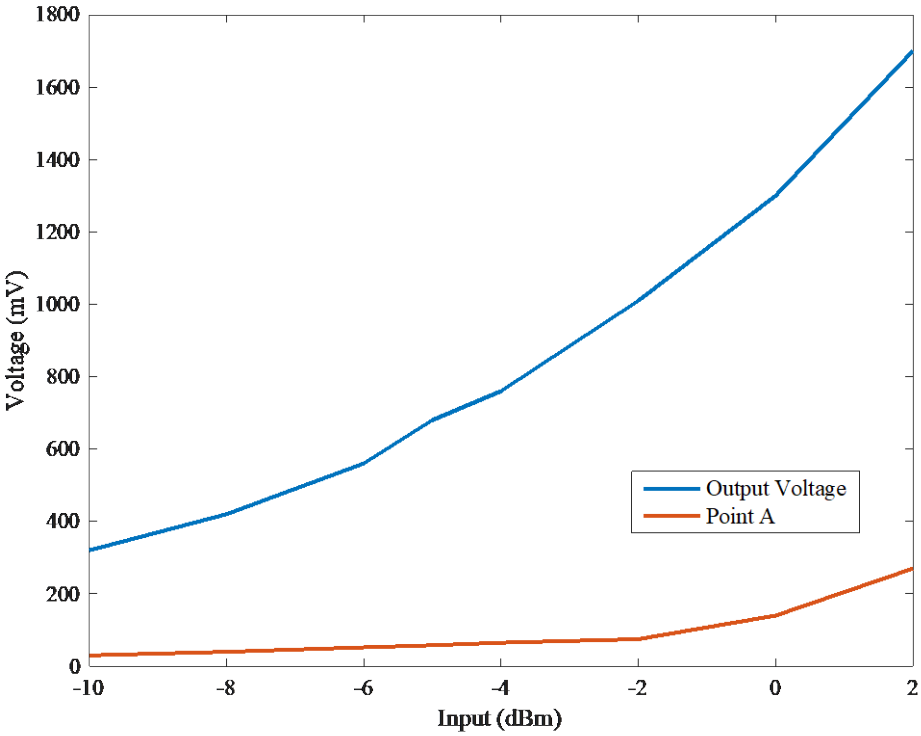

Figure 3.43 The output of 1-stage rectifier (with phase shifter), where the gained voltages of point A and output are shown for input range of -10dBm to 2dBm plotted in MATLAB.

Najmehossadat Nourieh
School of Physics, Engineering and Computer Science, University of Hertfordshire

TABLE 3.1 PARAMETERS OF THE PROPOSED RECTIFIERS

	1-stage rectifier	7-stage rectifier
Schottky diode	SMS7630-079LF	SMS7630-079LF
Capacitor	10nF	10nF
Input voltage	From -10dBm to 2dBm	From -10dBm to -6dBm
Output voltage	From 318mV to 1700mV	From 1220mV to 1550mV
Output resistor	3kΩ	20kΩ
Frequency	915MHz	915MHz

In Figure 3.43, the practical gained voltages at the output and point A for the range of input powers from -10dBm to 2dBm are plotted by Curve Fitting in MATLAB, where for the input signals of -10dBm, -8dBm, -6dBm and -4dBm the output is 318mV, 420mV, 560mV and 760mV respectively, as well as 1010mV, 1300mV and 1700mV for -2dBm, 0dBm and 2dBm in turn. Furthermore, the red graph illustrated with diamond points is plotted to show the voltages of point A in the range of inputs where

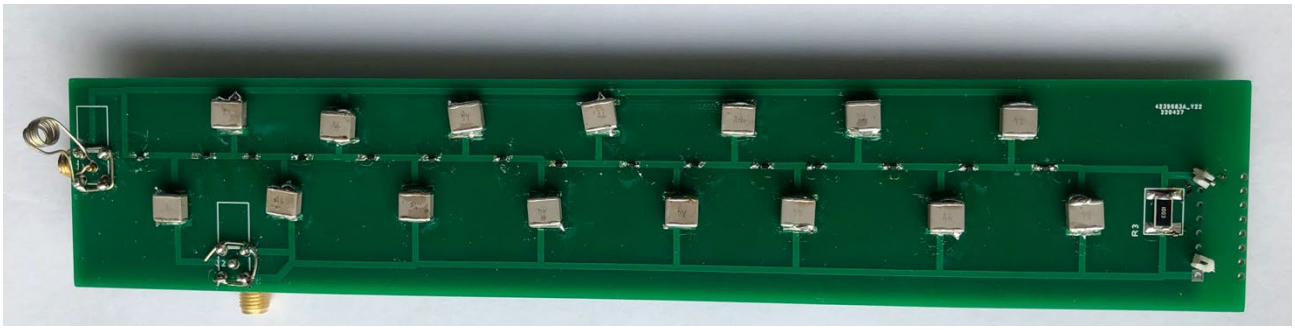

Figure 3.44 The PCB of the 7-stage rectifier prototype

Najmehossadat Nourieh
School of Physics, Engineering and Computer Science, University of Hertfordshire

30mV, 40mV, 52mV and 65mV were measured correspondingly for -10dBm, -8dBm, -6dBm and -4dBm. In addition, for input of -2dBm, 0dBm and 2dBm, the voltages of 75mV, 140mV and 270mV are obtained.

Following the tested 1-stage rectifier, the implementation and the practical results of the 7-stage rectifier were analysed. As shown in Figure 3.44, a PCB board of the proposed 7-stage rectifier with two inputs with 180° phase difference composed of Schottky diodes and 10nF capacitors, is manufactured. As shown in Figure 3.45, we tested the rectifier for input power of -10dBm, -8dBm and -6dBm; which are the safe available input power for Schottky diodes (Note: diodes can probably be damaged in higher

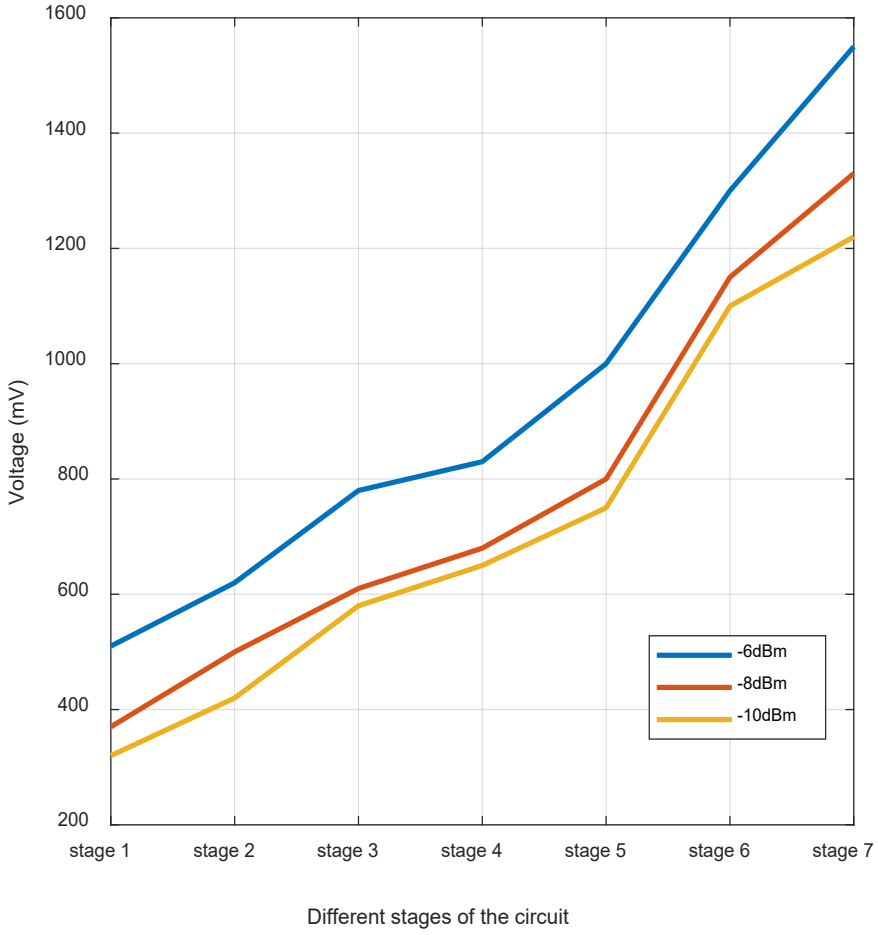

Figure 3.45 The output voltage of 7-stage rectifier (with phase shifter)

Najmehossadat Nourieh
School of Physics, Engineering and Computer Science, University of Hertfordshire

voltages). In this figure, we measured the voltages of different stages on the board, the numbers 1 to 7 refer to stages 1 to 7 respectively. The blue graph presents the outputs for the inputs of -6dBm while the red and yellow graphs show the results for -8dBm and -10dBm. At the main output of the rectifier that is at the end of the 7th stage, for input powers of -10dBm and -8dBm, we gained 1220mV and 1330mV, whereas 1550mV was attained for -6dBm. In addition, the efficiency of this circuit, considering the output resistor of 20kΩ, for -10dBm is 74% while it is 56% and 47% for -8dBm and -6dBm.

In Figure 3.46 to Figure 3.48, the gained outputs of the circuit for different inputs measured on the oscilloscope are shown. Furthermore, in Figure 3.49, a plotted graph for practical output results of 7-stage rectifier via different inputs is given.

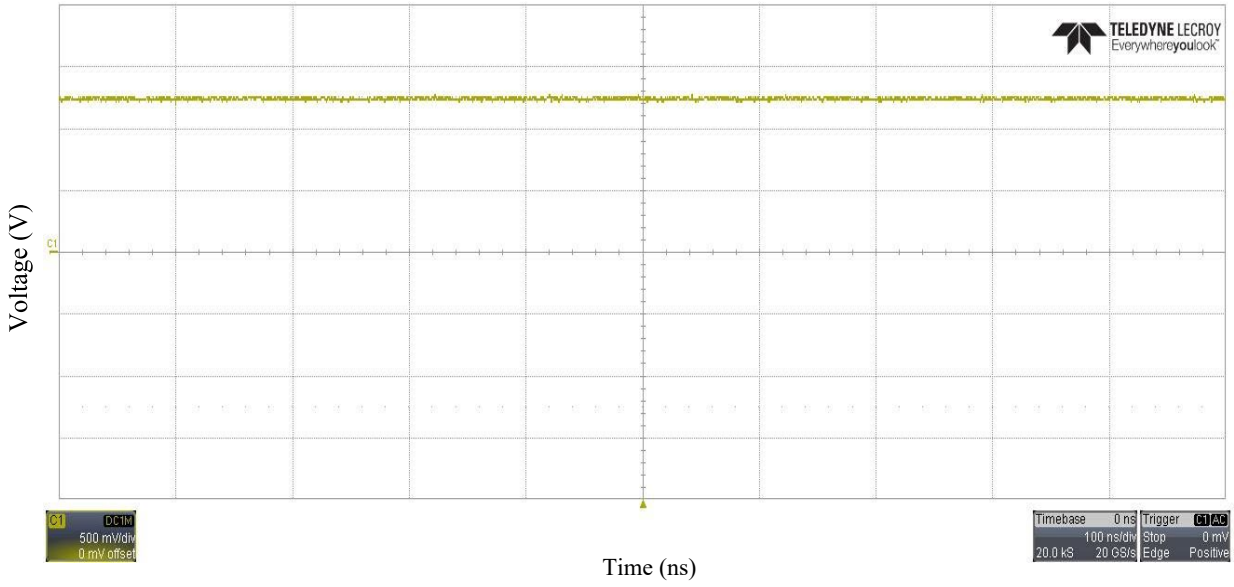

Figure 3.46 The output of the 7-stage rectifier (with phase shifter) for the input of -10dBm (500mV/div and 1ns/div).

Najmehossadat Nourieh
School of Physics, Engineering and Computer Science, University of Hertfordshire

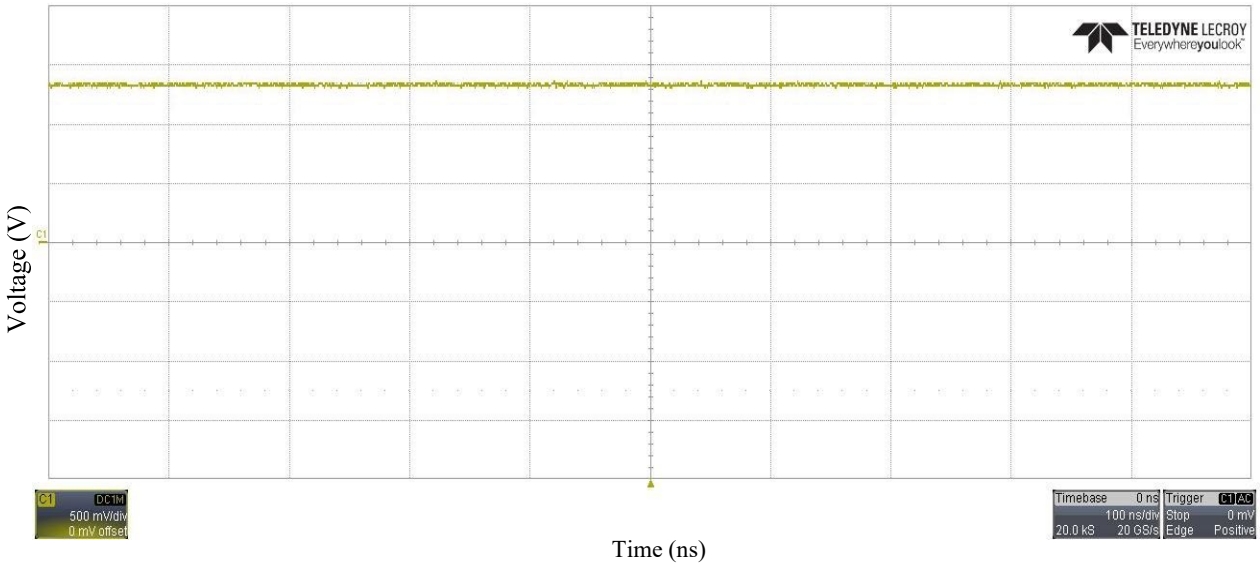

Figure 3.47 The output of the 7-stage rectifier (with phase shifter) for the input of -8dBm (500mV/div and 1ns/div).

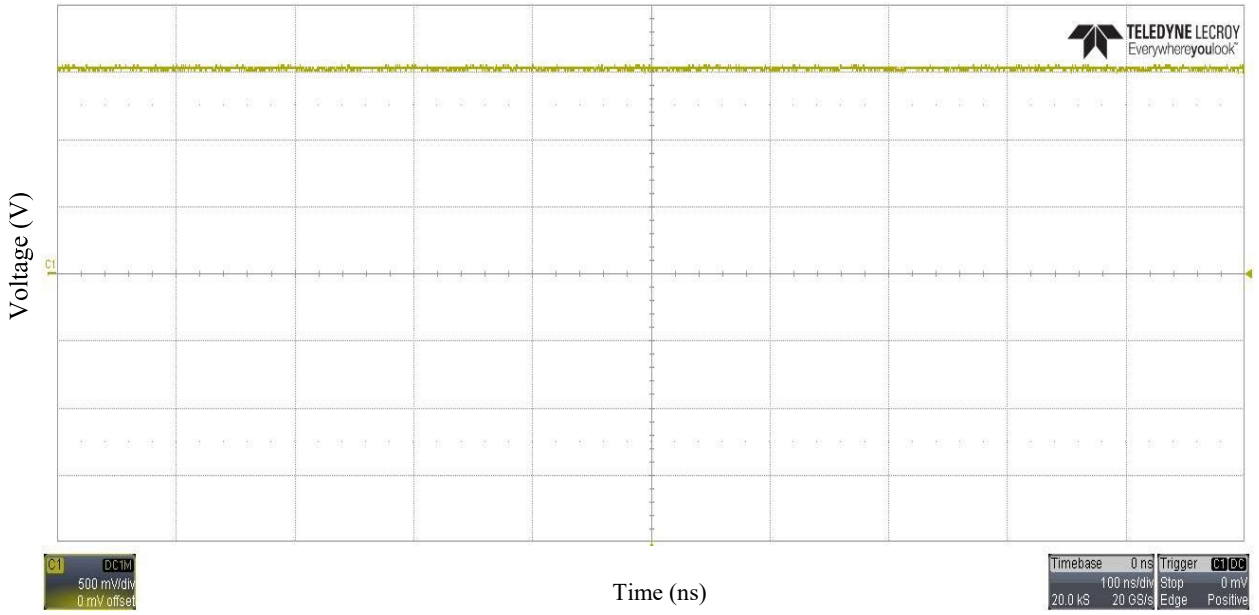

Figure 3.48 The output of the 7-stage rectifier (with phase shifter) for the input of -6dBm (500mV/div and 1ns/div).

Najmehossadat Nourieh
School of Physics, Engineering and Computer Science, University of Hertfordshire

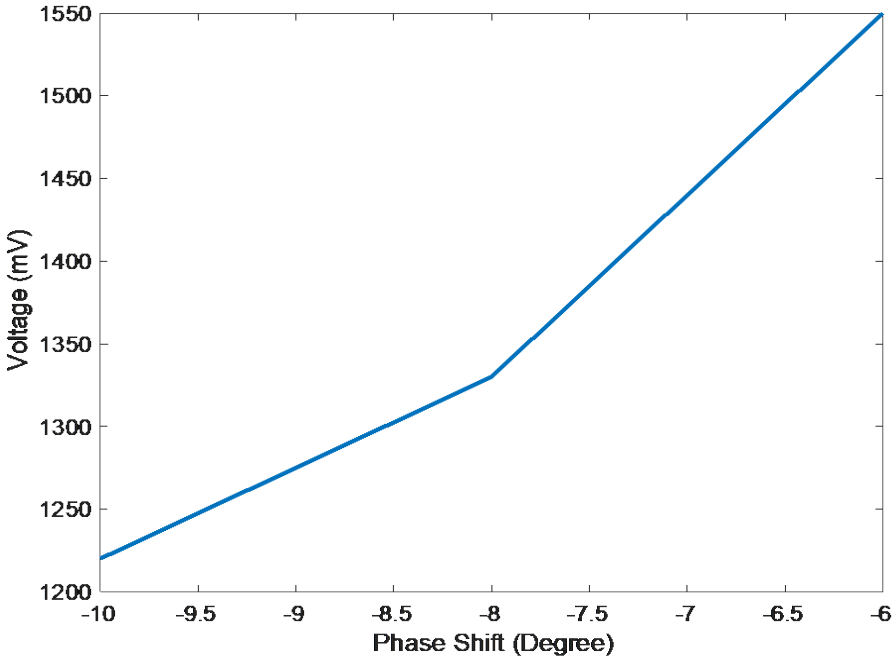

Figure 3.49 The practical results for output voltage vs different input signals.

3.7.3 RF Energy Harvesting Practical Test

After testing the proposed rectifiers with the signals produces by signal generator, we connect the designed circuits to an antenna to investigate the function of circuits with ambient signals. In this regard, the antenna that is used is Tl.92.2113.

As we wanted to see the output of antenna and circuits in the laboratory, we were limited to use the RFEH in the certain area of laboratory. So, the highest power that we could gain in the environment of laboratory is -15dBm with frequency of 916.5MHz (Note: if we test the RFEH closer to signal source such as Wi-Fi source or telecommunication tower or in another city/country, the signal power can be varied to be extremely more powerful or drastically weaker).

Najmehossadat Nourieh
School of Physics, Engineering and Computer Science, University of Hertfordshire

In Figure 3.50, the testing boards are shown, where the antenna is connected to IMN, phase shifter and rectifier. As we need to match the impedance of the circuit to antenna, we need to use the impedance matching network. The design of the IMN is explained in Appendix 1.

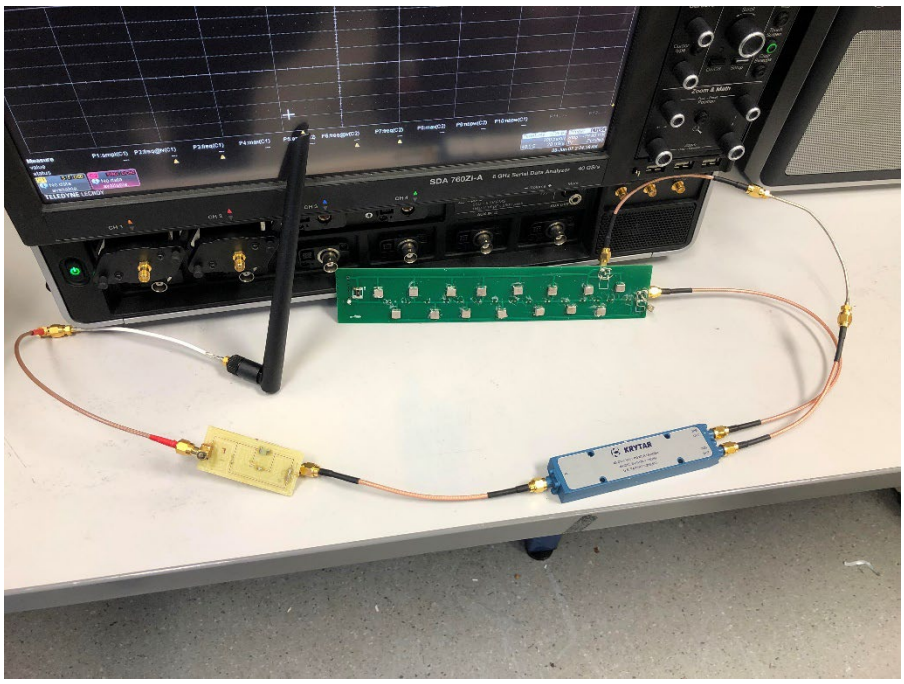

Figure 3.50 The circuit combination in the laboratory with an antenna

In Figure 3.51, the signal harvested from antenna is shown which has -15dbm power, 78mV_{p-p} voltage and its frequency is 916.5MHz (Note: This signal is the most powerful that we could get in the specific environment of laboratory).

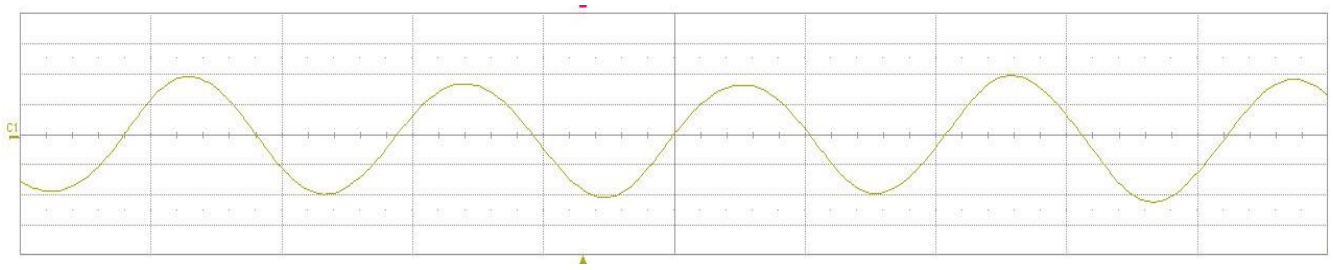

Figure 3.51 The signal harvested by the antenna (20mV/div and 500ps/div)

Najmehossadat Nourieh
School of Physics, Engineering and Computer Science, University of Hertfordshire

By testing the 7-stage circuit for the achieved signal from antenna, the output voltage is gained as 858mV, where the output load is 32K and the efficiency is obtained 69%. As the input signal is weaker with lower voltage, the output voltage is also lower, but the efficiency is still remained high. Figure 3.52 shows the output voltage of 858mV.

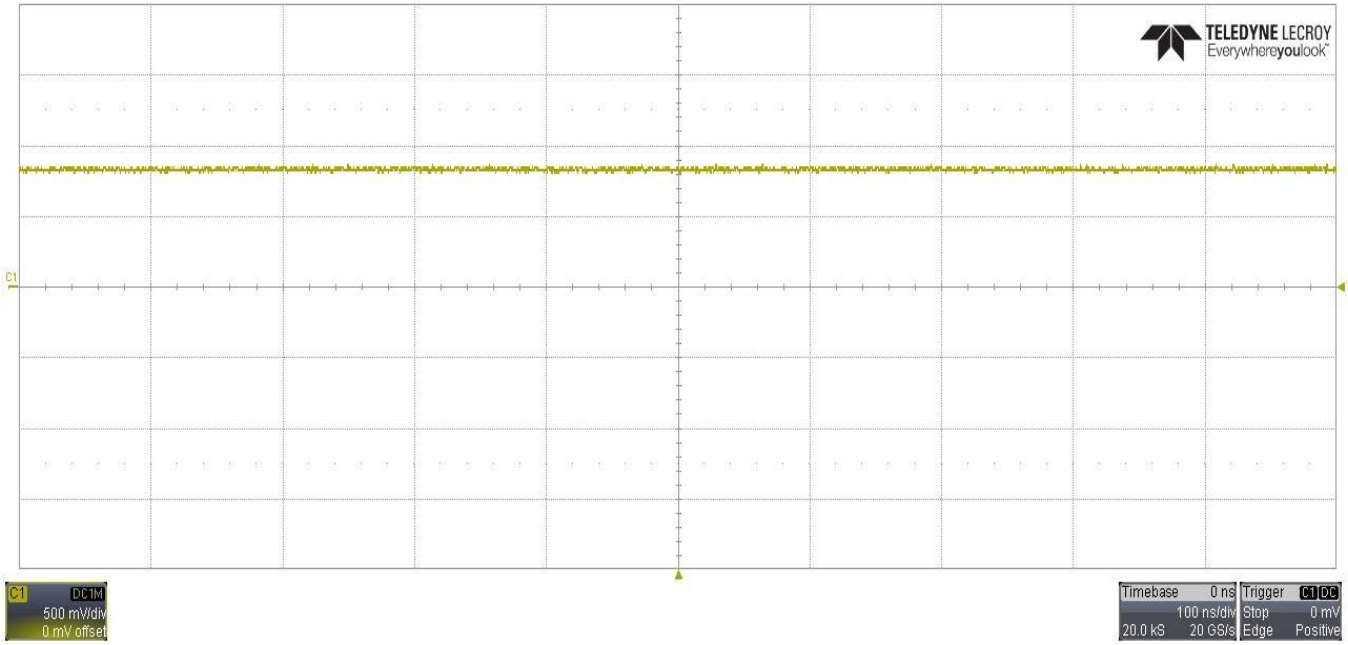

Figure 3.51 The output voltage of proposed circuit with antenna (500mV/div and 100ns/div)

Najmehossadat Nourieh
School of Physics, Engineering and Computer Science, University of Hertfordshire

3.7.4. Comparison Analysis

In Table 3.2 a comparison between the proposed rectifier of 7-stage and other works is presented. In this table, the input power, frequency and output voltage of [115, 116] and [118] are very close to the proposed work, while the efficiency of our circuit is higher than the other three works. Although the work presented in [117] covers nearly twice the frequency than our circuit, it has poor efficiency. Comparing the given two works in [120] and [121] with our circuit, the applied frequency is nearly same as the proposed circuits in this thesis, but for greater input power of 0dBm, the output voltage and the efficiency are lower in [121] while for lower input power of -15dBm, [120] shows the efficiency of only 39%. In [119], for the input power of 1dBm, the efficiency is 47% when frequency is 2.45GHz. Furthermore, [32] presents a circuit which is capable of working with very low input power of -30dBm, but it gains very poor

TABLE 3.2
COMPARISON OF THE MODIFIED 7-STAGE RECTIFIER AND OTHER WORKS

References	Input Power	Output Voltage	Efficiency	Rout	Frequency
[115]	-10dBm	1.17V	69%	13kOhm	937MHz
[116]	-5dBm	1.41V	63%	10kOhm	915MHz
[117]	-10dBm	not defined	30%	not de-fined	1.84GHz
[118]	-10dBm	5.7V	33%	1MOhm	902MHz
[119]	1dBm	1.71V	47%	5kOhm	902MHz
[120]	-15dBm	3.32V	39%	1MOhm	900MHz
[121]	0dBm	3.32V	48.19%	23kOhm	900MHz
[32]	-30dBm	0.164V	10%	300kOhm	2.4GHz
This Work	-10dBm	1.22V	74.4%	20kOhm	915MHz

Najmehossadat Nourieh
School of Physics, Engineering and Computer Science, University of Hertfordshire

efficiency of 10% in frequency of 2.4GHz. Concluding all, it is shown that the proposed rectifier has gained the best performance compared to other works.

3.8 Conclusion

Radio frequency energy harvesting systems experience a fast development because of the increasing number of transmitter sources and range of applications. This chapter shows a novel circuit for the voltage multiplier/rectifier at the frequency of 915MHz. The suggested circuit proposes a new method of deriving output characteristics of the rectification circuit in terms of two main factors, voltage and efficiency. The design consists of different stages of Dickson voltage multiplier rectifier. In this chapter, phase shifters and different Dickson rectifiers with two input signals in one and seven stages were discussed theoretically followed by simulation and practical results. In this chapter the prototype of 1-stage rectifier is presented where the input voltage is between -10dBm and 2dBm and the output voltage is gained from 318mV to 1700mV. Also, the prototype of 7-stage rectifier is presented where the input voltage is -10dBm, -8dBm and -6dBm and the output voltage is gained 1220mV, 1330mV and 1550mV.

Najmehossadat Nourieh
School of Physics, Engineering and Computer Science, University of Hertfordshire

4 The High Voltage Gain Resonant Zero-voltage Switching DC to DC Converters

Switched-mode power supplies can be applied to various applications, including DC to DC converters. Usually, although a DC power supply such as a battery might be available, it is possible that the converted output voltage is not convenient for the application being supplied. For instance, the motors used in driving electric automobiles require high voltages, in the range of 500V, which cannot be supplied by an individual battery. Even if a series of batteries were applied, the extra space and weight taking up would be significantly larger to be practically efficient. A solution to this problem is to boost the available DC voltage by a DC to DC step-up converter to meet the required level of voltages [122- 124].

In this chapter, a new non-isolated DC to DC resonant converter working under zero-voltage switching condition has been introduced, which can work in high frequencies with high power conversion rate and efficiency as well as low losses. The proposed converter can provide 5V output from 350mV input voltage with efficiency of 72.8%. Furthermore, we proposed an isolated DC to DC converter which provides the output voltage of 6V and more with efficiency of 68%. Due to the isolation, this converter is proper for applications required more safety. All the theoretical analyses are verified by MATLAB and circuits are simulated in PSIM.

4.1 Introduction

In many power electronic applications, there is a need for high gain DC to DC converters. A step-up (boost) converter is one of the simplest models of switched-mode converters. As its name implies, it takes the input voltage and increases it to the desired amount. All conventional boost (step-up) converters

Najmehossadat Nourieh
School of Physics, Engineering and Computer Science, University of Hertfordshire

include a diode, a switch (today a MOSFET mostly used, as you can get high-quality types), a capacitor and an inductor. As shown in Figure 4.1, this traditional type of converter can work merely with four elements [125- 128]. Theoretically, a conventional boost converter may achieve an infinite voltage gain when the duty cycle value is equal to 1. However, the high duty cycle results in high conduction and reverse recovery losses in active switches and diodes respectively. Also, the switch voltage stress will be higher as we gain higher output voltage by increasing the duty cycle.

Mode I:

In this mode, the circuit operation during the original period of the high-frequency square wave applied to the gate of MOSFET at the start-up point, is considered. During this period, the MOSFET conducts, setting a short-circuit from the right side of inductor to the negative terminal of the input supply. Hence, the current flows through between the negative and positive terminals, which saves energy in its own magnetic field. Though, there will be no flowing current in the rest of the circuit since the combination of diode, capacitor and the load provide a great larger impedance than the route directly through the conducted MOSFET.

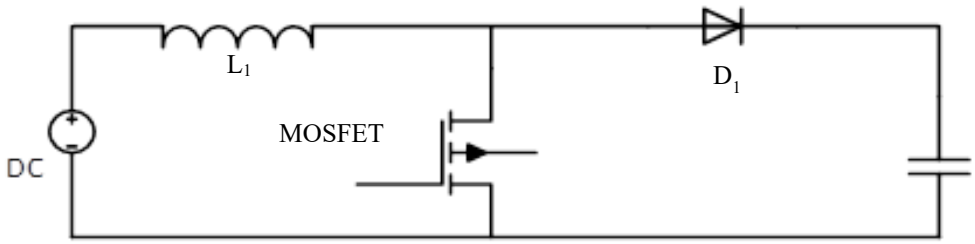

Figure 4.1 The conventional boost circuit

Mode II:

Najmehossadat Nourieh
School of Physics, Engineering and Computer Science, University of Hertfordshire

In second operational mode, the current pathway is through the low part of the switching square wave cycle. Since the MOSFET is quickly turned off, a sudden current drop causes the inductor to produce a back e.m.f, electromotive force (A back e.m.f. or Counter e.m.f., is the one produced across the inductor by changes of the magnetic flux around the conductor, created by changing current in the same inductor) in the reverse polarity to the voltage across the inductor throughout the ON period, to retain the current flowing. This can result in two voltages, one the supply voltage called V_{IN} and second the back voltage of V_L across inductor. The higher voltage of $V_{IN} + V_L$ (now that we have no current flowing through the MOSFET), will forward biases the diode. Hence, the resulting current in diode will charge up the capacitor to $V_{IN} + V_L - V_{f\text{-}diode}$, and further supplies the load [125].

The circuit operates during the ON periods of MOSFET after the initial start-up. Each time when the MOSFET conducts, the anode of the diode will be less positive than the cathode, due to the charge of the capacitor. Therefore, the diode is consequently turned off; thus, the output will be isolated from the input; however, the load remains to be supplied from the charge of capacitor with the voltage of $V_{IN} + V_L$. Although the charge of the capacitor is reduced by the load through this period, it will be recharged whenever MOSFET is off, thus it can maintain a relatively steady output voltage for the load

Although the conventional type of step-up converter is simple, low cost and small, for applications with frequencies more than 100KHz, this converter produces high thermal, switching and conductive losses.

In this chapter, two novel isolated and non-isolated DC to DC converters will be discussed. Both of these converters are working under ZVS conditions to provide high efficiency for applications with higher required voltages (more than 1.2V, which can be achieved by the designed Dickson rectifiers we have presented in chapter 3).

Najmehossadat Nourieh
School of Physics, Engineering and Computer Science, University of Hertfordshire

4.2 Proposed Step-up Power Converter Working under Zero-Voltage Switching

The proposed converter is the modified version of the conventional boost circuit which can perfectly work in higher frequency ranges such as MHz (In this thesis, we have considered the RF frequency of 915MHz). This chapter presents a DC to DC resonant converter with soft-switching conditions. The resonant network is composed of a capacitor and an inductor which provides soft-switching conditions for the main switch. By applying a ZVS method, the converter has advantages such as high efficiency, small size and low losses. In addition, this converter also benefits from a diode-connected MOSFET which provides ultra-low conduction loss. The output voltage/current of this circuit is 5V/25uA when the input voltage/current is 0.35V/500uA and the power efficiency is 72.8%. The simulated results in PSIM are also presented to verify the proposed converter. Having advantages of high efficiency, low switching, conducting and thermal losses, low EMI and high switching frequency ranges, this converter can be applied in different applications such as consumer electronics, biomedical devices and communications systems [73].

The proposed converter is shown in Figure 4.2 which has four operating modes shown in Figure 4.3. The switch MOS constitutes an inverter leg. The capacitor C_2 and inductor L_2 (along with the MOSFET parasitic output capacitance C_{oss}) are set to provide ZVS condition and resonance. The benefits of the resonant converter with ZVS condition have been mentioned below.

1. Zero voltage switching
    a. Low switching loss
    b. low capacitance loss
    c. high power density
2. Resonant converter

Najmehossadat Nourieh
School of Physics, Engineering and Computer Science, University of Hertfordshire

a. Increase switching frequency

b. Increase efficiency

c. Low EMI and noise.

For theoretical analyses, it is assumed that the converter is in the steady-state, all the circuit elements are ideal, and the output capacitor C_{out} is large enough to keep the output voltage constant during one switching cycle. In Eq. (4.1), Eq. (4.2) and Eq. (4.3), we define various parameters which will be used in the following discussion. The parameter ω_r is the angular frequency. In all operating modes $I_{number}=i_{r(tnumber)}$. In addition, Z_r, L_r, C_r and f_r are the resonance impedance, resonance inductor, resonance capacitor and the resonance frequency respectively.

$$\omega_r=2\pi f_r=\frac{2\pi}{T_r}=\frac{1}{\sqrt{L_rC_r}} \tag{4.1}$$

$$R_{out}=\frac{n^2V_o{}^2}{P_{out}} \tag{4.2}$$

$$Z_r=\sqrt{\frac{L_r}{C_r}} \tag{4.3}$$

All the operation modes of the suggested converter are simulated and verified by PSIM and MATLAB. The inherent mechanism of this converter considerably limits the switching frequency variations to small values (normally, 10% variations) which means that components can be selected/designed optimally. Furthermore, the capacitor of the MOSFET which is extremely tiny will be charged very fast. Figure 4.2 shows the schematic of the proposed converter where all the components are labelled. Also, in Figure 4.3, the key waveforms of converter are presented

In mode I, the capacitor C_2 should be large enough to protect the inductor L_2 from infinite current and it keeps the correct volt-second balance of the inductor. Here, Z_{eq} is the equivalent impedance of C_1, C_2 and L_2. Where ω_r is the resonant angular frequency, V_s is the source voltage, V_{out} and R_{out} are the output voltage and output resistance, respectively.

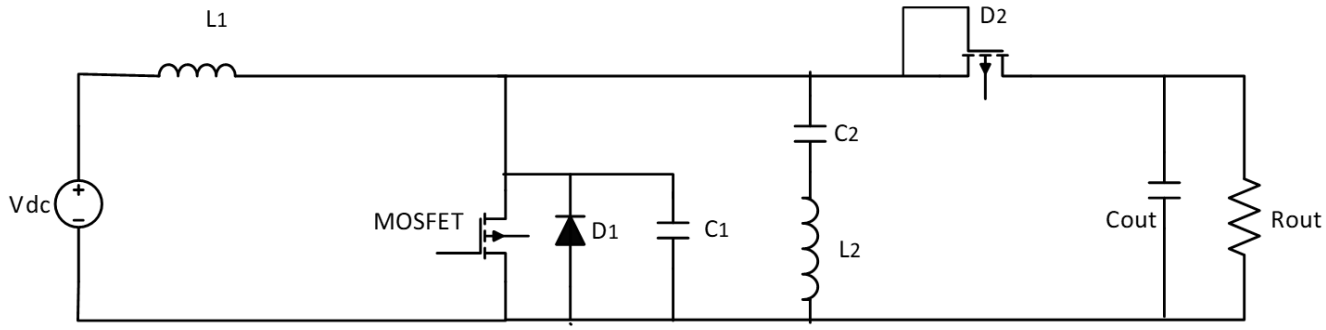

Figure 4.2 The schematic of the proposed converter

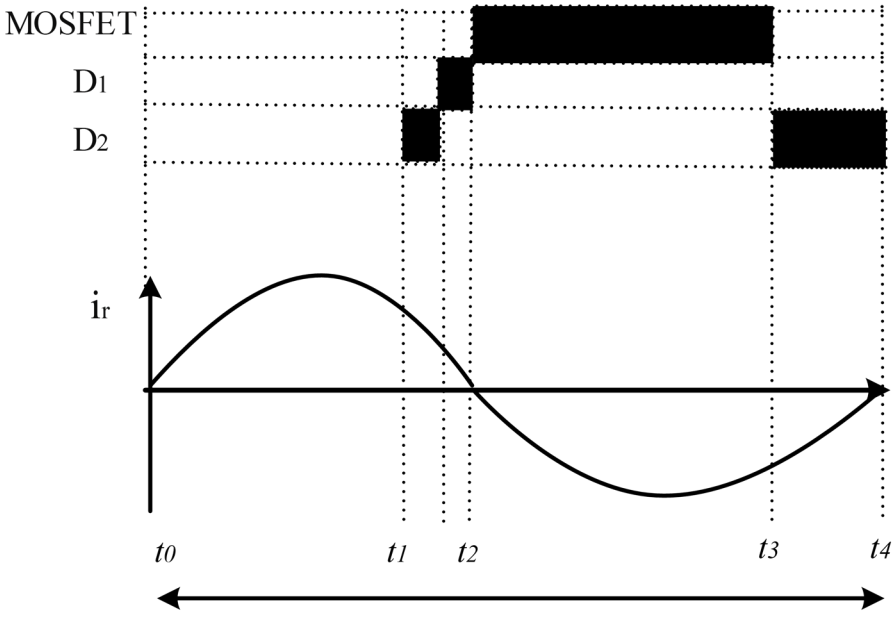

Figure 4.3 The key waveforms of the proposed converter

Mode I: In this interval, at t_0, the current flows through the inductors and capacitors named L_1, L_2, C_1 and C_2 until when the voltage of the cathode ($V_{cathode}$) of diode-connected MOSFET, D_2, reaches the threshold voltage ($V_{th,diode}$) i.e. $V_{cathode}>V_{th,diode}$. Thus, all the resonant elements will be charged by the input source.

Najmehossadat Nourieh
School of Physics, Engineering and Computer Science, University of Hertfordshire

Furthermore, the capacitor of the MOSFET, which is extremely small, will be charged very fast. In this mode, the capacitor C_2 should be large enough to protect the inductor L_2 from infinite current and it keeps the correct volt-second balance of the inductor. Here, Z_{eq} is the equivalent impedance of C_1, C_2 and L_2 and Z_L is the impedance of L_1 (Figure 4.4). By Eq. (4.4) the main current of converter is gained. Appling Eq. (4.5) and Eq. (4.6), the resonant voltage and current will be calculated.

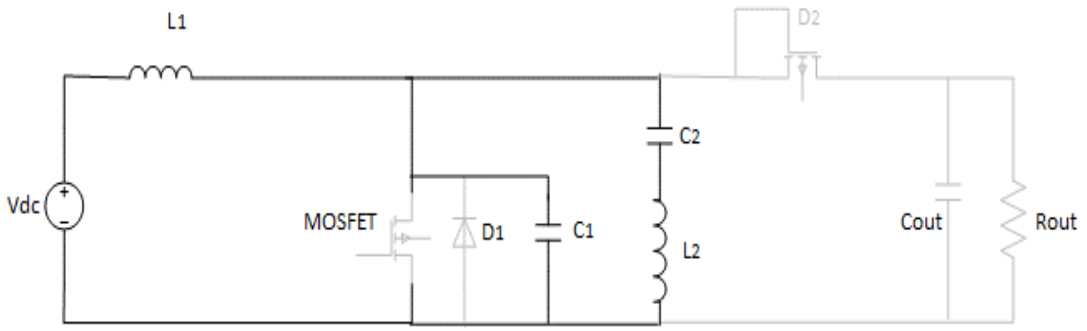

Figure 4.4 The schematic of the first mode.

$$I_{L1}(t)=\frac{V_S}{Z_{eq}+Z_L}\sin(\omega_r(t-t_0)) \tag{4.4}$$

$$V_{c2}(t)=V_s\left(1-\frac{(L_1+L_2)\omega_r}{Z_{eq}}\cos(\omega_r(t-t_0))\right) \tag{4.5}$$

$$I_{L2}(t)=\cos(\omega_r(t-t_0))\left[\left(\frac{V_s-V_{out}}{L_1}\right)\sin\left(\cos^{-1}\frac{V_mL_1}{\omega_rL_2(V_s-V_m)}\right)-\frac{V_m}{Z_{eq}}\right] \tag{4.6}$$

$$V_{c1}(t)=V_{c2}(t)+V_{L2}(t)=V_s\left[1-\frac{(L_1+L_2)\omega_r}{Z_{eq}}\cos(\omega_r(t-t_0))+\frac{\omega_rL_2}{Z_{eq}}\cos(\omega_r(t-t_0))\right] \tag{4.7}$$

Mode II:

Najmehossadat Nourieh
School of Physics, Engineering and Computer Science, University of Hertfordshire

This mode is the combination of the two very short modes. At t_1, when the cathode of the diode-connected MOSFET (D_2) exceeds $V_{th,diode}$, the diode will be turned-on and the energy stored in the inductor L_1 will not only be transferred to the output but will also continue charging C_2 and L_2 until the energy of L_1 reaches zero. This turns D_1 on for extremely short time. As the capacitor C_1 was fully charged in previous interval due to its small capacitance, it starts to be discharged through D_1 which means that the voltage of the drain-so of MOSFET will be zero in readiness for turning on under ZVS condition in the next mode (Figure 4.5). Appling Eq. (4.8) and Eq. (4.9), the resonant voltage and current will be calcuted.

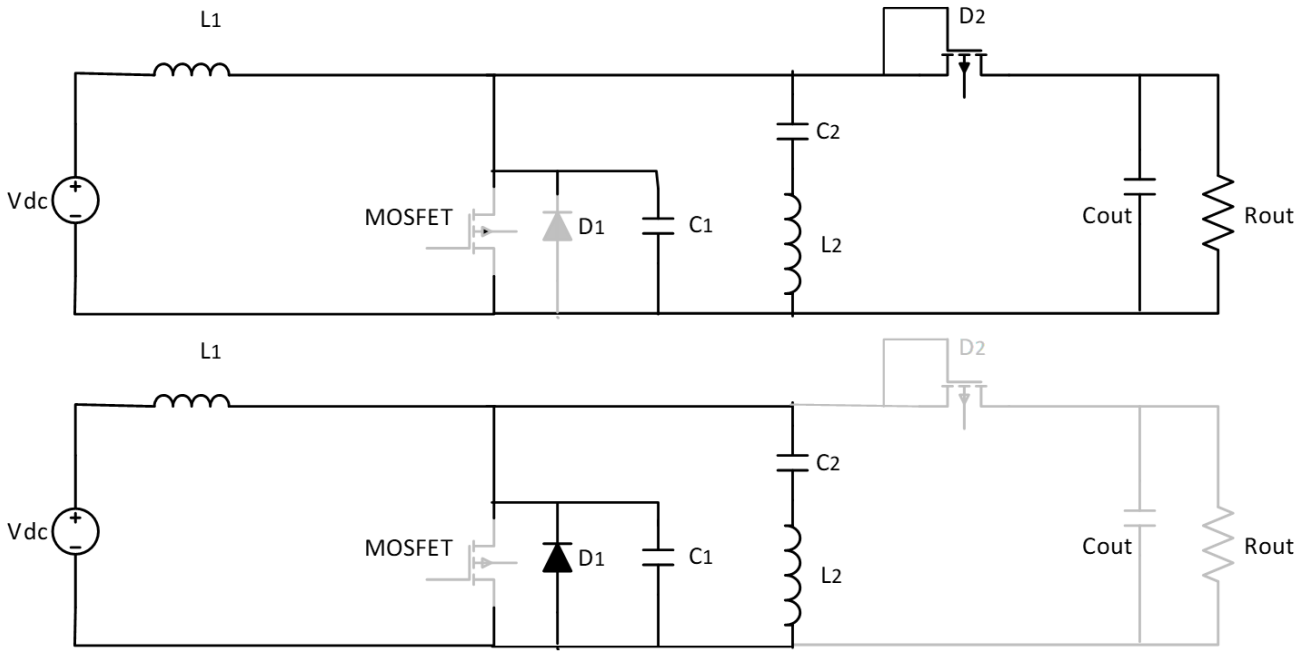

Figure 4.5 The schematic of the second mode.

$$V_{c2}(t)=V_{out}\left(1-\frac{(L_1+L_2)\omega_r}{Z_{eq}}\cos(\omega_r(t-t_1))\right) \tag{4.8}$$

$$I_{L2}(t)=\cos(\omega_r(t-t_2))\left[\left(\frac{V_s-V_{out}}{L_1}\right)\sin\left(\cos^{-1}\frac{V_{out}L_1}{\omega_r L_2(V_s-V_{out})}\right)-\frac{V_{out}}{R_{out}}\right] \tag{4.9}$$

Mode III:

Najmehossadat Nourieh
School of Physics, Engineering and Computer Science, University of Hertfordshire

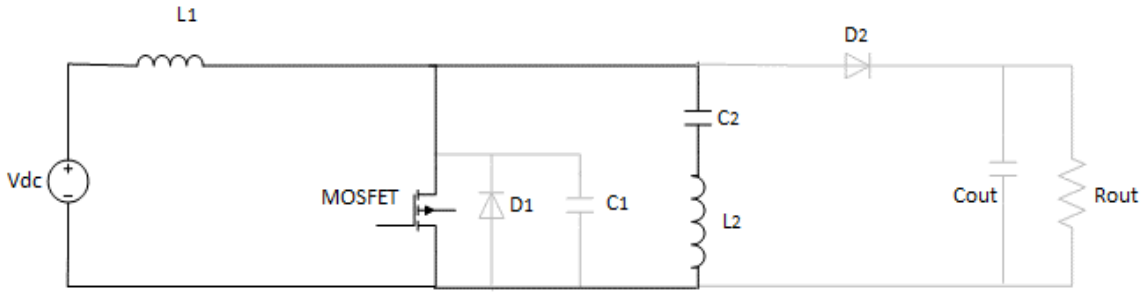

Figure 4.6 The schematic of the third mode.

In this mode at t_2, the MOSFET is turned-on under zero-voltage-switching condition, the main switch is turned-on or turned-off under soft-switching condition due to have the series of C_2 and L_2 where the spike of the voltage or current can be absorbed by these two elements. During this mode L_r is charged by the input source and the series of the capacitor and inductor resonate together. Figure 4.6 presents the schematic view of the circuit in this mode. Appling Eq. (4.10) and Eq. (4.11), the resonant voltage and current will be calculated.

$$I_{L2}(t)=\sin(\omega_r(t-t_2))\left[\left(\frac{V_s-V_{out}}{L_1}\right)\sin\left(\cos^{-1}\frac{V_{out}L_1}{\omega_r L_2(V_s-V_{out})}\right)-\frac{V_{out}}{R_{out}}\right]\sin\left(\omega_r(t_2-t_1)\right) \quad (4.10)$$

$$V_{c2}(t)=V_s\left[1-\frac{(L_1+L_2)\omega_r}{Z_{eq}}\cos(\omega_r(t-t_2))+\frac{\omega_r L_2}{Z_{eq}}\cos(\omega_r(t-t_2))\right] \quad (4.11)$$

Mode IV:

At t_3, the MOSFET is turned-off under ZVS condition. In this mode, the power of the input source goes through the inductor L_1 to reach the output stage. Besides, the energy stored in the series of the inductor and capacitor will also be transferred to the output. Hence, in this mode the existence of the series of capacitor and inductor is not only to provide the ZVS condition, but also to store and transfer the energy from the input stage to the output. In Figure 4.9, the schematic view of the circuit of this mode is

Najmehossadat Nourieh
School of Physics, Engineering and Computer Science, University of Hertfordshire

presented. By Eq. (4.12) the main current of converter is gained. Appling Eq. (4.13) and Eq. (4.14), the resonant voltage and current will be calculated.

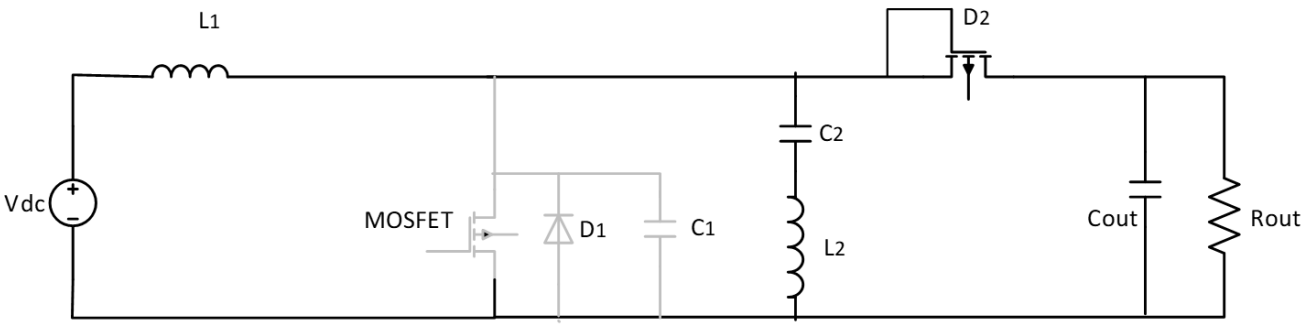

Figure 4.8 The schematic of the fourth mode.

$$I_{L1}(t)=\left(\frac{V_s-V_{out}}{L_1}\right)\sin(\omega_r(t-t_3))+\ I_{L1}(t_2) \tag{4.12}$$

$$I_{L2}(t)=\left(\frac{V_s-V_{out}}{L_1}\right)\sin(\omega_r(t-t_3))-\frac{V_{out}}{R_{out}}+I_{L1}(t_2) \tag{4.13}$$

$$V_{C2}(t)=\left(\frac{V_s-V_{out}}{L_1C_2\omega_r}\right)\cos\left(\omega_r(t-t_3)\right)-\frac{V_{out}}{C_2R_{out}}(t-t_3) \tag{4.14}$$

4.2.1 The Output Stage

As we considered 5V for the output voltage and the power is about 100uW, Eq. (4.15) gives us the output resistor of 350KΩ. To also have a proper ripple in the output voltage, the equation Eq. (4.16) is considered to set the ripple less than 0.01. Considering all the information given above, the elements of the converter are designed and set to the closest proper value to theoretical results for simulation in PSIM software. In

Najmehossadat Nourieh
School of Physics, Engineering and Computer Science, University of Hertfordshire

order to investigate the accuracy of all the presented equations, they are subsequently verified by MATLAB software.

$$P_{out}=\frac{(V_{out})^2}{R_{out}} \tag{4.15}$$

$$\frac{\Delta V_{out}}{V_{out}}<0.01 \tag{4.16}$$

4.3 Simulation Results

As previously stated, the verification of this circuit is proven by simulation in the environment of the PSIM software. In the following figures the main circuit schematic and the waveform result will be presented. In Figure 4.9, the complete design of the proposed converter in PSIM is presented, where the value of each element is shown beside it. Figure 4.10 shows drain-source voltage and current of the MOSFET where the ZVS condition is met. In Figure 4.11 the current of conductive diode D_1 is illustrated which defines the time when the diode is on.

In Figure 4.12 the output voltage of circuit (5.05V) is presented to show both transient and steady-state modes which shows the period it takes to reach the steady-state mode is about 58us.

In Table 4.1, the specification of this converter is shown, whereas Table 4.2 shows a comparison between the proposed converter and similar works published before.

Najmehossadat Nourieh
School of Physics, Engineering and Computer Science, University of Hertfordshire

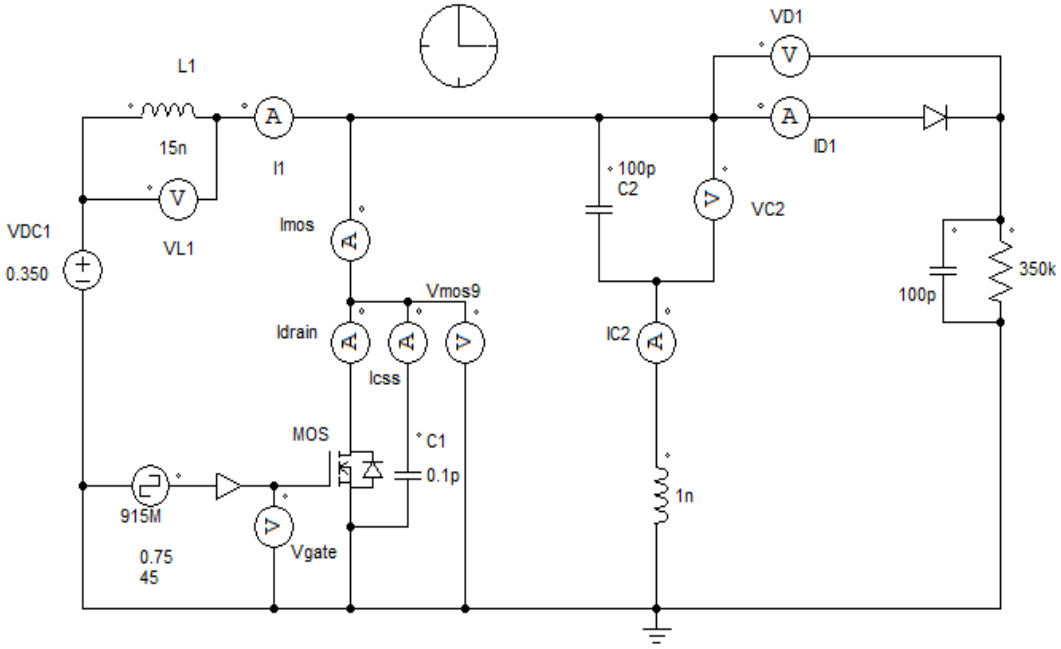

Figure 4.9 The schematic of the designed DC to DC converter in PSIM

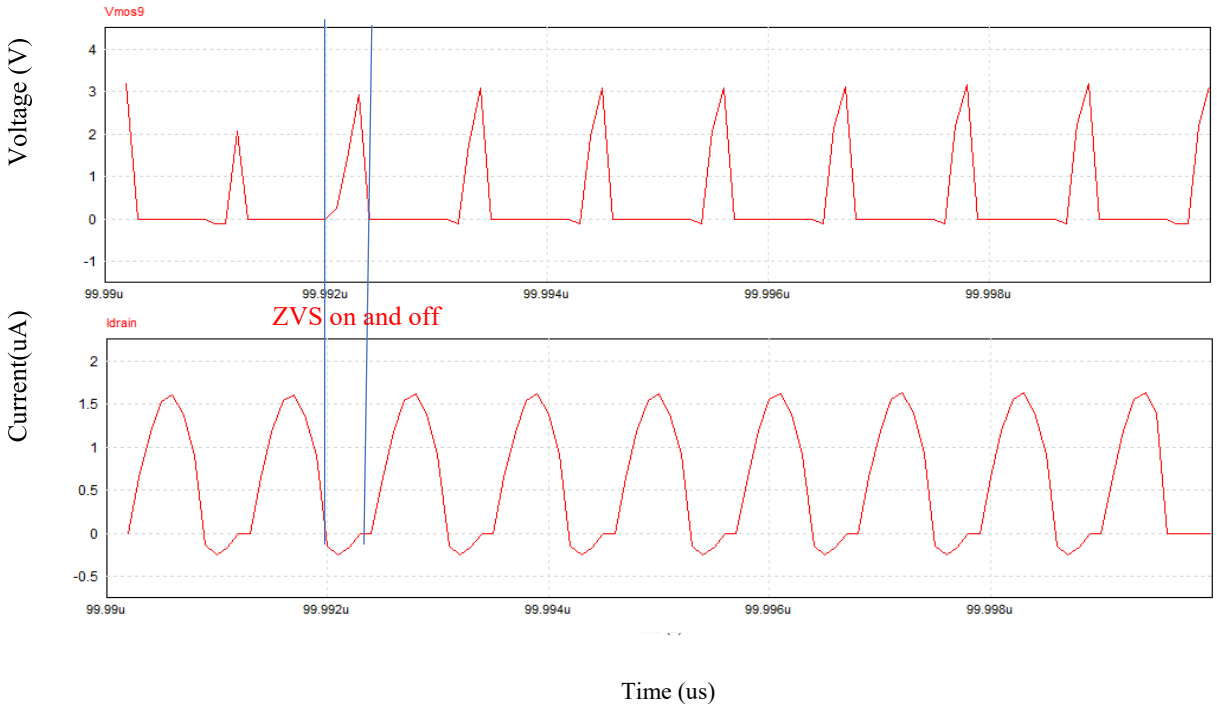

Figure 4.10 The waveforms of the drain-source voltage and current of the MOSFET

In Figure 4.13 the efficiency of the proposed circuit in PSIM for the range of full load, half load and light load is discussed. As it is shown in this figure the efficiency of the circuit is 72.8% for full load,

Najmehossadat Nourieh
School of Physics, Engineering and Computer Science, University of Hertfordshire

54.1% for half load and 32% for light load (20% load).

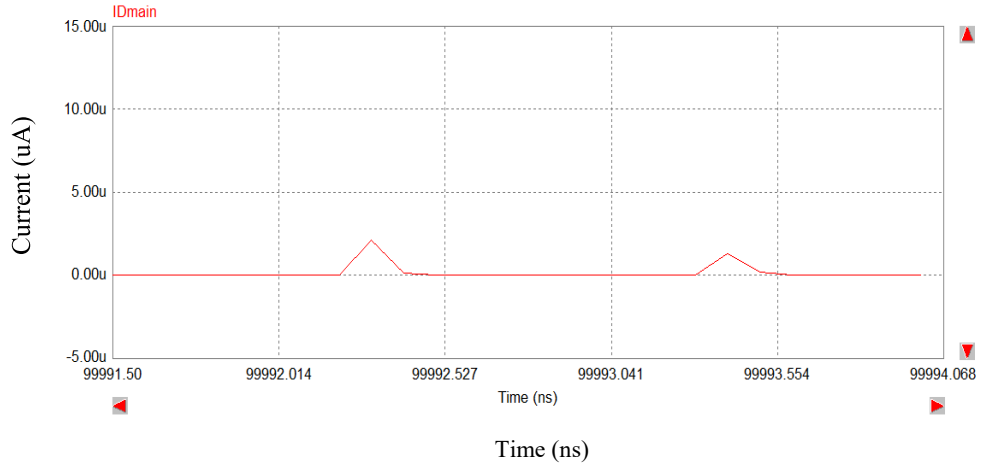

Figure 4.11 The waveforms of the current of diode D_1

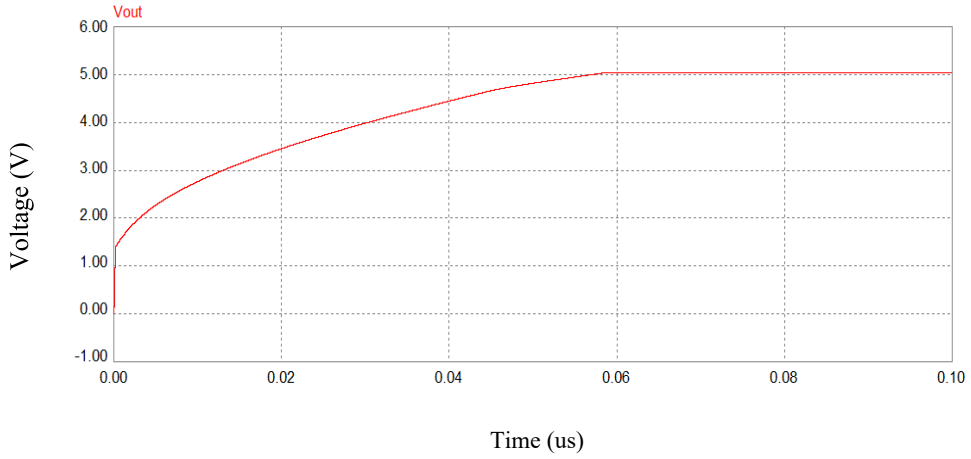

Figure 4.12 The output voltage of the circuit

In Table 4.2, a comparison between the proposed converter and some recently published works is presented, where soft-switch conditions, number of elements, common ground, voltage gain and input power are listed. From information given in this table, the proposed converter has a voltage gain of 14 while the voltage gains in [129- 131] are 4, 7.91 and 3, respectively.

Najmehossadat Nourieh
School of Physics, Engineering and Computer Science, University of Hertfordshire

All these converters provide soft switching and common ground operation. Referring to the input power, it is understood that the works presented in [129] and [130] are not suitable for low input power conversion. The circuit presented in [131] has an input power of 417μW which is around three times more than the proposed converter.

Furthermore, the total number of components in the converters presented in [129- 131] are 10, 15, and 7 respectively. In comparison our proposed converter comprises of 6 components, consequently, having lower losses and a smaller converter size.

TABLE 4.1
COMPONENTS OF THE PROPOSED CONVERTER

Component	**Value**	**Component**	**Value**
Vs	0.35V	R_g	0.5Ω
Vo	5.05V	C_g	1nF
f_s	915MHz	R_{out}	350kΩ
L_1	15nH	C_{out}	100pF
L_2	1nH	C_2	100nF
C_1	0.1pF	Efficiency Power	72.8%

Najmehossadat Nourieh
School of Physics, Engineering and Computer Science, University of Hertfordshire

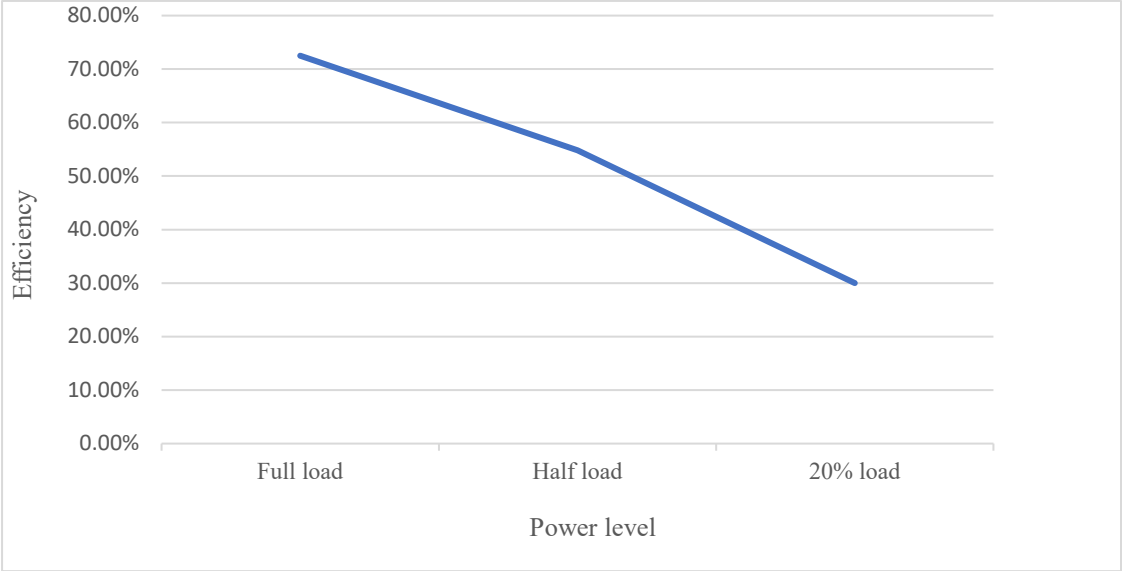

Figure 4.13 The efficiency of the circuit for the range of full load to light load

TABLE 4.2
COMPARISON OF THE PROPOSED CONVERTER WITH OTHER HIGH STEP-UP CONVERTERS

Converters	Voltage Gain	Soft Switching	Common Ground	Input Power	Number of Components	
					Active	Passive
[129]	4	✓	✓	100W	4	6
[130]	7.91	✓	✓	500W	8	7
[131]	3	✓	✓	417μW	5	2
Proposed	14	✓	✓	100μW	4	2

Najmehossadat Nourieh
School of Physics, Engineering and Computer Science, University of Hertfordshire

4.4 The Proposed Isolated Resonant DC to DC Converter Working under ZVS Condition

In this section, we propose a new isolated ZVS resonant DC to DC converter which has the advantages of producing higher output voltage and isolation for the applications where isolation and safety are very critical. This circuit also has the capability of producing wider range of output voltages which can cover more applications requirement. The schematic circuit of the proposed combination is presented in Figure 4.14 and the key waveforms are shown in Figure 4.15.

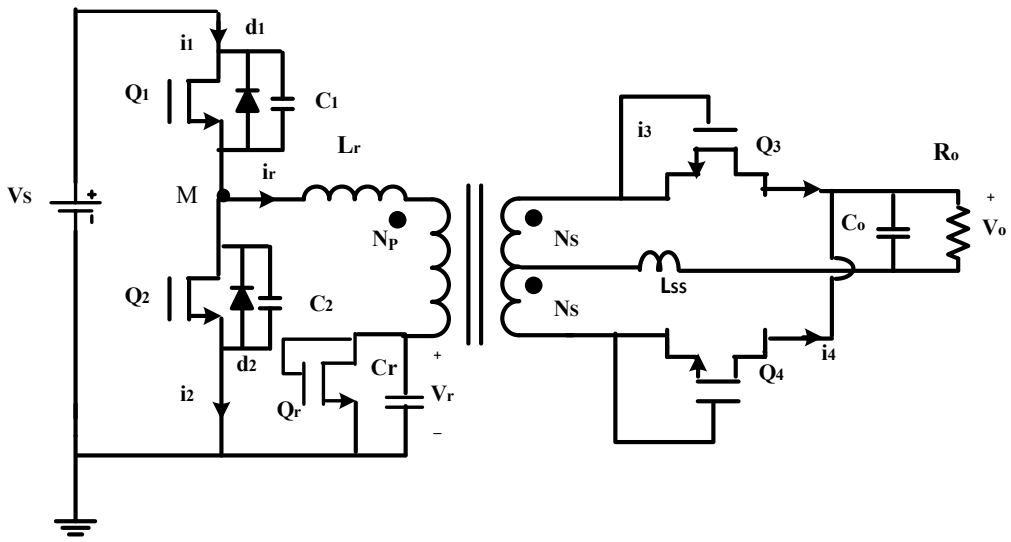

Figure 4.14 The propose isolated DC to DC circuit

This proposed circuit benefits from isolation, zero-voltage switching condition and resonance that each of these specifications adds advantages to the proposed circuits [139-141].

1. Zero voltage switching

    a. Low switching loss

    b. Low capacitance loss

Najmehossadat Nourieh
School of Physics, Engineering and Computer Science, University of Hertfordshire

c. High power density

2. Resonant converter

a. Increase switching frequency

b. Increase efficiency

c. Low EMI and noise.

3. MOSFETs in rectification part

a. Low conduction loss

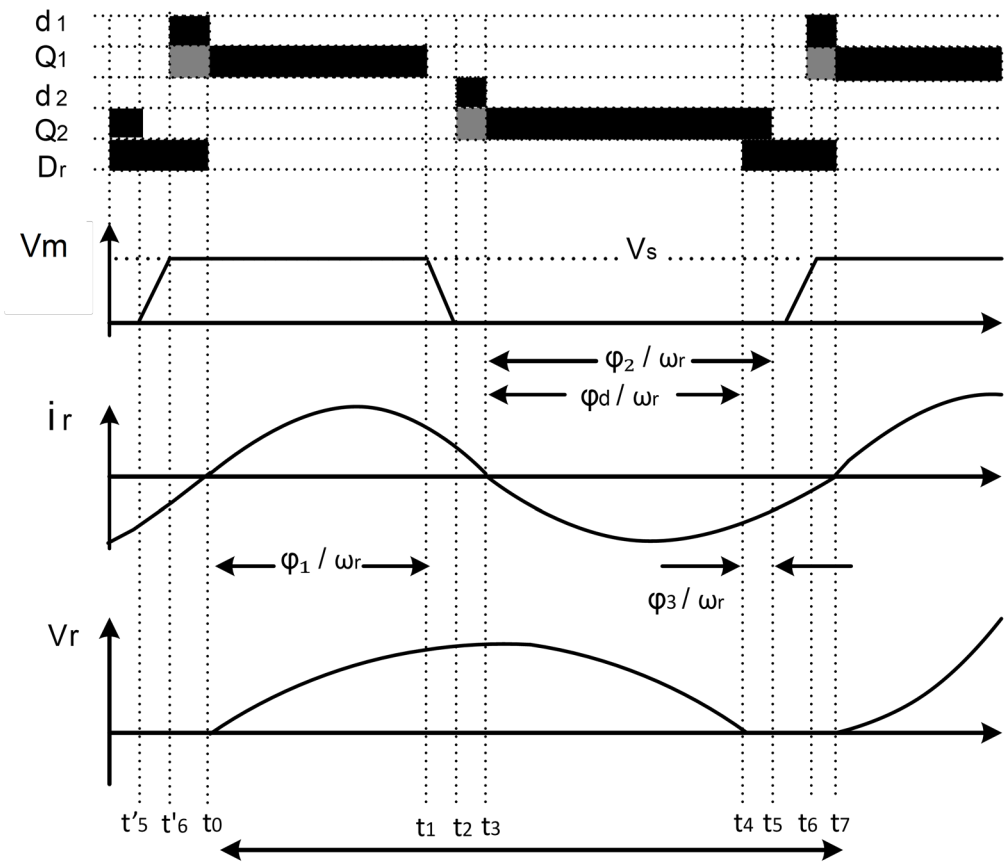

Figure 4.15 The key waveform of the proposed converter

Najmehossadat Nourieh
School of Physics, Engineering and Computer Science, University of Hertfordshire

b. Low thermal loss

4. Isolation

a. By changing the wounded wire layers we can boost the voltage very well

b. Buck or boost application

c. Increase safety as the output is separate from the input

d. Wide range of output voltages

$$\omega_r=2\pi f_r=\frac{2\pi}{T_r},\ R_o=\frac{n^2V_o{}^2}{P_{out}} \tag{4.17}$$

$$B=n\frac{V_o}{V_s}=nA,\ Z_r=\sqrt{\frac{L_r}{C_r}} \tag{4.18}$$

$$\alpha=\frac{C_r}{C_1+C_2},\ \beta=\frac{1+\alpha}{\alpha},\ \omega_\alpha=\sqrt{1+\alpha\omega_r} \tag{4.19}$$

This converter has seven operation modes which are explained in the following paragraphs. In Eq. (4.17) to Eq. (4.19) several parameters, which will be used in the following discussion, are defined. The parameter B is the converter normalized voltage gain, $B= nA = nV_o/V_s$ whereas α and β are used to simplify the equations. Shown in Figure 4.14, the conduction angles of Q_1 and Q_2 are defined as φ_1 and φ_2 respectively. In all operating modes $I_{number}=i_{r(tnumber)}$. Furthermore, the parasitic inductance is also used as resonant inductance since its total value is around nH which will be added to the 25μH resonant inductance. In addition, Z_r and f_r are the resonance impedance and the resonance frequency respectively.

Mode I:

In the interval before t_0, the diode d_1 is conducting to provide ZVS condition for Q_1 to be turned on at t_0. Thus, the energy from input source is transferred to output via Q_1, L_1, C_1, transformer and Q_3. Also,

Najmehossadat Nourieh
School of Physics, Engineering and Computer Science, University of Hertfordshire

resonant capacitor C_r is charged through resonance with L_r until t_1. Appling Eq. (4.20) and Eq. (4.21), the resonant voltage and current will be calculated.

$$V_r(t)= V_s(1-B)\left[1-\cos\left(\omega_r(t-t_0)\right)\right] \quad (4.20)$$

$$I_r(t)= \frac{V_s}{Z_r}\left[(1-B)\sin\left(\omega_r(t-t_0)\right)\right] \quad (4.21)$$

Mode II:

When the switch Q_1 is turned off at t_1, the remained current available in L_r will flow through capacitors C_1 and C_2. Hence, the voltage at node V_m (Eq. (4.22)) will be decreased from V_s to zero. The resonant current is gained by Eq. (4.23).

$$V_M(t)=V_s\left[1+\alpha(1-B)(1-\cos\varphi)-\alpha V(t)\right] \quad (4.22)$$

$$I_r(t)= \frac{V_s}{Z_r}\left[[(1-B)\cos\varphi_1/(\sqrt{1+\alpha})]\sin\left(\omega_\alpha(t-t_1)\right) + [(1-B)\sin\varphi_1]\cos\varphi_1(\omega_\alpha(t-t_1))\right] \quad (4.23)$$

Mode III:

At t_2, the diode d_2 is direct biased under ZVS condition at which the current flows until it reaches zero level at the time t_3. In this interval, the signal for switch Q_2 should be ready to turn this switch on in the following mode. The voltage of this mode is gained by Eq. (4.25).

$$T_3=1/\omega_r\left(\tan^{-1}\left(\frac{I_2}{(V_2+B)}\right)\right) \quad (4.24)$$

$$V_3=\sqrt{(-2(1-B)\cos\varphi_1+(1-B)^2+1+1/\alpha)} \quad (4.25)$$

Mode IV:

Najmehossadat Nourieh
School of Physics, Engineering and Computer Science, University of Hertfordshire

At t_3, the energy stored in resonant capacitor (C_r) will be transferred to output stage through the elements L_r and Q_2. Appling Eq. (4.26) and Eq. (4.27), the resonant voltage and converter current will be calculated.

$$V_r(t)= V_s(1-B)\, I_3 \sin\left(\omega_r(t-t_3)\right) \tag{4.26}$$

$$I(t)= (B-V_3)\, \sin\left(\omega_r(t-t_3)\right) \tag{4.27}$$

$$I_3= (B-V_3)^{\,2} - B^2 \tag{4.28}$$

Mode V:

At t_4, the diode D_r is turned on under ZVS condition and the current i_r flows through it. The energy remained in L_r provides ZVS condition to turn the switch Q_1 on. Hence, the switch Q_2 will be turned off at t_5 under ZVS condition. In this mode the energy stored in L_r is transferred to the output stage. By calculation of Eq. (4.29), the resonant voltage is obtained.

$$V_r(t)=V_s \left[1+\alpha(1-B)\left(1-\cos(\omega_r(t-t_4))\right)\right] \tag{4.29}$$

$$I(t)=B\omega_r(t-t_4)+I_4 \tag{4.30}$$

Mode VI:

In this mode, the voltage of node M (called V_m) will reach the zero level which leads to set the voltage of diode d_1 to make it ready to be turned on in the next mode and provide the ZVS turn-on condition for switch Q_1. Appling Eq. (4.31) and Eq. (4.32), the resonant voltage and converter current will be gained. At t_5, Q_2 is turned off.

$$V_r(t)=V_s \left[1+\alpha(1-B)\sin(\omega_r(t-t_5))+\cos(\omega_r(t-t_5))\right] \tag{4.31}$$

Najmehossadat Nourieh
School of Physics, Engineering and Computer Science, University of Hertfordshire

$$I_6=-\sqrt{I_5^2-\left(\frac{1+2B}{\alpha}\right)} \tag{4.32}$$

Mode VII:

In t_6, d_1 is turned on under ZVS condition and the resonant current flows through it until it reaches the zero level at t_7. In this mode, the gate signal of Q_1 will be ready to turn it on in the next interval mode. By calculation of Eq. (4.33) and Eq. (4.34), the resonant current and voltage are obtained.

$$I_r(t)=(1+B)\sin(\omega_r(t-t_6))+I_6 \tag{4.33}$$

$$V_r(t)= V_s[(1-B)(1/\sqrt{\alpha})\sin(\omega_r(t-t_6)) + B\cos(\omega_r(t-t_6))] \tag{4.34}$$

In Table 4.3 the specification of the converter is presented.

TABLE 4.3
PARAMETERS AND COMPONENTS OF THE CIRCUIT

Symbol	Full-Load
Vs	0.35V
V_{out}	6.07V
P_{in}	100uW
f_s	242kHz
C_r	1nF
L_r	25nH
C_1	0.25nF
C_2	0.25nF

Najmehossadat Nourieh
School of Physics, Engineering and Computer Science, University of Hertfordshire

4.5 Simulation Results

In the following figures the simulation results of the proposed converter in PSIM are presented in Figure 4.16 to Figure 4.20. In Figure 4.16 the schematic of the simulated converter is shown while in Figure 4.17 and Figure 4.18, the drain-source voltages of Q_1 and Q_2 are illustrated respectively where the on

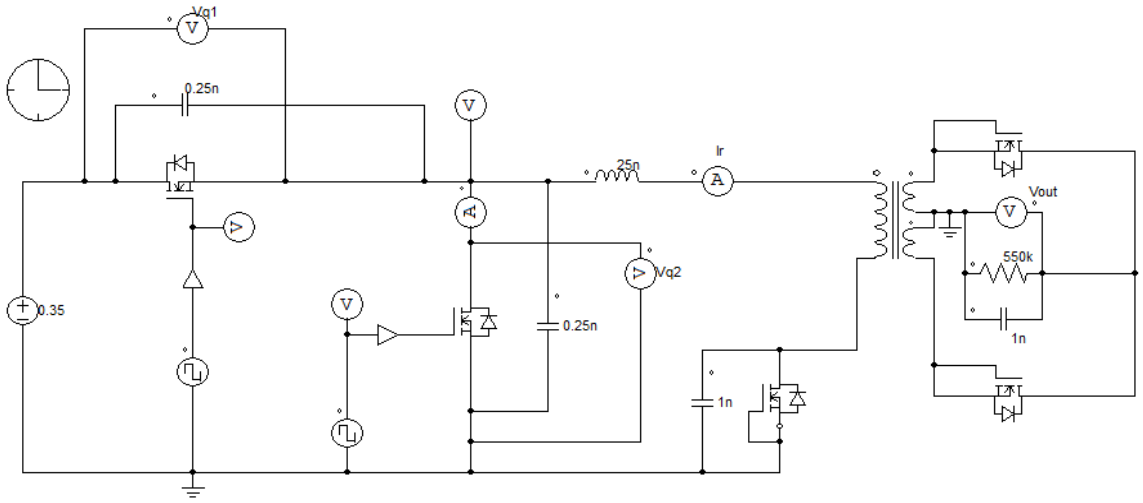

Figure 4.16 The schematic of the proposed isolated DC to DC converter

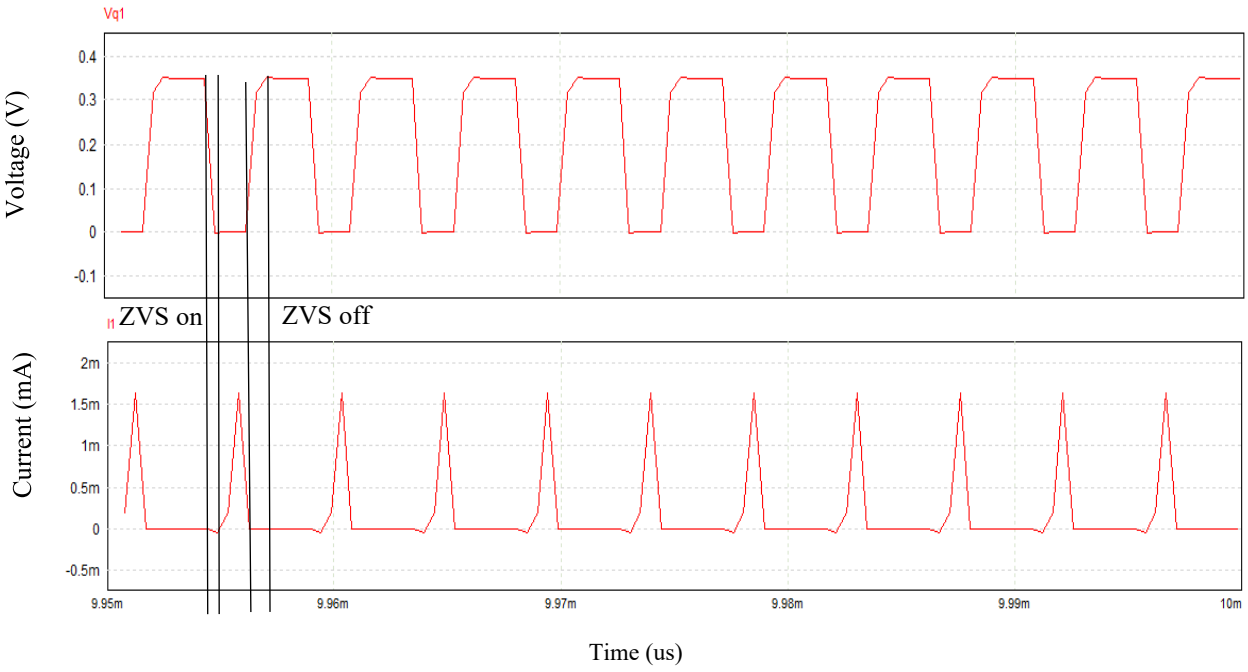

Figure 4.17 The voltage of drain-source in Q_1

Najmehossadat Nourieh
School of Physics, Engineering and Computer Science, University of Hertfordshire

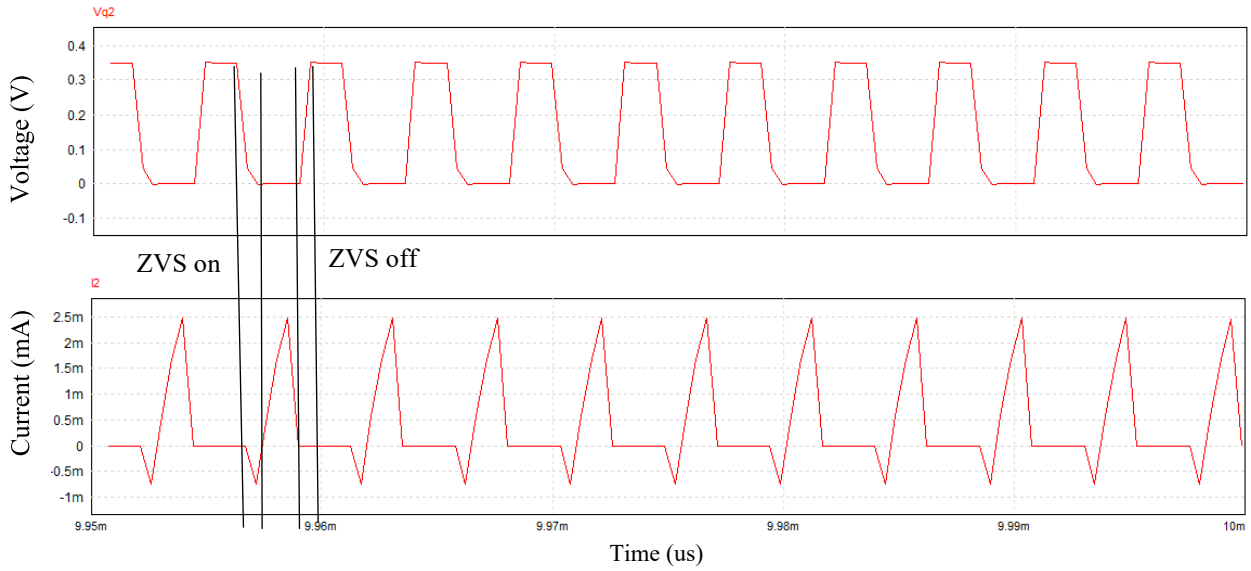

Figure 4.18 The voltage of drain-source in Q_2

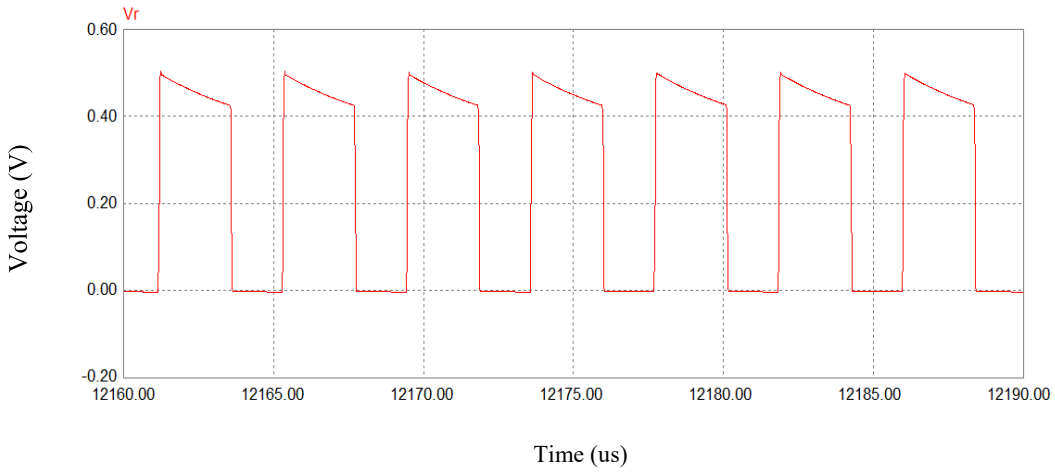

Figure 4.19 The voltage of V_{Cr}

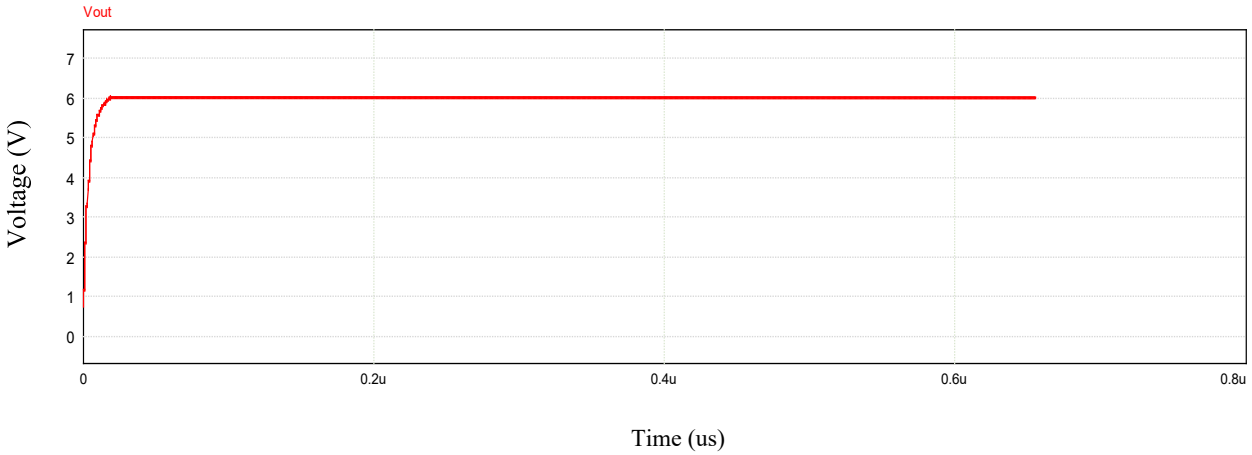

Figure 4.20 The output voltage of the circuit

period of these two switches are defined. Then, the voltage of V_{Cr} is presented in Figure 4.19 (the peak

Najmehossadat Nourieh
School of Physics, Engineering and Computer Science, University of Hertfordshire

voltage of C_r is 0.5V), and the graph for output voltage (6.07V) is shown in Figure 4.20. To run MOSFETs, the gate signals are set to turn on Q_1 and Q_2 for 39% and 44% of the cycle.

5.6 Performance Comparisons of Suggested Converters with Other Works

Table 4.4 compares the proposed converters with other published works. This comparison shows the better performance of the proposed converter, as the input power of proposed converter is greatly lower than other works with higher voltage gain. Comparing to [134] which has input power of 22uWatt with the efficiency of 62.30% and voltage gain of 2, the proposed isolated converter has the efficiency of 68% while it is 73% for the non-isolated proposed converter. The voltage gain for isolated and non-isolated proposed circuits is 17.34 and 14.42 respectively.

TABLE 4.4
COMPARISON OF TWO PROPOSED CONVERTERS AND OTHER WORKS

Previous works	Input Power	Input Voltage	Voltage gain	Efficiency
[132]	10mWatt	2V	1.5	77%
[133]	16mWatt	3.2V	1.3	55%
[134]	22.4uWatt	0.7V	2	62.30%
[135]	100mWatt	1V	2	40%
[136]	120mWatt	1.2V	2.75	97.50%
[137]	330mWatt	3.3V	2.12	77%
[138]	500mWatt	10V	1.5	78%
Isolated DC to DC converter	100uWatt	0.35V	17.34	68%
DC to DC converter	100uWatt	0.35V	14.42	72.8%

Najmehossadat Nourieh
School of Physics, Engineering and Computer Science, University of Hertfordshire

4.7 Conclusion

In this chapter, a new non-isolated DC to DC resonant converter working under zero-voltage switching condition has been introduced, which can work in high frequencies with high power conversion rate and efficiency as well as low losses. The proposed converter can provide 5V output from 350mV input voltage with efficiency of 72.8%. Furthermore, we proposed an isolated DC to DC converter which provides the output voltage of 6V and more with efficiency of 68%. Due to the isolation, this converter is proper for applications required more safety. All the theoretical analyses are verified by MATLAB and circuits are simulated in PSIM.

Najmehossadat Nourieh
School of Physics, Engineering and Computer Science, University of Hertfordshire

5 The Combination of Phase Shifter, Rectifier, and DC to DC Converters

Radio frequency energy obtained from free space typically possesses low power density as the electric field power density declines proportional to distance from the RF source [142], this is an issue that most of recent works try to resolve to make this greatly available power source applicable for different applications.

In this chapter, two combinations of high voltage gain circuits are introduced for low power applications such as RF energy harvesting (RFEH). The first combination consists of a phase shifter, 1-stage rectifier and resonant ZVS DC to DC converter which has the output voltage of 6V with the efficiency of 71%. The second, consists of a phase shifter, 1-stage rectifier and isolated resonant ZVS DC to DC converter with output voltage and efficiency of 5V and 65% respectively.

5.1 Introduction

The availability of many ambient energy harvesting techniques such as thermal, solar, vibration, RF, wind, etc., is now one of the interesting topics of research community since last decade [143]. In this thesis, a special attention has been paid to the RF energy harvesting circuits. Although RFEH is one of the least powerfull sources of practical electrical energy, it has many advantages, which make it superior to other ambient energy harvesting solutions. RFEH can provide a regular energy source, specifically for indoor areas, where natural light is not strong enough. Furthermore, it is proven in the survey [144] that there is no large-scale fluctuation in the RF power levels which makes it more reliable. Besides, RF sources are always available regardless of time and they are negligibly affected by weather conditions, unlike wind and solar energy. Another advantage could be the tiny size of the RFEH without any movable

Najmehossadat Nourieh
School of Physics, Engineering and Computer Science, University of Hertfordshire

part, making it simpler to use for specific applications. Therefore, RFEH is easy to manufacture and maintain, and more cost effective than solar panels or other energy harvesting systems [145].

In RFEH circuits, one of the main blocks is rectifier. Rectification is the most popular purpose of diodes, which refers to the conversion of AC to DC. In power harvesting circuits, the RF signal recovered in an antenna has a sinusoidal waveform. The signal will be rectified and boosted to satisfy the appropriate voltage/current demands of the considered applications [146, 147].

The metal–oxide semiconductor field-effect transistor (MOSFET) technology overcomes the weaknesses of diodes and is becoming an essential alternative solution for boosting and rectifying. Having MOSFET technology, the Dickson multiplier can be integrated in an Integrate Circuits (IC) by substituting diodes with PMOS or NMOS. Relatively, the low threshold voltage and high-power conversion rate are the main points of this design [148, 149].

Voltage multiplier is a particular type of rectifier which rectifies and boosts AC input to DC output. In some cases, where the rectified output power is not enough to meet the power requirement of the application, there is a necessity to boost the output DC by using rectifiers, which is further called voltage multiplier [150, 151].

In this chapter, we will propose two combinations of both rectifier and voltage multiplier with their analyses. The first suggested combination is to have 1-stage of modified Dickson rectifier followed with a novel non-isolated DC to DC boost converter which can produce high voltages with satisfying efficiency. The second proposed solution is to have an isolated DC to DC boost converter following the 1-stage Dickson rectifier with two input sources. Both applied 1-stage Dickson rectifiers work with a phase shifter (which provides two input signals with 180° phase difference). All the suggested combinations are analysed theoretically and verified by simulation results. Each of these suggestions has its own pros and cons that make them suitable for a range of applications. Finally, we compare all the proposed RF to DC circuits in this thesis with each other.

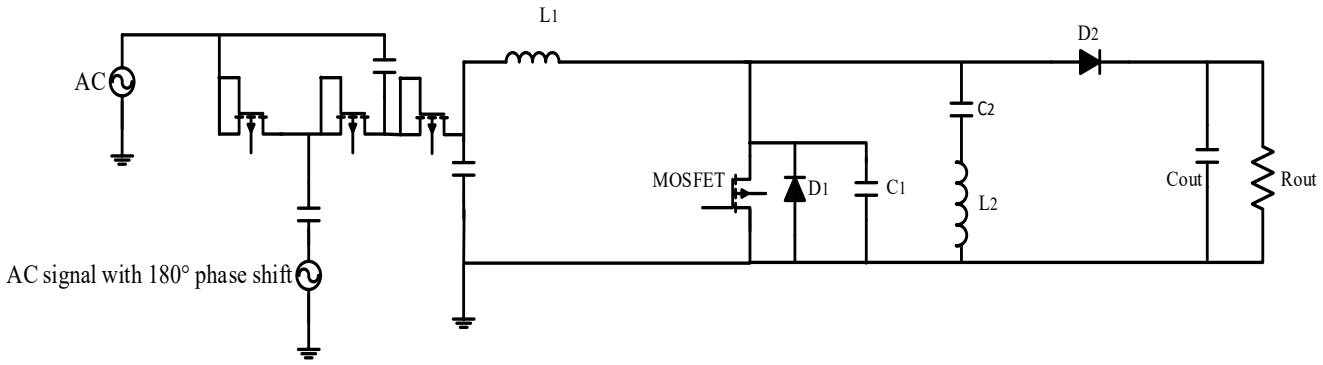

Figure 5.1 The schematic of the proposed combination of rectifier and resonant converter

5.2 1-Stage of Modified Dickson Rectifier/Multiplier with LC Boost Converter

As discussed in the chapter 3, considering the trade-off between the number of stages in Dickson rectifier and the efficiency (the input power delivery to the rectifier circuit), we propose two other combinations of circuits for the purpose of having a wider range of applications requiring higher output voltages.

For this combination, we will use the 1-stage modified Dickson rectifier working with a resonant ZVS step-up converter which has the capability of boosting the voltage by more than 1.2V (we set it to gain an output voltage of 5V). This circuit has advantages such as working under ZVS condition which enables the circuit to work at high frequencies such as 915MHz (the desired frequency of this thesis).

In the following paragraphs, we will discuss the theory and simulation of the proposed combination. The schematic of the suggested circuit is given in Figure 5.1. In this section, we present the theory analyses of the proposed combination where the simulation verification of each mode is given.

As it has been discussed in chapter 4, the proposed resonant converter has four main modes where the initial input source can be replaced by the output of given 1-stage rectifier in chapter 3. Hence, the operation modes of the new combined circuits will be verified in section 5.21 below.

Najmehossadat Nourieh
School of Physics, Engineering and Computer Science, University of Hertfordshire

5.2.1 Operation Modes of The Proposed Combination of Rectifier and Resonant Converter

The different operation modes of the combination of proposed rectifier with diode connected MOSFETs and the ZVS resonant converter are theoretically analysed in the following. The parameter ω_r is the angular frequency. In all operating modes $I_{number}=i_{r(tnumber)}$. In addition, Z_r, L_r, C_r and f_r are the resonance impedance, resonance inductor, resonance capacitor and the resonance frequency respectively.

$$\omega_r=2\pi f_r=\frac{2\pi}{T_r}=\frac{1}{\sqrt{L_rC_r}} \tag{5.1}$$

$$R_{out}=\frac{n^2V_o{}^2}{P_{out}} \tag{5.2}$$

$$Z_r=\sqrt{\frac{L_r}{C_r}} \tag{5.3}$$

Considering Eq. (5.1) to Eq. (5.3), all other equations were calculated.

Mode I:

The MOSFET was turned-off in the last mode of the previous period under ZVS condition. At t_0, when the cathode of diode D_2 exceeds $V_{th,diode}$, it is turned-on and the energy stored in inductor L_1 is not only transferred to the output stage, but also continues charging C_2 and L_2 by transferring energy from input source which is produced by the proposed rectifier at its output capacitor. By Eq. (5.4), Eq. (5.6) and Eq. (5.7), main current of converter and resonant current and voltage are obtained.

$$I_{L1}(t)=\frac{\left(2V_s+I_s\left(-jX_C+Z_D\right)\right)-V_M}{Z_{eq}}\sin\left(\omega_r(t-t_0)\right) \tag{5.4}$$

$$I_{L2}=I_{L1}-I_r \tag{5.5}$$

Najmehossadat Nourieh
School of Physics, Engineering and Computer Science, University of Hertfordshire

$$I_{L2}=\left(\frac{\left(2V_s+I_s\left(-jX_C+Z_D\right)\right)-V_{out}}{L_1}\sin\left(\cos^{-1}\frac{V_mL_1}{\omega_rL_2(V_s-V_m)}\right)\right)-\frac{V_m}{Z_{eq}} \quad (5.6)$$

$$V_{c1}=\left(2V_s+I_s\left(-jX_C+Z_D\right)\right)\left[1-\frac{(L_1+L_2)\omega_r}{Z_{eq}}\cos\left(\omega_r(t-t_0)\right)+\frac{\omega_rL_2}{Z_{eq}}\cos\left(\omega_r(t-t_0)\right)\right] \quad (5.7)$$

Mode II:

In this mode, at t_1, the current flows through inductors and capacitors named L_1, L_2, C_1 and C_2 until when the voltage of the cathode of diode D_2 reaches $V_{cathode}>V_{th}$. All the resonant elements will be charged by the input source. Furthermore, the capacitor of the MOSFET which is extremely tiny, is charged very fast. In this mode, the capacitor C_2 should be large enough to protect L_2 from infinite current and it keeps the correct volt-second balance of the inductor. In this mode, we have considered Z_{eq} as the equivalent impedance of the circuit. When the capacitor C_1 is fully charged, it starts to be discharged and the current will be reversed due to the reverse current coming from the energy stored in the series of C_2 and L_2 (which are discharged through the capacitor C_1). Besides, the voltage of the drain-source of the MOSFET will be zero to be ready for turning the MOSFET on under ZVS condition in the next mode. Appling Eq. (5.9) and Eq. (5.11), the resonant current and voltage are gained.

$$V_{c2}(t)=\left(2V_s+I_s\left(-jX_C+Z_D\right)\right)\left(1-\frac{(L_1+L_2)\omega_r}{Z_{eq}}\cos\left(\omega_r(t-t_1)\right)\right) \quad (5.9)$$

$$V_{c1}(t)=V_{c2}(t)+V_{L2}=\left(2V_s+I_s\left(-jX_C+Z_D\right)\right)\left[1-\frac{(L_1+L_2)\omega_r}{Z_{eq}}\cos\left(\omega_r(t-t_1)\right)+\frac{\omega_rL_2}{Z_{eq}}\cos\left(\omega_r(t-t_1)\right)\right] \quad (5.10)$$

$$I_{L2\text{ and }C2}=\cos\left(\omega_r(t-t_1)\right)\left[\left(\frac{\left(2V_s+I_s\left(-jX_C+Z_D\right)\right)-V_{out}}{L_1}\right)\sin\left(\cos^{-1}\frac{V_{out}L_1}{\omega_rL_2(V_s-V_{out})}\right)-\frac{V_{out}}{R_{out}}\right] \quad (5.11)$$

Najmehossadat Nourieh
School of Physics, Engineering and Computer Science, University of Hertfordshire

Mode III:

In this mode at t_2, the MOSFET is turned-on under zero voltage switching condition, due to having the series of C_2 and L_2, as the spike of voltage or current can be absorbed by these two elements. During this mode, L_r is charged by the input source (which is the output of rectifier) and the series of capacitor and inductor resonate together. Eq. (5.12) shows the resonant current at the end of third mode while Eq. (5.13) is the resonant current calculated for this mode.

$$V_{c2}(t)=\left(2V_s+I_s\left(-jX_C+Z_D\right)\right)\left[1-\frac{(L_1+L_2)\omega_r}{Z_{eq}}\cos\left(\omega_r(t-t_2)\right)+\frac{\omega_r L_2}{Z_{eq}}\cos\left(\omega_r(t-t_2)\right)\right] \tag{5.12}$$

$$I_{L2}=\sin(\omega_r(t-t_2))\left[\left(\frac{\left(2V_s+I_s\left(-jX_C+Z_D\right)\right)-V_{out}}{L_1}\right)\sin\left(\cos^{-1}\frac{V_{out}L_1}{\omega_r L_2\left(\left(2V_s+I_s\left(-jX_C+Z_D\right)\right)-V_{out}\right)}\right)-\frac{V_{out}}{R_{out}}\right]\sin\left(\omega_r(t_2-t_1)\right) \tag{5.13}$$

Mode IV:

In this mode, the power of the input sources goes through the inductor L_1 to reach the output stage. Besides, the energy stored in the series of inductor and capacitor will be further transferred to the output stage too. Hence, in this mode, the existence of the series of capacitor and inductor is not only to provide the ZVS condition, but also to store and transfer the energy from input to output. By Eq. (5.14), Eq. (5.15) and Eq. (5.16), main current of converter, resonant current and voltage are obtained.

$$I_{L1}=\left(\frac{\left(2V_s+I_s\left(-jX_C+Z_D\right)\right)-V_{out}}{L_1}\right)\sin\left(\omega_r(t-t_3)\right)+I_{L1}(t_2) \tag{5.14}$$

Najmehossadat Nourieh
School of Physics, Engineering and Computer Science, University of Hertfordshire

$$I_{L2}=\left(\frac{\left(2V_s+I_s\left(-jX_C+Z_D\right)\right)-V_{out}}{L_1}\right)\sin\left(\omega_r(t-t_3)\right)-\frac{V_{out}}{R_{out}}+I_{L1}(t_2) \tag{5.15}$$

$$V_{C2}=\left(\frac{\left(2V_s+I_s\left(-jX_C+Z_D\right)\right)-V_{out}}{L_1C_2\omega_r}\right)\cos\left(\omega_r(t-t_3)\right)-\frac{V_{out}}{C_2R_{out}}(t-t_0) \tag{5.16}$$

5.2.2 Simulation Results of The Combination of Phase Shifter + 1-Stage Rectifier and DC/DC Converter

To verify the operation of this suggested combination, in the following paragraphs the results of simulated circuit in the environment of PSIM will be given. In Figure 5.2, the schematic of simulated circuit is presented. In Figure 5.3, the waveform of current I_{C2} is presented (it changes from -0.18uA to +0.18uA) while in Figure 5.4 the waveform of voltage V_{C2} is given (the peak voltage is 0.58V). Respectively, the

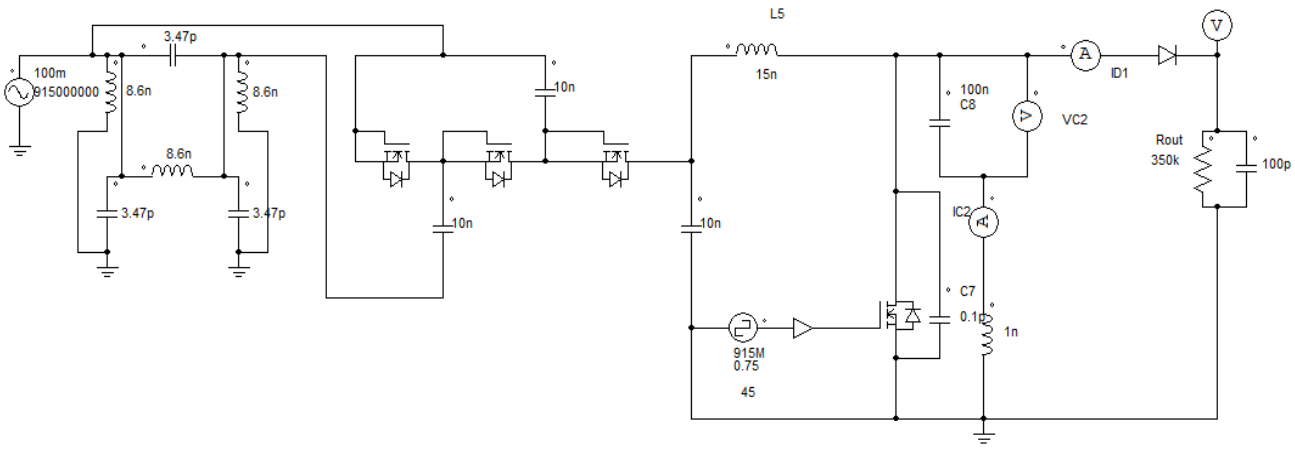

Figure 5.2 The schematic of the simulated circuit in PSIM

Najmehossadat Nourieh
School of Physics, Engineering and Computer Science, University of Hertfordshire

waveforms for I_{L1} (moves between 0.155uA and 0.185uA) and $V_{DS,MOSFET}$ are given in Figure 5.5 and Figure 5.6 respectively.

Relatively, in Figure 5.7, the output voltage (5V) of the combination of the proposed circuits is presented.

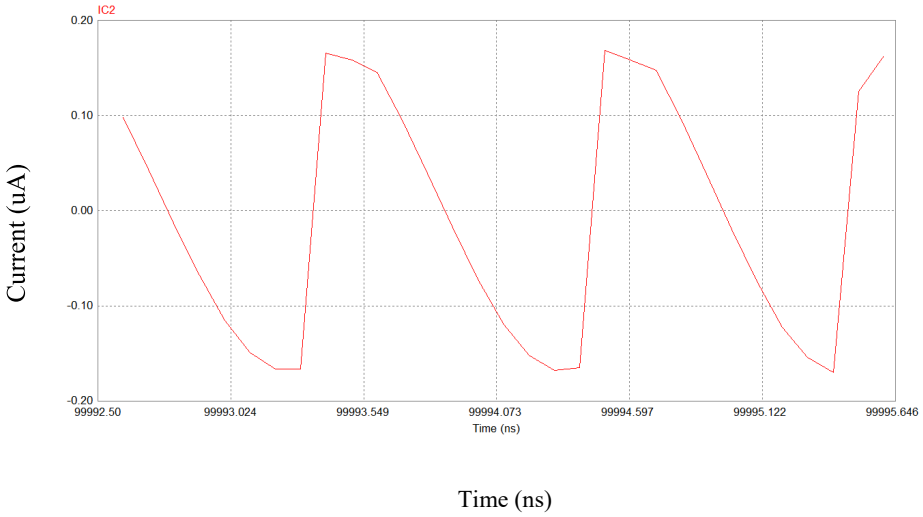

Time (ns)

Figure 5.3 The simulated waveform for I_{C2} and I_{L2}

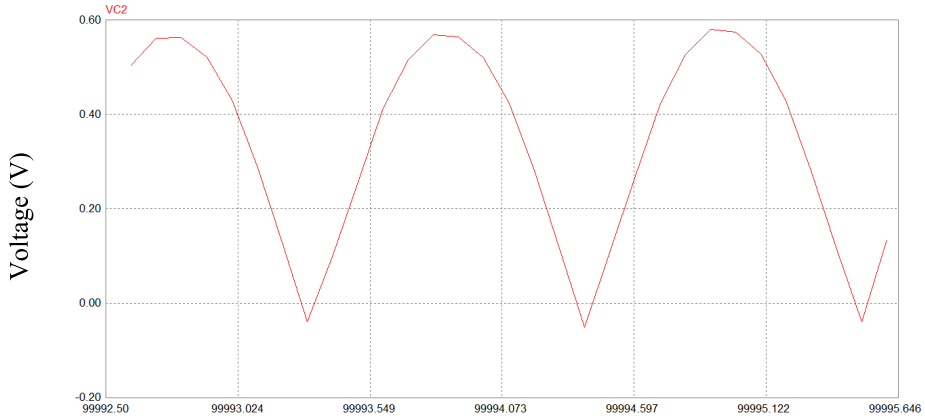

Figure 5.4 The simulated waveform for V_{C2}

Najmehossadat Nourieh
School of Physics, Engineering and Computer Science, University of Hertfordshire

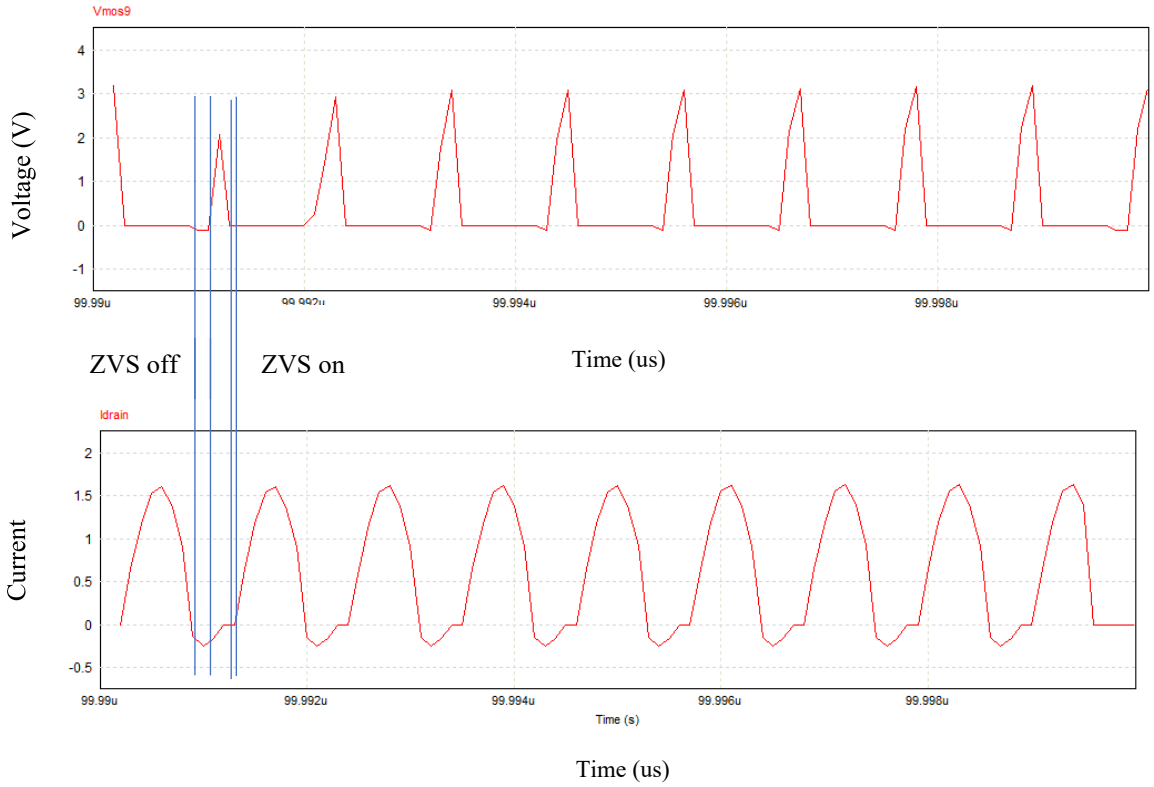

Figure 5.6 The simulated waveform for $V_{DS,MOSFET}$

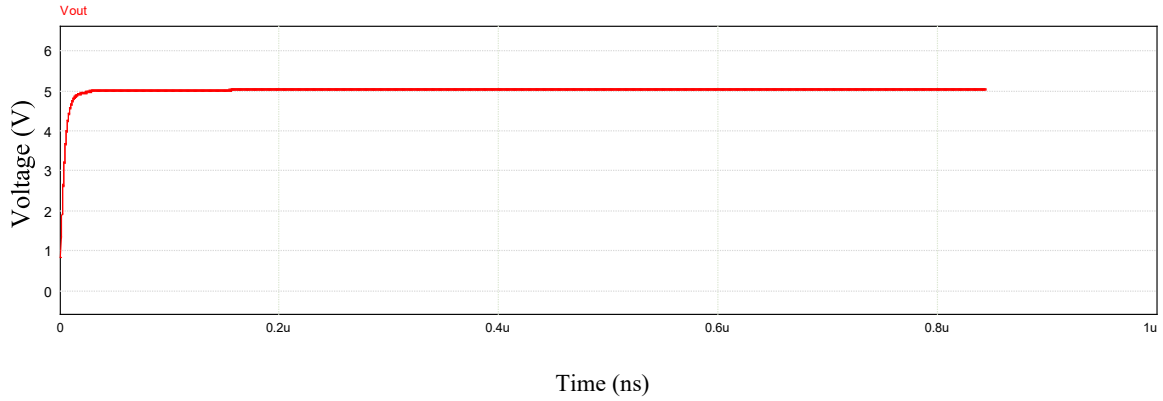

Figure 5.7 The output voltage of the proposed combination showing the steady state time

5.2.3. Practical Results of The Proposed Combination of Phase Shifter + Dickson Rectifier with non-Isolated Resonant DC to DC Converter Working under ZVS Condition

In this section, the practical results of non-isolated DC to DC converter are presented. As it is shown in the simulation of the circuit in PSIM, the value of main inductor L_1 =15nH, L_2= 1nH, C_2= 100p, R_{out}= 350K, diode, MOSFET and gate driver are SMS7630-079LF, LND150N3-G and FL73282. The switching frequency is also chosen to be 220kHz. The LND150n-3 is a high voltage N-channel depletion mode (normally-on) transistor utilizing Supertex's lateral DMOS technology. The gate is ESD protected. We need to use this type of MOSFETs as it always on until we apply very low voltage to the to turn it off. Hence, the energy consumed to turn MOSFET on and off is considerably low. By choosing this type of MOSFET (LND150N-3), the maximum calculated loss to run MOSFET is 11uWatt ($I_g=Q_g/t_{off}$=11uA , so the calculated power will be $P=I_g*V_g$ = 11uWatt). The threshold voltage of MOSFET to be turned off is -1V, which is lower for our application as I_d is around 1mA. However, we apply -1V (which will make more loss and therefore lower efficiency) to be sure the on/off time of MOSFET is compatible with the considered switching frequency. For V_{gs}=-1V, Q_g=16nC and the turn off time of MOSFET is 1.45uS. Therefore, the energy consumed by MOSFET to be turn on and off is 11uWatt.

In order to reduce the power loss in MOSFET, it is strongly recommended (for the future works) to use self-driven method with the Same type of MOSFETs, if the circuit will be applied in energy harvesting applications. Then, the circuit will be independent which can generate the gate signal from the harvested energy.

In Figure 5.8, the laboratory environment to test ZVS DC to DC converter along with 1-stage rectifier and phase shifter is shown. The initial input power and voltage is considered to be -10dBm and 100mV respectively. The circuit has been tested for different input power of -10dBm, -8dBm and -6dBm. As all three circuits are designed to work with -10dBm, we cannot apply more powerful signal more than -6dBm to not damage components. We used the specified cables as phase shifter (which is discussed in Chapter 3).

Najmehossadat Nourieh
School of Physics, Engineering and Computer Science, University of Hertfordshire

Figure 5.9 presents the output voltage of proposed combination for input power of -6dBm, -8dBm and -10dBm. For input power of -10dBm, the output voltage is 4.75V, for -8dBm and -6dBm it is 5.2V and 5.95V respectively.

Figure 5.10 shows practical performance of DC to DC converter with 1-stage rectifier for range of different output voltages. For the input power of -10dBm, the output voltage for resistor of 350kΩ is 4.75V and the efficiency is equal to 63.1%. Then, the input power of -8dBm increases the output voltage to 5.2V, but the efficiency is dropped to 49%. Moreover, for the input power of -6dBm, the output voltage and efficiency are 5.95V and 40.2% respectively.

In Figure 5.11, the ZVS condition of proposed circuit is shown. As it is defined in figure, MOSFET turns on and off under ZVD condition, which means the switching loss is close to be zero.

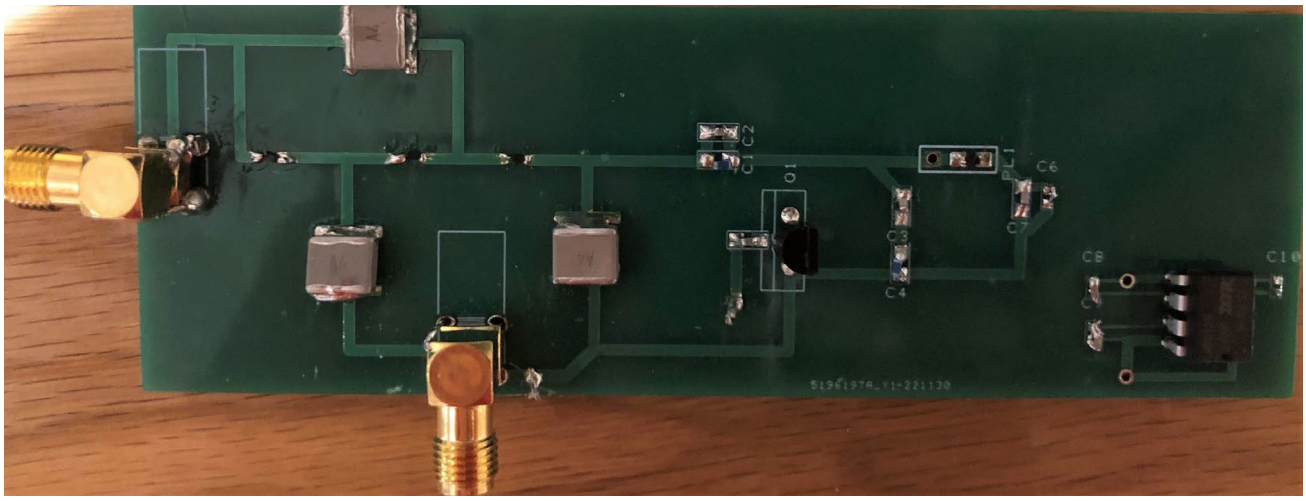

Figure 5.8 The PCB board of proposed combination

Najmehossadat Nourieh
School of Physics, Engineering and Computer Science, University of Hertfordshire

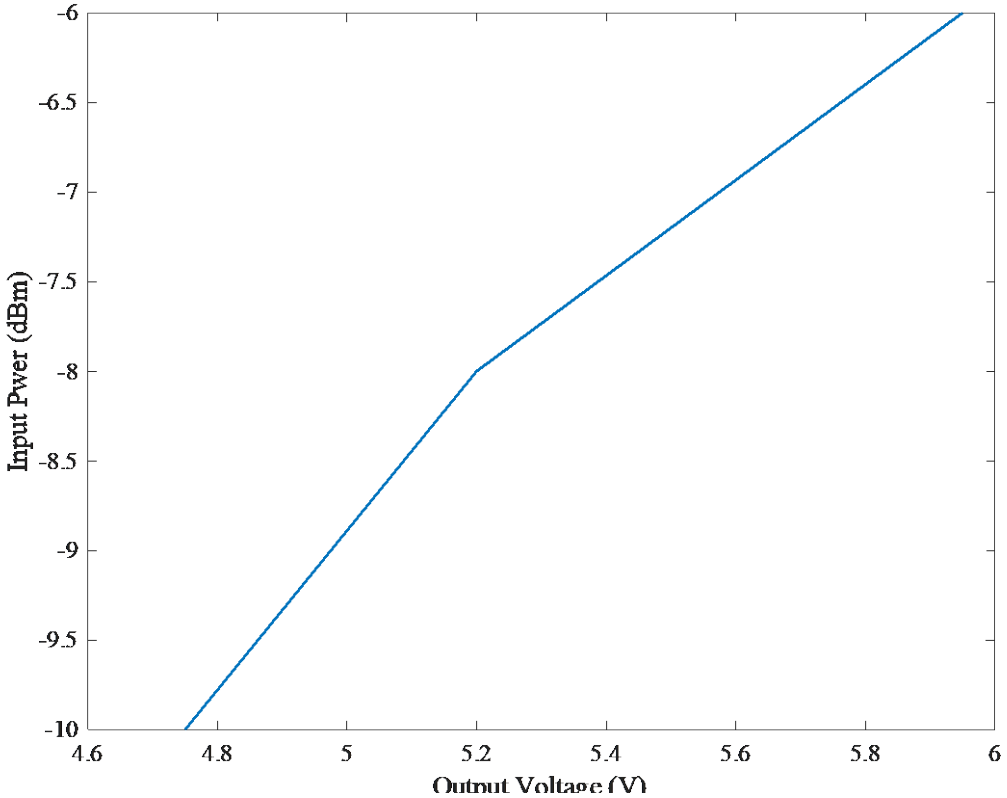

Figure 5.9 The output voltage of circuits for -10dBm, -8dBm and -6dBm.

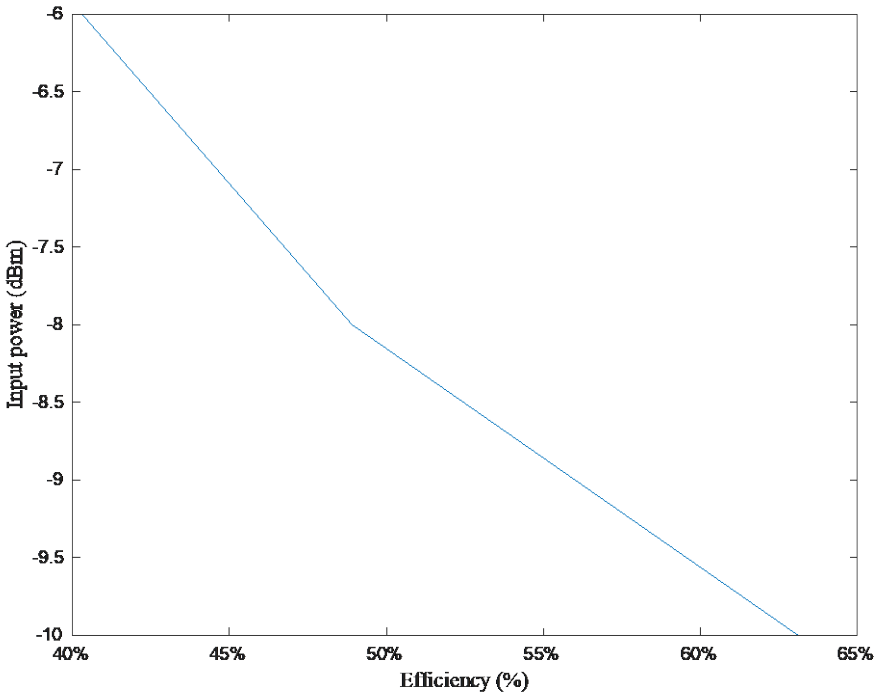

Figure 5.10. The input power via efficiency for -10dBm, -8dBm and -6dBm.

Najmehossadat Nourieh
School of Physics, Engineering and Computer Science, University of Hertfordshire

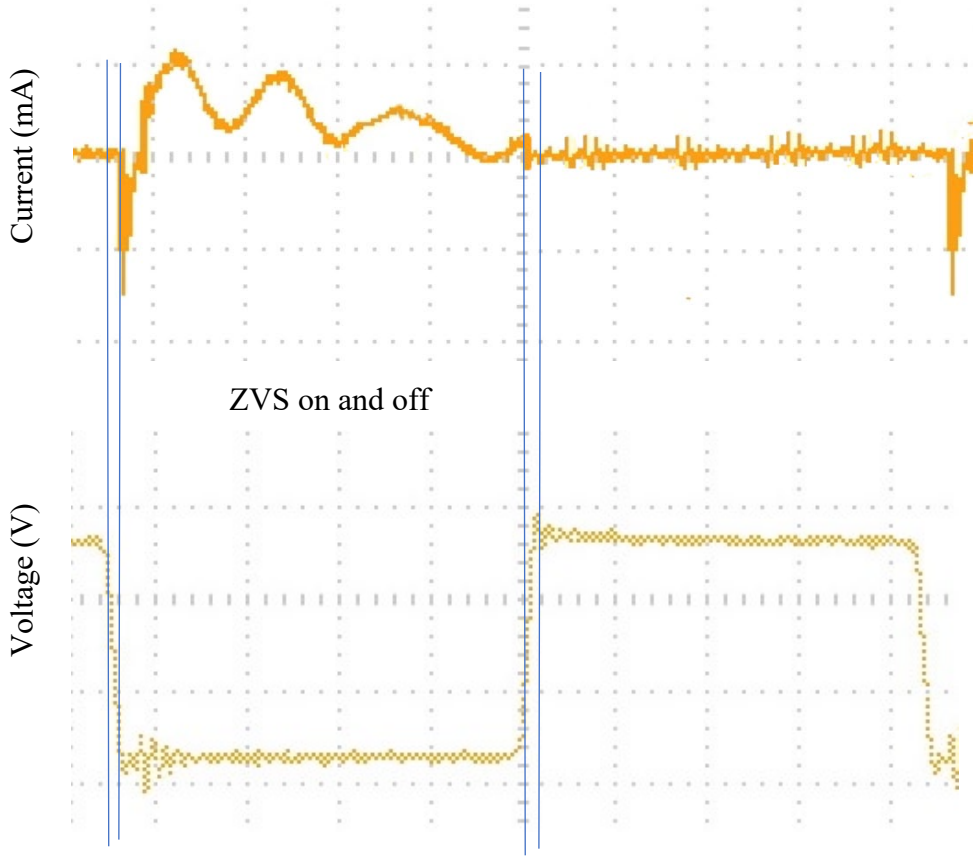

Figure 5.11. The drain-source current and voltage of MOSFET which show ZVS turn-on and turn-off condition (500ns/div , 1mA/div, 100mV/div)

5.3 The Proposed Combination of Phase Shifter + Dickson Rectifier with Isolated Resonant DC to DC Converter Working under ZVS Condition

As we have discussed before, the suggested 7-stage Dickson rectifier has restriction on the range of produced output voltage leading to limit the appropriate applications. To solve this issue, we have proposed the combination of phase shifter, 1-stage of modified Dickson rectifier following an isolated resonant DC to DC converter which gives us more capability to produce higher output voltages, providing larger range of applications for this RF energy harvesting system.

Najmehossadat Nourieh
School of Physics, Engineering and Computer Science, University of Hertfordshire

In this section, we will propose a new combination of Dickson rectifier with two input sources working with an isolated ZVS resonant DC to DC converter which has the advantage of isolation in the applications where it is more critical. The schematic circuit of the proposed combination is presented in Figure 5.8.

In this combination, shown in Figure 5.12, the output power of 1-stage rectifier will be used as the input source of DC to DC converter. The operation of rectifier with dual input sources (with 180° phase shift) was discussed in previous chapter. In this chapter, we will focus on the operation of converter working along with the rectifier. The parameters, α and β are used to simplify equations and B is the converter normalized voltage gain, $B=nA=nV_o/V_s$. The parameters φ_1 and φ_2 are the conduction angles of Q_1 and Q_2 respectively. In each operation mode $I_{number} = i_r(t_{number})$.

$$\omega_r=2\pi f_r=\frac{2\pi}{T_r},\ R_o=\frac{n^2V_o^{\ 2}}{P_{out}} \tag{5.17}$$

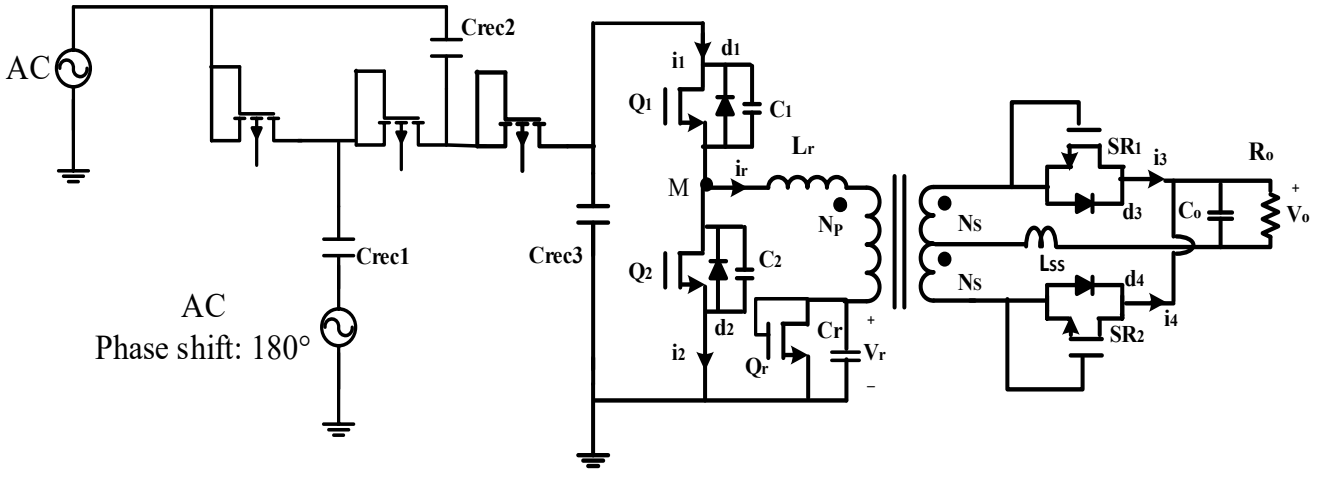

Figure 5.12 The schematic of the proposed combination

Najmehossadat Nourieh
School of Physics, Engineering and Computer Science, University of Hertfordshire

$$B=n\frac{V_o}{V_s}=nA,\ Z_r=\sqrt{\frac{L_r}{C_r}} \tag{5.18}$$

$$\alpha=\frac{C_r}{C_1+C_2},\ \beta=\frac{1+\alpha}{\alpha},\ \omega_\alpha=\sqrt{1+\alpha\omega_r} \tag{5.19}$$

Mode I:

In the mode before t_1, the diode d_1 was conducting to provide ZVS condition for switch Q_1 to be turned on at t_1. Thus, resonant capacitor C_r is charged through resonance with L_r until t_1. Appling Eq. (5.20) and Eq. (5.21), the resonant voltage and current are achieved.

$$V_r(t)=(2V_s+I_s(-jX_C+Z_D))(1-B)\left[1-\cos\left(\omega_r(t-t_0)\right)\right] \tag{5.20}$$

$$I_r(t)=\frac{(2V_s+I_s(-jX_C+Z_D))}{Z_r}\left[(1-B)\sin\left(\omega_r(t-t_0)\right)\right] \tag{5.21}$$

Mode II:

When the switch Q_1 is turned off at t_1, the remained current available in L_r will flow through C_1 and C_2. Hence, the voltage at node V_m (Eq. 5.22) will be decreased from Vs to zero. Eq. (5.23) shows resonant current.

$$V_M(t)=(2V_s+I_s(-jX_C+Z_D))\ [1+\alpha(1-B)(1-\cos\varphi)-\alpha V(t)] \tag{5.22}$$

$$I_r(t)=\frac{(2V_s+I_s(-jX_C+Z_D))}{Z_r}\left[[(1-B)\cos\varphi_1/(\sqrt{1+\alpha})]\sin\left(\omega_\alpha(t-t_1)\right)+[(1-B)\sin\varphi_1]\cos\varphi_1\left(\omega_\alpha(t-t_1)\right)\right] \tag{5.23}$$

Mode III:

At t_2, the diode d_2 is direct biased under ZVS condition at which the current flows until it reaches zero at t_3. In this interval, the signal for Q_2 will be ready to turn Q_2 on in the next operational mode.

Najmehossadat Nourieh
School of Physics, Engineering and Computer Science, University of Hertfordshire

$$T_3=1/\omega_r\left(\tan^{-1}\left(\frac{I_2}{(V_2+B)}\right)\right) \quad (5.24)$$

$$V_3=\sqrt{(-2(1-B)\cos\varphi_1+(1-B)^2+1+1/\alpha)} \quad (5.25)$$

Mode IV:

At t_3, the energy stored in resonant capacitor will be transferred to the output stage through L_r and Q_2. Eq. (5.26) and Eq. (5.28), show the resonant voltage and the current at the end of this mode.

$$V_r(t)=(2V_s+I_s(-jX_C+Z_D))(1-B)(\sin\omega_r(t-t_3)) \quad (5.26)$$

$$I(t)=(B-V_3)\sin\omega_r(t-t_3) \quad (5.27)$$

$$I_4=(B-V_3)^2-B^2 \quad (5.28)$$

Mode V:

At t_4, the diode D_r is turned on under ZVS condition and the current i_r flows through it. The energy remained in L_r provides ZVS condition to turn the switch Q_2 off. Hence, the switch Q_2 will be turned off at t_5 under ZVS condition. In this mode, the energy stored in L_r is transferred.

$$V_r(t)=(2V_s+I_s(-jX_C+Z_D))\left[1+\alpha(1-B)\left(1-\cos(\omega_r(t-t_4))\right)\right] \quad (5.29)$$

$$I(t)=B\omega_r(t-t_4)+I_4 \quad (5.30)$$

Mode VI:

In this mode, the voltage V_m will reach zero level and the voltage of d_1 is set to be turned on in the next mode. Appling Eq. (5.31) and Eq. (5.32), the resonant voltage and current are achieved.

Najmehossadat Nourieh
School of Physics, Engineering and Computer Science, University of Hertfordshire

$$V_r(t)=(2V_s+I_s(-jX_C+Z_D))[1+\alpha(1-B)\sin(\omega_r(t-t_5))+\cos(\omega_r(t-t_5))] \quad (5.31)$$

$$I_6=-\sqrt{I_5^2-\left(\frac{1+2B}{\alpha}\right)} \quad (5.32)$$

Mode VII:

In t_6, the diode d_1 is turned on under ZVS condition and the resonant current flows through it until it reaches the zero level. In this mode, the gate signal of Q_1 will be ready to turn it on in the next mode. Calculating Eq. (5.20) and Eq. (5.21), the resonant voltage and current are achieved.

$$I_r(t)=(1+B)\sin\left(\omega_r(t-t_6)\right)+I_6 \quad (5.33)$$

$$V_r(t)=(2V_s+I_s(-jX_C+Z_D))\left[(1-B)(1/\sqrt{\alpha})\sin\left(\omega_r(t-t_6)\right)+B\cos\left(\omega_r(t-t_6)\right)\right] \quad (5.34)$$

The verification of given formulas and analyses gained from MATLAB software have been given in Appendix 2.

5.3.1 Simulation results of the combination of Phase Shifter, 1-Stage Rectifier and An Isolated DC to DC Converter in PSIM Software

In this section, all the simulation results obtained for the proposed circuit combination are presented. In Figure 5.13, the schematic of the proposed circuit designed in PSIM software is presented. Figure 5.14 shows the waveform of output voltage (6V). In Figure 5.15, the simulation results of $V_{drain\text{-}source}$ of Q_1 and drain-source current are presented to show ZVS condition is met for this switch.

Respectively, in Figure 5.16, the simulation results of $V_{drain\text{-}source}$ of Q_2 and drain-source current are presented to show ZVS condition is met for this switch.

Najmehossadat Nourieh
School of Physics, Engineering and Computer Science, University of Hertfordshire

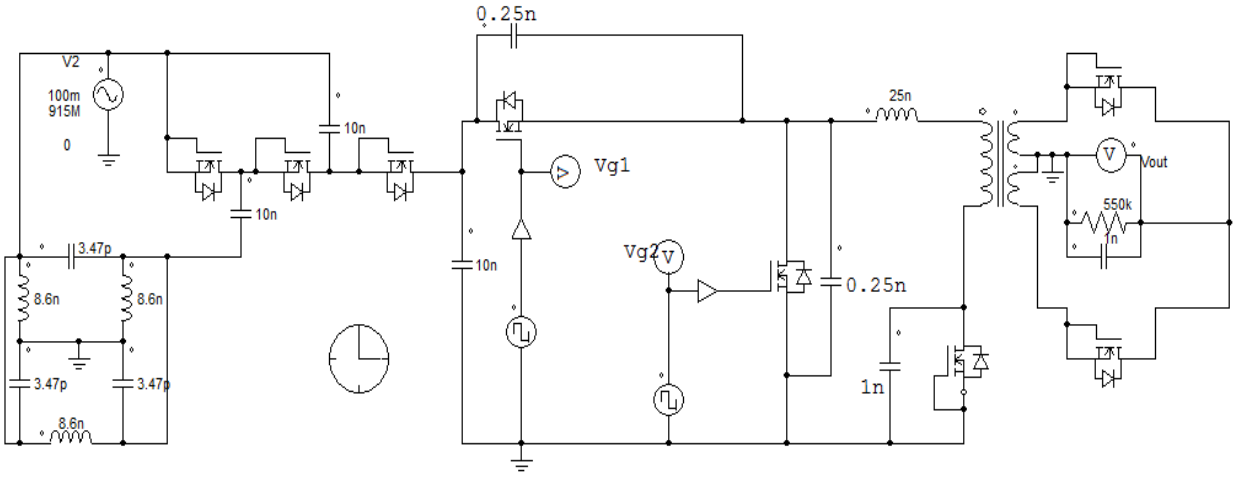

Figure 5.13 Schematic of three circuits working together

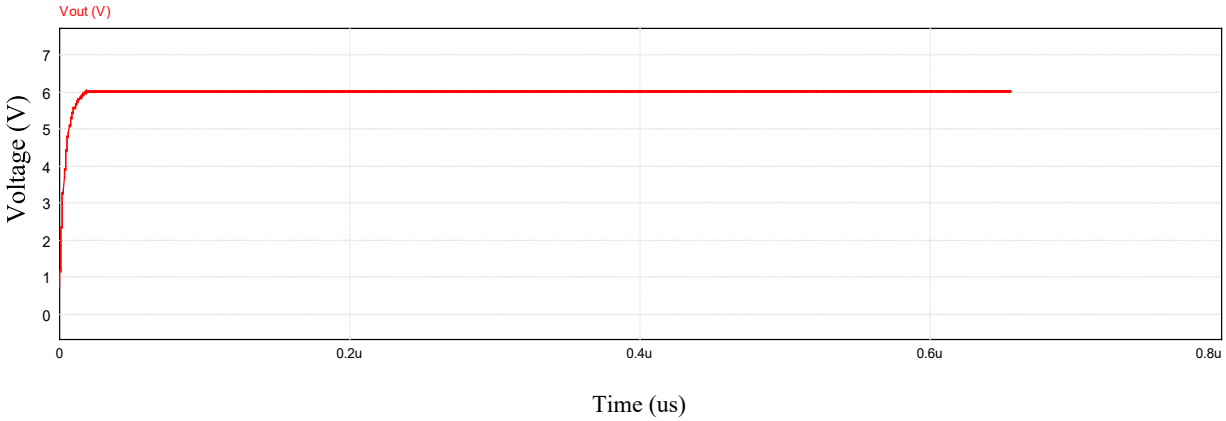

Figure 5.14 The graph of output voltage

Najmehossadat Nourieh
School of Physics, Engineering and Computer Science, University of Hertfordshire

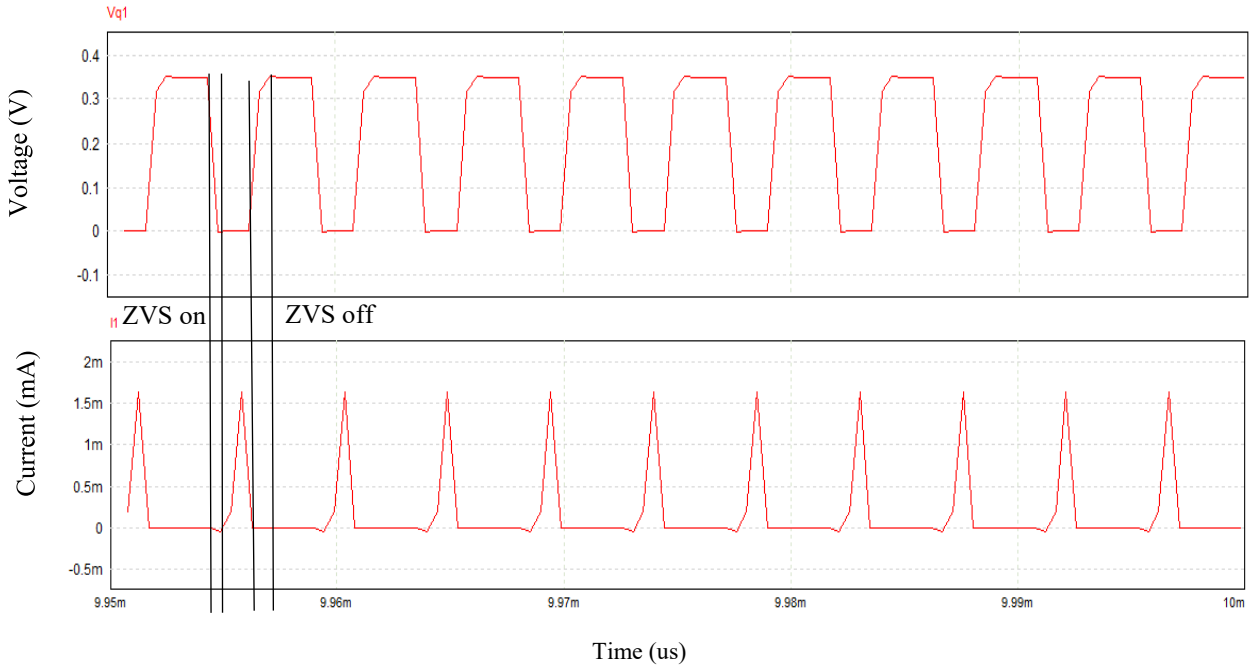

Figure 5.15 The voltage and current of drain-source in Q_1 with ZVS condition

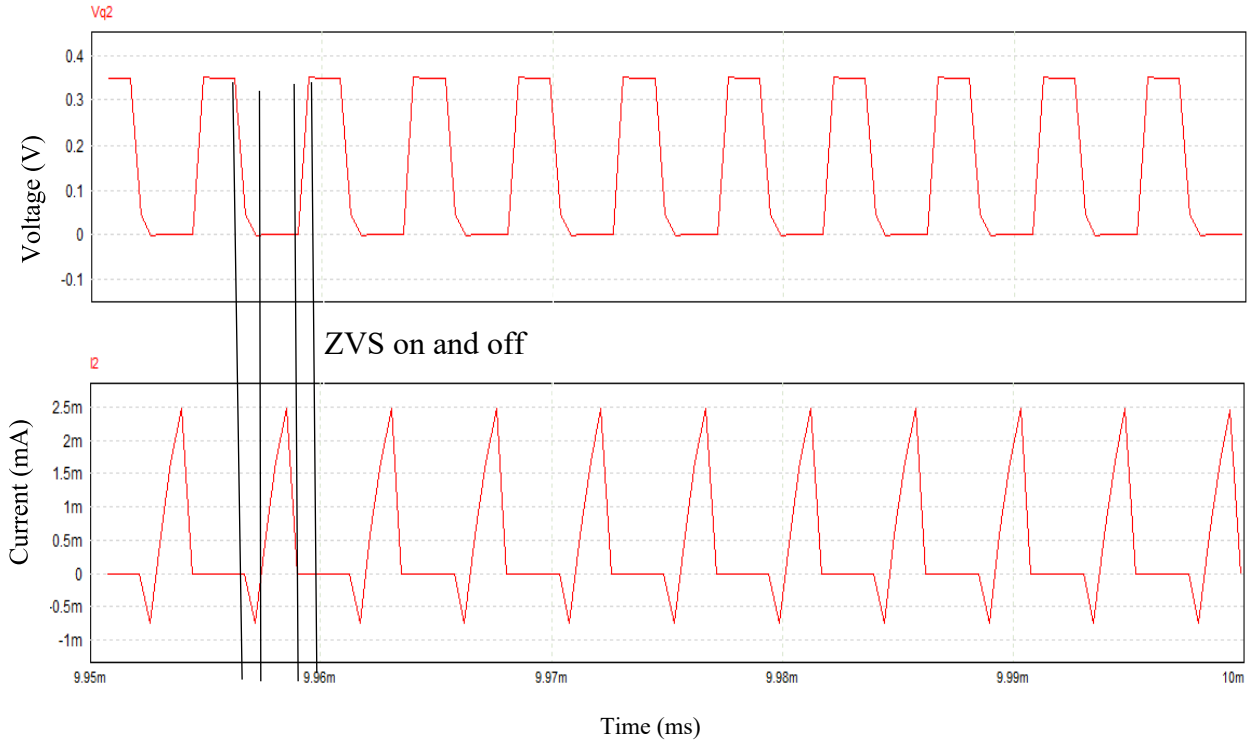

Figure 5.16 The voltage and current of drain-source in Q_2 with ZVS condition

5.4 Conclusion

Najmehossadat Nourieh
School of Physics, Engineering and Computer Science, University of Hertfordshire

In this chapter, two combinations of high voltage gain circuits are introduced for low power applications such as RFEH. The first combination consists of a phase shifter, 1-stage rectifier and resonant ZVS DC to DC converter which produces the output voltage of 6V with the efficiency of 71%. The second, consists of a phase shifter, 1-stage rectifier and isolated resonant ZVS DC to DC converter with the output voltage and efficiency of 5V and 65% respectively. These two circuits are theoretically discussed, and the simulation results are presented to verify their operation.

Najmehossadat Nourieh
School of Physics, Engineering and Computer Science, University of Hertfordshire

6 Conclusion and Future Work

6.1 Conclusion

The sources for WEH are available in many forms, such as solar power, wind energy, thermal energy, electromagnetic energy, kinetic energy, etc. Among them, electromagnetic energy is abundant in space and can be retrieved without limitation. Electromagnetic waves come from a variety of sources such as satellite station, wireless internet, radio station, and digital multimedia broadcasting. A radio frequency power harvesting system can capture and convert electromagnetic energy into a usable direct current (DC) voltage.

This PhD research proposed new RF to DC circuits to amplify the voltage of low power sources in different applications such as radio frequency energy harvesting (RFEH). The presented circuits were discussed in theory, simulation and implementation phases. The presented works are novel energy-efficient circuits including phase shifter, modified Dickson rectifier with one and seven stages and isolated/non-isolated resonant ZVS DC to DC converters. These circuits maximized the energy harvested from RF sources and converted it to DC output with the desired range of voltages for different applications. Proposing the novel techniques to harvest energy from radio waves, is involved in designing novel circuits capable of gaining energy from RF sources and converting RF to DC (rectifier) which could also amplify the voltage, followed by DC to DC converters with specific output voltages. In this thesis, the analysis and design of the dual input rectifiers (1-stage and 7-stage), isolated and non-isolated DC to DC converters, and phase shift circuit were presented.

The key units of an RF power harvesting system are the antenna and rectifier circuit that allows the RF power or alternating current (AC) to be converted into DC energy. The processing of battery wastes is a critical problem. Most batteries end up in landfills, leading to the pollution of the land and water

underneath. The most effective solution for reducing battery wastes is to replace them with possible alternatives. Applying WPH technology will help to reduce the dependency on batteries, which will ultimately have a positive impact on the environment.

In this thesis, comprehensive analysis and discussions of various designs of rectifiers, isolated and non-isolated DC to DC converters and phase shifters in addition to their trade-offs for RF energy harvesting purposes are included. After discussions, simulation results and analysis are presented of some recent works are presented.

This thesis shows a novel analytical model for the voltage multiplier/rectifier at the frequency of 915MHz. The suggested model proposes a new method of deriving output characteristics of the rectification circuit in terms of two main factors, voltage and current. The design consists of different stages of Dickson voltage multiplier rectifier. In chapter 3, phase shifters and different Dickson rectifiers with two input signals in one and seven stages were discussed theoretically followed by simulation and practical results. In this chapter the prototype of 1-stage rectifier is presented where the input voltage is between -10dBm and 2dBm and the output voltage is gained from 318mV to 1700mV. Also, the prototype of 7-stage rectifier is presented where the input voltage is between -10dBm and -6dBm and the output voltage is gained from 1220mV to 1550mV.

In addition, a new non-isolated DC to DC resonant converter working under zero-voltage switching condition has been introduced, which can work in high frequencies with high power conversion rate and efficiency as well as low losses. The proposed converter can provide 5V output from 350mV input voltage with efficiency of 72.8%. Furthermore, we proposed an isolated DC to DC converter which provides the output voltage of 6V and more with efficiency of 68%. Due to the isolation, this converter is proper for applications required more safety. All the theoretical analyses are verified by MATLAB and circuits are simulated in PSIM. The two DC to DC converters have advantages such as zero voltage switching (a. Low switching loss, b. Low capacitance loss, c. High power density), resonance (a. Increase switching

Najmehossadat Nourieh
School of Physics, Engineering and Computer Science, University of Hertfordshire

frequency, b. Increase efficiency, c. Low EMI and noise), and diode-connected MOSFETs in rectification part (a. Low conduction loss, b. Low thermal loss). For the isolated converter the advantage of isolation gives more safety to the system for the applications which circuit safety is very critical (such as medical application).

In this thesis, two combinations of high voltage gain circuits are introduced for low power applications such as RFEH. The first combination consists of a phase shifter, 1-stage rectifier and resonant ZVS DC to DC converter which produces the output voltage of 6V with the efficiency of 71%. The second, consists of a phase shifter, 1-stage rectifier and isolated resonant ZVS DC to DC converter with the output voltage and efficiency of 5V and 65% respectively. These two circuits are theoretically discussed, and the simulation results are also presented to verify their operation.

As shown in Table 6.1, the 7-stage diode-based rectifier with dual input signals (produced by phase shifter to have 180° phase difference) provides an output voltage of 1220mV with the efficiency of 74%, where the combination of phase shifter, 1-stage diode-connected MOSFET rectifier with two inputs, and isolated DC to DC converter can produce 6V with 65% of efficiency. Furthermore, the combination of phase shifter, 1-stage diode-connected MOSFET rectifier with two inputs, and non-isolated DC to DC converter provides output voltage and efficiency of 5V and 71% respectively.

Najmehossadat Nourieh
School of Physics, Engineering and Computer Science, University of Hertfordshire

TABLE 6.1
COMPARISON OF ALL PROPOSED CIRCUITS IN THIS THESIS

	Test Environment	Number of Elements	Input Power(uWatt)	Input Voltage(mV)	Output Power(uWatt	Output Voltage(V)	Efficiency
Isolated DC/DC converter	Simulation	10+External gate driver	100	350	77.28	6.07	68%
DC/DC converter	Simulation	8+External gate driver	100	350	81.76	5.05	73%
1-stage Dickson rectifier with diode	Practical circuit	7	100	100	34.13	0.32	34.13%
7-stage Dickson rectifier with diode	Practical circuit	29	100	100	74	1.22	74%
1-stage Dickson rectifier with diode-connected MOSFET	Simulation	7	100	100	38.5	0.34	38.50%
7-stage Dickson rectifier with diode-connected MOSFET	Simulation	29	100	100	79.38	1.26	79.38%
1-stage Dickson rectifier with diode-connected MOSFET + Isolated DC/DC converter	Simulation	17+External gate driver	100	100	65	6	65%
1-stage Dickson rectifier with diode-connected MOSFET + DC/DC converter	Simulation	15+External gate driver	100	100	71	5	71%
1-stage Dickson rectifier with diode-connected MOSFET + DC/DC converter	Practical circuit	15+External gate driver	100	100	63.1	4.75	63%

Najmehossadat Nourieh
School of Physics, Engineering and Computer Science, University of Hertfordshire

6.2 Future Work

This thesis basically offers three combinations of different circuits to be used for low power applications specifically RF energy harvesting systems. Along with the proposed circuits, this thesis suggests future improvements on the suggested system to develop the whole system offering a wider range of applications.

6.2.2 Dickson Rectifier

For the proposed Dickson rectifier, we used diode-connected MOSFET as a rectifying component, we also applied two input signals with a 180° phase difference. For this circuit, if we use the ON resistance of the MOSFET by generating the proper gate signal to turn transistors on, the drop voltage on each rectifying device should be less.

Furthermore, we can run all the MOSFETs by generating signals from coupled inductors, using the inductor in phase shift circuit. In this system, we will apply self-driven method to generate proper signals for turning MOSFETs on.

To enhance this circuit, if the MOSFETs are run to transfer energy, a control system will be required to also analyse feedback loops, controlling all rectifying devices.

6.2.3 Isolated DC to DC Converter

The proposed isolated resonant DC to DC converter provides zero-voltage-switching condition for all switches. This step-up converter is offered to boost the voltage for specific applications. In order to further enhance this circuit, the main improvement should be design of self-driven method to run the main switch and get rid of external gate driver.

To have better function, we can increase the switching frequency to have smaller size components which consequently produce less losses and operate more efficiently with smaller package.

Moreover, the design of the transformer can be developed to be smaller by trying different kinds of transformer cores and setting smaller gaps between two sides of the core which can significantly affect the leakage inductance and capacitance of the transformer.

Another potential future work could be the study on the control circuit which can relatively work with feedback loops to control both switches in the primary side of transformer. Furthermore, by applying synchronous rectifier at the secondary section of this converter, the advantages such as less losses and higher efficiency can be achieved.

6.2.4 Non-Isolated Resonant DC to DC Converter

In chapter 4, a new resonant DC to DC converter is introduced. This converter has high voltage gain with relatively high efficiency comparing to other works. An important development for this circuit can be the self-driven method to run the main switch of this circuit. It can be easily applied if we use coupled inductors for the main inductor in the initial section. We can also use the resonant inductor to be coupled with another one and produce the signal to run the MOSFET.

In addition, by studying the combination of the resonant capacitor and inductor, another potential future work is to increase the resonant frequency which consequently requires smaller components with better operation.

Najmehossadat Nourieh
School of Physics, Engineering and Computer Science, University of Hertfordshire

REFERENCES

[1] Z. Khonsari, T. Bjorninen Manos, M. Tentzeris, L. Sydanheimo and L. Ukkonen, "Inkjet-printed monopole antenna and voltage doubler on cardboard for RF energy harvesting", IEEE APS/URSI, pp. 1312-1313, 19–24 July 2015.

[2] Z. Hameed and K. Moez, "Design of impedance matching circuits for RF energy harvesting systems", Microelectronics Journal, vol. 62, pp. 49-56, April 2017.

[3] H. Dai, Y. Lu, M.-K. Law, S.-W. Sin, S.-P. U and R.P. Martins, "A review and design of the on-chip rectifier for RF energy harvesting", IEEE International Wireless Symposium, pp. 1-4, 30 Mar.-l Apr. 2015.

[4] N. Pournoori, M. W. A. Khan, L. Ukkonen and T. Björninen, "RF Energy Harvesting System Integrating a Passive UHF RFID Tag as a Charge Storage Indicator", IEEE International Symposium on Antennas and Propagation & USNC/URSI National Radio Science Meeting, 2018.

[5] Y. Zhu et al., "An Energy Autonomous 400 MHz Active Wireless SAW Temperature Sensor Powered by Vibration Energy Harvesting", IEEE Trans. Circuits and Systems. I, Reg. Papers, Vol. 62, No. 4, pp. 2015.

[6] Y. Sun and J. K. Fidler, "Design method for impedance matching networks", IEE Proc. Circuits, Devices and Systems, Vol. 143, No. 4, pp 186 – 194, 1996.

[7] M. K. Karami and K. Moez, "Systematic Co-Design of Matching Networks and Rectifiers for CMOS Radio Frequency Energy Harvesters" IEEE Trans. on Circuits and Systems, 1109/TCSI.2019.2902506, AUG 2019.

[8] T. Soyata, L. Copeland and W. Heinzelman, "RF Energy Harvesting for Embedded Systems: A Survey of Tradeoffs and Methodology", IEEE Circuits Syst. Mag., vol. 16, no. 1, pp. 22–57, 1st Quart, 2016.

[9] A. Khaligh, P. Zeng and C. Zheng, "Kinetic Energy Harvesting Using Piezoelectric and Electromagnetic Technologies—State of The Art", IEEE Trans. Ind. Electron., Vol. 57, No. 3, pp. 850–860, Mar. 2010.

[10] X. Lu and S.-H. Yang, "Thermal Energy Harvesting for WSNs", in Proc. IEEE Int. Conf. Syst., Man Cybern., Oct. 2010, pp. 3045–3052.

Najmehossadat Nourieh
School of Physics, Engineering and Computer Science, University of Hertfordshire

[11] V. Raghunathan, A. Kansal, J. Hsu, J. Friedman, and M. Srivastava, "Design Considerations for Solar Energy Harvesting Wireless Embedded Systems", in Proc. IEEE IPSN, Apr. 2005, pp. 457–462.

[12] J. Qian et al., "A Passive UHF Tag For RFID-Based Train Axle Temperature Measurement System", in Proc. IEEE Custom Integr. Circuits Conf. San Jose. USA, pp. 1–4, Sep. 2011.

[13] P. Saffari, A. Basaligheh, V. J. Sieben, and K. Moez, "An RF-Powered Wireless Temperature Sensor for Harsh Environment Monitoring with Nonintermittent Operation", IEEE Trans. Circuits Syst. I, Reg. Papers, Vol. 65, No. 5, pp. 1529–1542, May 2018.

[14] M. H. Ouda, M. Arsalan, L. Marnat, A. Shamim, and K. N. Salama, "5.2-GHz RF Power Harvester In 0.18-µm CMOS For Implantable Intraocular Pressure Monitoring", IEEE Trans. Microw. Theory Techn, Vol. 61, No. 5, pp. 2177–2184, May 2013.

[15] Z. Hameed, K. Moez, "Hybrid Forward and Backward Threshold- Compensated RF-DC Power Converter for RF Energy Harvesting", IEEE Journal on Emerging and Selected Topics in Circuits and Systems ,Vol. 4, No. 3, 2014

[16] U. Karthaus and M. Fischer, "Fully Integrated Passive UHF RFID Transponder IC with 16.7-/muW Minimum RF Input Power", IEEE J. Solid-State Circuits, Vol. 38, No. 10, pp. 1602–1608, Oct. 2003.

[17] H. Jabbar, Y. Song, and T. Jeong, "RF Energy Harvesting System and Circuits for Charging of Mobile Devices", IEEE trans. Consum. Electron., Vol. 56, No. 1, pp. 247–253, Feb. 2010.

[18] J. P. Curty, N. Joehl, C. Dehollain, andM. J. Declercq, "Remotely Powered Addressable UHF RFID Integrated System", IEEE J. Solid State Circuits, Vol. 40, No. 11, pp. 2193–2202, Nov. 2005.

[19] F. Kocer and M. P. Flynn, "A New Transponder Architecture with On-Chip ADC For Long-Range Telemetry Applications", IEEE J. Solid-State Circuits, Vol. 41, No. 5, pp. 1142–1148, May 2006.

[20] Y. Sun, J. Moritz and X. Zhu, "Adaptive impedance matching and antenna tuning for green software defined and cognitive radio", (Invited Paper), 54th IEEE MWSCAS, Seoul, Korea, August 2011.

[21] Y. Tan, Y. Sun and D. Lauder, "Automatic impedance matching and antenna tuning using quantum genetic algorithms for wireless and mobile communications", IET Antenna, Microwave and Propagation, Vol.7, No.8, pp.693-700, 2013.

[22] B. Li, X. Shao, N. Shahshahan, N. Goldsman, T. Salter, and G.Metze, "An Antenna Co-Design Dual Band RF Energy Harvester", IEEE Trans. Circuits and Systems. I, Reg. Papers, Vol. 60, No. 12, pp. 3256–3266, Dec. 2013.

[23] T. Le, K. Mayaram, and T. Fiez, "Efficient Far-Field Radio Frequency Energy Harvesting for Passively Powered Sensor Networks", IEEE J. Solid-State Circuits, Vol. 43, No. 5, pp. 1287–1302, May 2008.

[24] J. Shin, I. Y. Chung, Y. J. Park, and H. S. Min, "A New Charge Pump Without Degradation in Threshold Voltage Due to Body Effect [Memory Applications] ", IEEE J. Solid-State Circuits, Vol. 35, No. 8, pp. 1227–1230, Aug. 2000.

[25] D-S. Liu, F.-B. Li, X.-C. Zou, Y. Liu, X-M. Hui, and X- F. Tao, "New Analysis and Design of a RF Rectifier for RFID and Implantable," Sensors, Vol. 11, No. 7, pp. 6494–6508, 2011.

[26] K-H. Choi, J-M. Park, J-K. Kim, T-S. Jung, and K-D Suh, "Floating-Well Charge Pump Circuits for Sub-2.0 V Single Power Supply Flash Memories," in Proc. Symp. VLSI Circuits, pp. 61–62, 1997.

[27] Z. Wang and S. Mirabbasi, "A low-voltage CMOS rectifier with on-chip matching network and a magnetic field focused antenna for Wirelessly powered medical implants", IEEE Trans. Biomed. Circuits Syst., Vol. 13, No. 3, pp. 554-565, Jun. 2019.

[28] S. Eardprab and C. Chanadee, "Implementation of RF Energy Harvesting System with Efficiency Improvement by Using Metamaterials," 2021 7th International Conference on Engineering, Applied Sciences and Technology (ICEAST), 2021.

[29] G. Saini, L. Somappa and M. S. Baghini, "A 500-nW-to-1-mW Input Power Inductive Boost Converter With MPPT for RF Energy Harvesting System," in IEEE Journal of Emerging and Selected Topics in Power Electronics, Vol. 9, No. 5, pp. 5261-5271, Oct. 2021.

[30] Z. Liang and J. Yuan, "An Event-Driven Multi-Input Multi-Output BuckBoost Converter with Adaptive MPPT for Wide Power Range RF Energy Harvesting," 2021 IEEE International Symposium on Circuits and Systems (ISCAS), 2021.

[31] C. P. Singh, S. Kumar Pandey and J. Singh, "Body Connection Assessment of MOS-Diodes for MOS-Quadruple based RF Energy Harvesting Circuit," 2021 Devices for Integrated Circuit (DevIC), 2021.

[32] R. Wang, Y. Qi and H. M. Lavasani, "A Highly Efficient CMOS Rectifier for Ultra-Low-Power Ambient RF Energy Harvesting," 2021 IEEE International Midwest Symposium on Circuits and Systems (MWSCAS), 2021.

[33] Y. Luo, L. Pu and L. Lei, "Impact of Varying Radio Power Density on Wireless Communications of RF Energy Harvesting Systems," in IEEE Transactions on Communications, Vol. 69, No. 3, March 2021.

[34] X. Y. Pu, S. Y. Zheng, J. Liu, Y. Li, and Y. Long, "Novel multi-way broadband differential phase shifter with uniform reference line using coupled line structure," IEEE Microw. Wireless Compon. Lett., Vol. 25, No. 3, pp. 166–168, Mar. 2015.

[35] H. Zhu and Y. J. Guo, "Wideband filtering phase shifter using transversal signal-interference techniques," IEEE Microw. Wireless Compon. Lett., Vol. 29, No. 4, pp. 252–254, Apr. 2019.

[36] Y.-P. Lyu, L. Zhu, and C.-H. Cheng, “Proposal and synthesis design of differential phase shifters with filtering function,” IEEE Trans. Microw. Theory Techn., Vol. 65, No. 8, pp. 2906–2917, Aug. 2017.

[37] K. Rawat and F. M. Ghannouchi, “Design methodology for dualband Doherty power amplifier with performance enhancement using dual-band offset lines,” IEEE Trans. Ind. Electron., Vol. 59, No. 12, pp. 4831–4842, Dec. 2012.

[38] A. M. Zaidi, S. A. Imam, B. K. Kanaujia, K. Rambabu, K. Srivastava, and M. T. Beg, "A new dual band 4 × 4 butler matrix with dual band 3 dB quadrature branch line coupler and dual band 45_ phase shifter", AEU-Int. J. Electron. Commun., Vol. 99, pp. 215–225, Feb. 2019.

[39] Y.-P. Lyu, L. Zhu, and C.-H. Cheng, "Dual-band differential phase shifter using phase-slope alignment on coupled resonators, " IEEE Microw. Wireless Compon. Lett., Vol. 28, No. 12, pp. 1092–1094, Dec. 2018.

[40] Q. Dong, Y. Wu, W. Chen, Y. Yang, and W. Wang, "Single layer dual-band bandwidth-enhanced filtering phase shifter with two different predetermined phase-shifting values, " IEEE Trans. Circuits Syst. II, Exp. Briefs, Vol. 68, No. 1, pp. 236–240, Jan. 2021.

[41] L. L. Qui and L. Zhu, "Dual-Band Filtering Differential Phase Shifter Using Cascaded Wideband Phase Shifter and Band stop Network with Two Same Phase Shifts", IEEE Microwave and Wireless Components Letters, Vol. 31, No. 3, March 2021.

[42] X. Tang and K. Mouthaan, "A broadband 180° phase shifter with a small phase error using lumped elements," 2009 Asia Pacific Microwave Conference, pp. 1315-1318, 2009.

[43] Q. Shao, F. -C. Chen, Y. Wang and Q. -X. Chu, "Design of 4 × 4 and 8 × 8 Filtering Butler Matrices Utilizing Combined 90° and 180° Couplers," IEEE Transactions on Microwave Theory and Techniques, Vol. 69, No. 8, pp. 3842-3852, Aug. 2021.

[44] S. Y. Zheng, W. S. Chan and K. F. Man, "Broadband Phase Shifter Using Loaded Transmission Line," IEEE Microwave and Wireless Components Letters, Vol. 20, No. 9, pp. 498-500, Sept. 2010.

[45] J. Helszajn, "Ridge, Coaxial, and Stripline Phase-shifters," Microwave Polarizers, Power Dividers, Phase Shifters, Circulators, and Switches, IEEE, 2019.

[46] C. Ekkaravarodome, A. Bilsalam, P. Tantiviwattanawongsa and P. Thounthong, "High Step-Up DC-DC Push-Pull Resonant Based on low-Cost half-wave Class-D Rectifier," 2019 Research, Invention, and Innovation Congress (RI2C), 2019.

[47] Truman S. Gray, "Rectifier Circuits", in Applied Electronics: A First Course in Electronics, Electron Tubes, and Associated Circuits, MIT Press, pp.277-364, 1954.

Najmehossadat Nourieh
School of Physics, Engineering and Computer Science, University of Hertfordshire

[48] Marcelo Godoy Simes; Felix A. Farret, "Power Electronics", in Modeling Power Electronics and Interfacing Energy Conversion Systems, IEEE, pp.61-81, 2017.

[49] Tran, LG., Cha, HK. & Park, WT. RF power harvesting: a review on designing methodologies and applications. Micro and Nano Syst Lett 5, 14 (2017).

[50] F. Yan, J. Zhao, H. Qu; X. Xu, "Energy-Efficient Cooperative Strategy in RF Energy Harvesting Cognitive Radio Network", Chinese Journal of Electronics, Vol. 03, No. 63, 2019.

[51] Y. Berkovich, B. Axelrod, D. Shoshani and Y. Beck, "DC-DC converter based on the bipolar boost converter and Dickson voltage multiplier," 2018 IEEE International Energy Conference (ENERGYCON), 2018.

[52] M. abdallah, J. costantine, A. H. Ramadan, Y. Tawk,"Enhanced Radio Frequency Rectifier with a Power Splitting/Combining Topology for Wireless Energy Transfer and Harvesting", IET Microwaves, Antennas & Propagation, 2019.

[53] B. Axelrod Y. Berkovich A. Shenkman G. Golan,"Diode – Capacitor Voltage Multipliers Combined with Boost-Converters Topologies and Characteristics", IET Power Electronics, 2012.

[54] H. Gao, M. K. Marion, M. Dusan, J. P. Linnartz, P. Baltus,"A Design of 2.4GHz Rectifier In 65nm CMOS With 31% Efficiency", IEEE Conferences on Circuits and Systems, 978-1-4799-3206-1/13, 2013.

[55] D. Baderna, A. Cabrini, M. Pasotti, G. Torelli,"Power Efficiency Evaluation in Dickson and Voltage Doubler Charge Pump Topologies", Microelectronics Journal, Issue. 10, Vol. 37, 2006.

[56] G. Papotto, F. Carrara, and G. Palmisano,"A 90-nm CMOS Threshold Compensated RF Energy Harvester", IEEE J. Solid-State Circuits", Vol. 46, No. 9, 2011.

[57] M. Al-Absi, S. Al-Batati, "Hybrid Internal Vth Cancellation Rectifiers for RF Energy Harvesting", IEEE Access, Vol. 8, 2020.

[58] H. Lin, K. Chang, and S. Wong, "Novel High Positive and Negative Pumping Circuits for Low Supply Voltage", in Proc. IEEE Int. Symp. Circuits Syst., 1999, Vol. 1, pp. 238–241.

[59] H. Nakamoto, D. Yamazaki, T. Yamamoto, H. Kurata, S. Yamada, K. Mukaida, T.inomiya, T. Ohkawa, S. Masui, and K. Gotoh, "A Passive UHF RF Identification CMOS Tag IC Using Ferroelectric RAM In 0.35- Technology", IEEE J. Solid-State Circuits, Vol. 42, No. 1, Jan. 2007.

[60] G. Zhang, Z. Wu, S. S. Yu, H. Trinh and Y. Zhang, "Four Novel Embedded Z-Source DC–DC Converters," in IEEE Transactions on Power Electronics, Vol. 37, No. 1, Jan. 2022.

[61] J. F. Dickson, "Voltage multiplier employing clock gated transistor chain", U.S. Patent 4 214 174, Jul. 22, 1980.

Najmehossadat Nourieh
School of Physics, Engineering and Computer Science, University of Hertfordshire

[62] I. Alhurayyis, A. Elkhateb and J. Morrow, "Isolated and Nonisolated DC-to-DC Converters for Medium-Voltage DC Networks: A Review", IEEE Journal of Emerging and Selected Topics in Power Electronics, Vol. 9, No. 6, Dec. 2021.

[63] T. Shanthi, S. U. Prabha and K. Sundaramoorthy, "Non-Isolated n-Stage High Step-up DC-DC Converter for Low Voltage DC Source Integration", IEEE Transactions on Energy Conversion, Vol. 36, No. 3, Sept. 2021.

[64] DC/DC converter | definition and usage (videocide.com).

[65] S. Moury and J. Lam, "A Soft-Switched, Multiport Photovoltaic Power Optimizer with Integrated Storage Interface and Output Voltage Regulation", IEEE Transactions on Industrial Electronics, Vol. 68, No. 5, May 2021.

[66] N. Kim and B. Parkhideh, "PV-Battery Series Inverter Architecture: A Solar Inverter for Seamless Battery Integration with Partial-Power DC–DC Optimizer", IEEE Transactions on Energy Conversion, Vol. 34, No. 1, March 2019.

[67] Y. Zhu, J. Wu, R. Wang, Z. Lin and X. He, "Embedding Power Line Communication in Photovoltaic Optimizer by Modulating Data in Power Control Loop", IEEE Transactions on Industrial Electronics, Vol. 66, No. 5, May 2019.

[68] O. Khan and W. Xiao, "An efficient modeling technique to simulate and control submodule-integrated PV system for single-phase grid connection", IEEE Trans. Sustain. Energy, Vol. 7, No. 1, Jan 2016.

[69] A. Kulshreshtha, A. R. Saxena and M. Veerachary, "Non-Isolated Fourth-Order Boost DC-DC Converter for Power Management in Low Voltage Low Power DC Grids: Design and Interaction Analysis", IEEE Access, Vol. 8, 2020.

[70] V. Meleshin, S. Sachkov and S. Khukhtikov, "Three-level boost converters. Modes, sub-modes and asymmetrical regime of operation", 2014 16th European Conference on Power Electronics and Applications, 2014.

[71] S. Raghavendran, K. S. Kumar, A. Tirupathi and C. B, "An Improved Three-level DC-DC Boost Converter for Renewable energy Systems with High Gain", 2020 3rd International Conference on Energy, Power and Environment: Towards Clean Energy Technologies, 2021.

[72] S. Folmer and R. Stala, "DC-DC High Voltage Gain Switched Capacitor Converter With Multilevel Output Voltage and Zero-Voltage Switching", IEEE Access, Vol. 9, 2021.

[73] S. Kumaravel and P. E. Babu, "Reduced Switch Voltage Stress Ultra-Gain DC-DC Converter for High Voltage Low Power Applications", IEEE Trans. on Circuits and Systems II: Express Briefs, Vol. 69, No. 3, pp. 1277-1281, March 2022.

[74] M. Alexander, R. Blanchard and R. Severn, "Mosfets Move In on Low Voltage Rectifier", MOS-POWER Applications Handbook", Siliconix Technical Article, PP. 5-87-5-84, 1984, Siliconix Inc.

[75] K. Jin, L. Gue, and J. Wang, "A 10-MHz Resonant Converter with a Synchronous Rectifier for Low-Voltage Applications", IEEE Trans. on Power Electronics, Vol. 34, No. 4, 2019.

[76] S. M. Salehi, S. Hasanzadeh and H. Shojaeian, "A Dual Switch/Inductor Isolated High Voltage gain Based on Voltage Lift", 2021 12th Power Electronics, Drive Systems, and Technologies Conference (PEDSTC), pp. 1-5, 2021.

[77] S. Raghavendran and K. Sateesh Kumar, "A Self-Balanced High Gain Multi-Port Converter for Photovoltaic and Fuel Cell based Power Generation Systems", 2022 IEEE International Conference on Power Electronics, Smart Grid, and Renewable Energy (PESGRE), pp. 1-5, 2022.

[78] www.rfpage.com, RF based wireless energy harvesting and its applications, RF Page.

[79] iotdesignpro.com, An Overview of RF Energy Harvesting, Working and Applications. ieeeaps.org , APS | IEEE Antennas and Propagation Society | Antennas for RF Energy Harvesting and Wireless Power Transfer Applications.

[80] Y. C. Wong, P. C. Tan, M. M. ibrahim, A. R. Syafeeza and N. A. Hamid, "Dickson Charge Pump Rectifier using Ultra-Low Power (ULP) Diode for BAN Applications", Journal of Telecommunication, Electronic and Computer Engineering, 2016.

[81] P. Mitcheson and T. Tzern, "Power Management Electronics", Energy Harvesting for Autonomous Systems, pp.1-57, 2010.

[82] D. Corte, F. Massimo, M. Bellizzi, G. Carotenuto and I. Riccardo, "Temperature Effects on the Efficiency of Dickson Charge Pumps for Radio Frequency Energy Harvesting", IEEE Access, 2018.

[83] H. Evans, P. Gale, and A. Sambell, “Performance of 4×4 sequentially rotated patch antenna array using series feed,” Electron. Lett., Vol. 39, No. 6, pp. 493-494, Apr. 2003.

[84] L. Bian, Y. X. Guo, and X. Q. Shi, “Wideband circularly polarized slot antenna,” IET Microw. Antenna Propag., Vol. 2, No. 5, pp. 497- 502, Jul. 2008.

[85] W. Qin, L. Shi, W. Sun, W. Yang, L. Ge and J. Chen, "A Wideband LTCC Quad-Phase Power Dividing Network and its Application to Ceramic-Based Quadrifilar Helix Antennas," in IEEE Access, Vol. 7, pp. 141094-141103, 2019.

[86] W. Qin, L. -H. Shi and J. -X. Chen, "LTCC Wideband 1-to-4 Power Dividing Networks with 90° or 180° Output Phase Differences," 2020 IEEE MTT-S International Microwave Workshop Series on Advanced Materials and Processes for RF and THz Applications (IMWS-AMP), pp. 1-3, 2020.

Najmehossadat Nourieh
School of Physics, Engineering and Computer Science, University of Hertfordshire

[87] T. Nakura, H. Matsui and K. Asada, "Comparative Study of RF Energy Harvesting Rectifiers and Proposal of Output Voltage Universal Curves for Design Guideline", IEICE Electronics Express, Vol. 12, No.3, 2015.

[88] H. Greinacher, "Erzeugung einer Gleichspannung vom vielfachen Betrage einer Wechselspannung ohne Transformator", Bull Schweiz Elektrotechn Vereins. 1986.

[89] Y. Shi, Y. Fan, J. Jing, L. Yang, Y. Li and M. Wang, "An efficient fractal rectenna for RF energy harvest at 2.45 GHz ISM band", International Journal of RF and Microwave Computer-Aided Engineering, Issue. 9, Vol. 28, 2018.

[90] E. Ali, N. Z. Yahaya, P. Nallagownden, M. A. Zakariya, "Design of Microstrip Patch Antenna at 900 MHz for charging Mobile applications", Journal of Engineering and Applied Sciences, Vol. 12, Issue. 4, 2017.

[91] E. Ali, N. Z. Yahaya, P. Nallagownden, M. A. Zakariya, "Design of RF to DC rectifier at GSM band for energy harvesting applications". Journal of Engineering Science and Society, Vol. 10, No. 2, 2014.

[92] E. Ali, N. Z. Yahaya, P. Nallagownden, M. A. Zakariya, "Design and development of harvester rectenna at GSM band for battery charging applications", J Eng Appl Sci, 2015.

[93] Prusayon N, Ufuk M, David L, Kaushik C, "Design optimization and implementation for RF energy harvesting circuits", IEEE J Emerg Select Top Circ Syst, 2012.

[94] B. Razavi, "RF Microelectronics (2nd Edition) (Prentice Hall Communications Engineering and Emerging Technologies Series) (2nd. ed.) ", Prentice Hall Press, USA, 2011.

[95] W. Liu, K. Huang, T. Wang, J. Hou and Z. Zhang, "A Compact Ultra-Broadband RF Rectifier Using Dickson Charge Pump", IEEE Microwave and Wireless Components Letters, Vol. 32, No. 6, pp. 591-594, June 2022.

[96] L. G. d. Carli, Y. Juppa, A. J. Cardoso, C. Galup-Montoro, and M. C. Schneider, "Maximizing the Power Conversion Efficiency of Ultra-LowVoltage CMOS Multi-Stage Rectifiers," IEEE Trans. on Circuits and Systems I: Regular Papers, Vol. 62, pp. 967-975, 2015.

[97] R. V. Garver, “Broad-band diode phase shifters,” IEEE Trans. Microwave Theory Tech., Vol. MTT-20, pp. 9-14, May 1972.

[98] D. Adler and R. Popovich, "Broadband switched-bit phase shifter using all-pass networks", IEEE MTT-S Dig., pp. 265- 268, 1991.

[99] Y. Wang, H. Zhu, Y. Wang, X. Chen and Y. Wang, "Efficient Half-Period Phase Histogram Equalization for General Phase-Shifting Algorithms with Phase Shift Errors", IEEE Transactions on Instrumentation and Measurement, Vol. 71, pp. 1-10.

Najmehossadat Nourieh
School of Physics, Engineering and Computer Science, University of Hertfordshire

[100] I. J. Baul and D. Conway, "L- and S-band compact octave bandwidth 4-bit MMIC phase shifters", IEEE Trans. Microwave Theory Tech., Vol. 56, No. 2, pp. 293-299, Feb. 2008.

[101] M. A. Morton, J. P. Comeau, J. D. Cressler, M. Mitchell and J. Papapolymerou, "Sources of phase error and design considerations for silicon-based monolithic high-pass/low-pass microwave phase shifters", IEEE Trans. Microwave Theory Tech., Vol.54, No. 12, pp. 4032-4040, Dec. 2006.

[102] S. Pellerano, J. Alvarado, and Y. Palaskas, "A mm-wave powerharvesting RFID tag in 90 nm CMOS", IEEE J. of Solid-State Circuits, Vol. 45, No. 8, pp. 1627–1637, 2010.

[103] S. Eom, "Broadband 180º bit phase shifter using a λ/2 coupled line and parallel λ/8 stubs", IEEE Microw. Wireless Compon. Lett., Vol.14, No. 5, pp. 228-230, May 2004.

[104] G. Sung, R. Kasim, J. Ryu and B. Kim, "Broadband 180º bit Xband phase shifter using parallel coupled lines", in European Radar Conference EuRAD, pp. 319-321, 2005.

[105] X. Tang and K. Mouthaan, "180º and 90º phase shifting networks with an octave bandwidth and small phase errors", accepted in IEEE Microw. Wireless Compon. Lett. 2009.

[106] X. Tang and K. Mouthaan, "A broadband 180° phase shifter with a small phase error using lumped elements", 2009 Asia Pacific Microwave Conference, 2009, pp. 1315-1318, 2009.

[107] H. Hayashi, M. Mauraguchi,"An MMIC active phase shifter using a variable resonant circuit [and MESFETs]," IEEE Trans. On Microwave Theory and Techniques, Vol. 47, No. 10, Oct 1999.

[108] K. Miyaguchi, M. Hieda, K. Nakahara, H. Kurusu, M. Nii, M. Kasahara, T. Takagi, S. Urasaki, "An ultra-broad-band reflection-type phase-shifter MMIC with series and parallel LC circuits," Microwave Theory and Techniques, IEEE Trans. on, Vol.49, No.12, pp.2446-2452, Dec 2001.

[109] F. Ellinger, W. Bachtold, "Novel principle for vector modulator-based phase shifters operating with only one control voltage," IEEE Journal of Solid-State Circuits, Vol.37, No.10, pp. 1256- 1259, Oct 2002.

[110] N. Gupta, R. Tomar, P. Bhartia, "A Low-Loss Voltage-Controlled Analog Phase-Shifter Using Branchline Coupler and Varactor Diodes," Microwave and Millimeter Wave Technology, 2007. ICMMT '07. International Conference on, Vol., No., pp.1-2, 18-21 April 2007 doi: 10.1109/ICMMT.2007.381435

[111] Microwave101 website - High Pass Low Pass phase shifters http://www.microwaves101.com/encyclopedia/phaseshifters_HPLP.cfm [Last accessed 2012-09-19]

[112] P. V. Nikitin, K. Rao, and S. Lazar, "An overview of near field uhf RFID", in Proc. IEEE Int. Conf. RFID, 2007, vol. 167.

[113] M. S. Trotter, J. D. Griffin, and G. D. Durgin, "Power-optimized waveforms for improving the range and reliability of RFID systems", in Proc. IEEE Int. Conf. RFID, 2009, pp. 80–87.

[114] M. S. Trotter and G. D. Durgin, "Range estimation for passive RFID systems that use power-optimized waveforms", in Proc. IEEE Int. Conf. RFID, 2012, pp. 102–109.

[115] M. S. Papadopoulou et al., "Dual-Band RF-to-DC Rectifier with High Efficiency for RF Energy Harvesting Applications", 2020 9th International Conference on Modern Circuits and Systems Technologies (MOCAST), 2020.

[116] H. You, M. Yuan, R. Das, H. Heidari and R. Ghannam, "An Efficient RF-DC Rectifier Design for RF Energy Harvesting Systems", 2020 27th IEEE International Conference on Electronics, Circuits and Systems (ICECS), 2020.

[117] H. Zhang, N. Lu, R. Song and J. Li, "Stochastic Analysis on Ambient RF Energy Harvesting", 2020 IEEE 6th International Conference on Computer and Communications (ICCC), 2020.

[118] M. Basim, D. Khan, Q. Ul Ain, K. Shehzad, M. Asif and K. Y. Lee, "A High Efficient RF-DC Converter for RF Energy Harvesting Applications", 2020 International SoC Design Conference (ISOCC), 2020.

[119] D. Khan et al., "A CMOS RF Energy Harvester With 47% Peak Efficiency Using Internal Threshold Voltage Compensation", IEEE Microw. Wireless Compon. Letter, vol. 29, no. 6, pp. 415-417, June 2019.

[120] D. Khan et al., "A Design of Ambient RF Energy Harvester with Sensitivity of -21dBm and Power Efficiency of a 39.3% Using Internal Threshold Voltage Compensation", MDPI Energies, Vol. 11, No. 5, May 2018.

[121] S.-Y Kim et al., "A -20 to 30 dBm Input Power Range Wireless Power System with a MPPT-based Reconfigurable 48% Efficient RF Energy Harvester and 82% Efficient A4WP Wireless Power Receiver with Open Loop Delay Compensation", IEEE Trans. Power Electronics, Vol. 34, No. 7, July 2019.

[122] A. Sinha, R. Kumar, "Generation of high voltage using Cockcroft–Walton voltage multiplier circuit", International Research Journal of Engineering and Technology, 2018.

[123] J. W. Yang and H. L. Do, "High-Efficiency ZVS AC-DC LED Driver Using a Self-Driven Synchronous Rectifier", IEEE Trans. On Circuit and Systems I, Vol. 61, No. 8, 2014.

[124] W. X. Zhong, S. Y. Hui, W. C. Ho and X. Liu, "Using Self Driven AC–DC Synchronous Rectifier as a Direct Replacement for Traditional Power Diode Rectifier", IEEE Trans. On Industrial Electronics, Vol. 59, No. 1, 2012.

[125] https://learnabout-electronics.org/PSU/psu32.php

Najmehossadat Nourieh
School of Physics, Engineering and Computer Science, University of Hertfordshire

[126] S. Sadaf, M. S. Bhaskar, M. Meraj, A. Iqbal and N. Al-Emadi, "Transformer-Less Boost Converter with Reduced Voltage Stress for High Voltage Step-Up Applications", IEEE Trans. On Industrial Electronics, Vol. 69, No. 2, Feb. 2022.

[127] M. Rezaie and V. Abbasi, "Ultrahigh Step-Up DC–DC Converter Composed of Two Stages Boost Converter, Coupled Inductor, and Multiplier Cell," IEEE Trans. On Industrial Electronics, Vol. 69, No. 6, June 2022.

[128] V. K. Goyal and A. Shukla, "Two-Stage Hybrid Isolated DC–DC Boost Converter for High Power and Wide Input Voltage Range Applications", IEEE Trans. On Industrial Electronics, Vol. 69, No. 7, July 2022.

[129] H. Shayeghi, S. Pourjafar, S. M. Hashemzadeh and Frede. Blaadjerg, "A high efficiency soft-switched DC–DC converter with high voltage conversion ratio ", International Journal of Circuit Theory and Applications, 2020.

[130] D. Sivaraj, and M. Arounassalame, "High gain quadratic boost switched capacitor converter for photovoltaic applications", in Power Control Signals and Instrumentation Engineering (ICPCSI) 2017 IEEE International Conference, 2017.

[131] R. L. Radin, M. Sawan, C. Galup-Montoro and M. Ch. Schneider, "A 7.5-mV-Input Boost Converter for Thermal Energy Harvesting With 11-mV Self-Startup ", IEEE Trans. On Circuits and Systems, Vol. 67, No. 8, 2020.

[132] M. -C. Lee, C. -H. Li and X. -X. Yang, "Implementation of DC-DC PFM Boost Power Converter for Low-power Energy Harvesting Applications," 11th International Conference on Power, Energy and Electrical Engineering (CPEEE), 2021.

[133] J. D. López-Cardona et al., "Optimized Power-over-Fiber System to Remotely Feed Smart Nodes for Low-Power Consumption Applications", 13th Spanish Conference on Electron Devices (CDE), 2021.

[134] G. Mekhael, N. Morgan, M. Patnala, T. Ytterdal and M. Rizkalla, "GNRFET-Based DC-DC Converters for Low Power Data Management in ULSI System, a Feasibility Study", IEEE International Symposium on Circuits and Systems (ISCAS), 2021.

[135] F. Galea, O. Casha, I. Grech, E. Gatt and J. Micallef, "An Ultra Low Power CMOS MPPT Power Conditioning Circuit for Energy Harvesters", 2020 IEEE International Symposium on Circuits and Systems (ISCAS), 2020.

[136] S. Khan, S. Azeemuddin and M. A. Sohel, "A low power low ripple Schmitt trigger based PWM Boost Converter for Energy Harvesting Applications", 2020 IEEE 17th India Council International Conference (INDICON), 2020.

[137] M. Gendensuren, J. woong Park, C.-S. Lee and N.-S. Kim, "Low power integrated 0.35µm CMOS voltage-mode DC-DC boost converter", 4th International Conference on Power Engineering Energy and Electrical Drives, May. 2013.

[138] B. Pollet, G. Despesse and F. Costa, "A New Non-Isolated Low-Power Inductorless Piezoelectric DC–DC Converter", IEEE Trans. On Power Electronics, Vol. 34, No. 11, 2019.

[139] https://components101.com/articles/boost-converter-basics-working-design

[140] S. Sudevalayam and P. Kulkarni, "Energy harvesting sensor nodes: Survey and implications", IEEE Commun. Survey Tuts., Vol. 13, No. 3, 3rd Quart. 2011.

[141] U. Muncuk, K. Alemdar, J. D. Sarode and K. R. Chowdhury, "Multi-band ambient RF energy harvesting circuit design for enabling battery-less sensors and IoTs", IEEE Internet Things Journal., Vol. 5, No. 4, Aug. 2018.

[142] G. Verma and V. Sharma, "A Novel RF Energy Harvester for Event-Based Environmental Monitoring in Wireless Sensor Networks," in IEEE Internet of Things Journal, Vol. 9, No. 5, March. 2022.

[143] M. Hata, "Empirical formula for propagation loss in land mobile radio services", in IEEE Trans. On Vehicular Technology, Vol. 29, No. 3, pp. 317-325, Aug. 1980.

[144] Radiom S, Vandenbosch G, Gielen G, "Impact of antenna type and scaling on scavenged voltage in passive RFID tags", International workshop on antenna technology: small antennas and novel metamaterials, 2008.

[145] K. Kotani, A. Sasaki, and T. Ito, "High-efficiency differential-drive CMOS rectifier for UHF RFIDs," IEEE Journal of Solid-State Circuits, Vol. 44, No. 11, 2009.

[146] J. Hardy, High Frequency Circuit Design, Reston Publishing Company, 1979, 353 pages.

[147] G. Gosset and D. Flandre, "Fully-Automated and Portable Design Methodology for Optimal Sizing of Energy-Efficient CMOS Voltage Rectifiers", in IEEE Journal on Emerging and Selected Topics in Circuits and Systems, Vol. 1, No. 2, June 2011.

[148] A. Facen and A. Boni, "CMOS power retriever for UHF RFID tags", Electron Letters, 1424 -1425, 2007.

[149] https://www.murata.com/en-eu/tool/sparameter/inductor, [Online] Accessed: 08-Sep-2020.

Najmehossadat Nourieh
School of Physics, Engineering and Computer Science, University of Hertfordshire

Appendix 1

Shown in Figure 1, in this section the combination of the rectifier and phase shift circuit together will be discussed. To design the appropriate impedance matching network, the equivalent impedance of these two circuits should be substitute and in the circuit combination, the final impedance will be calculated to be further considered in the Smith chart method.

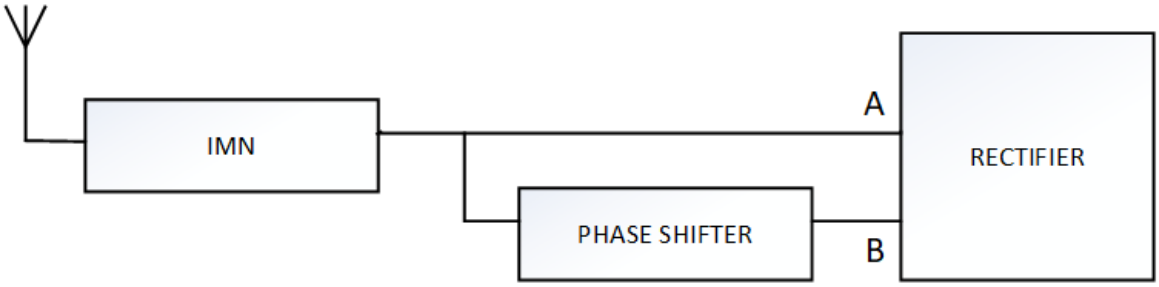

Figure 1 The whole scheme of the IMN, phase shifter and rectifier together in the

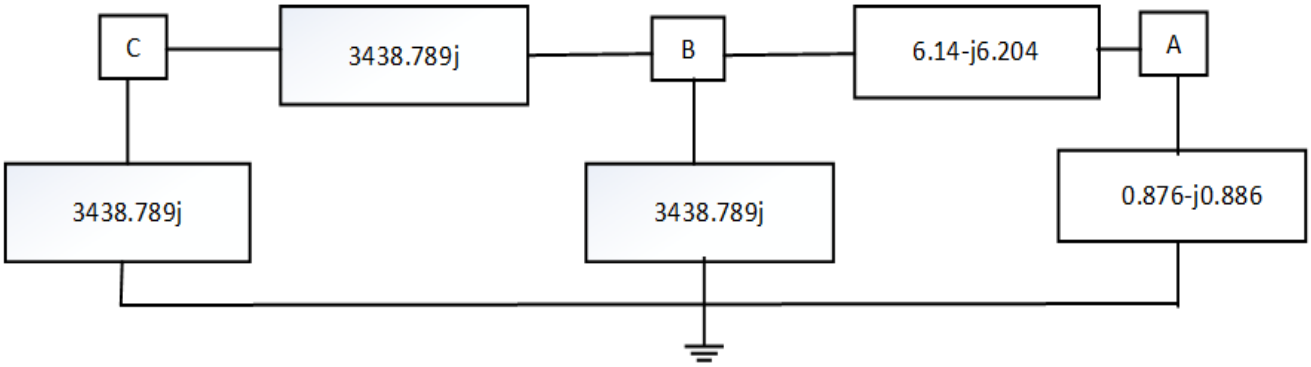

Figure 2 The impedance of the phase shifter and rectifier together in the proposed

In Figure 2, the substituted impedances of the rectifier and phase shift circuit has been illustrated which gives us the view of a star and a delta (Y and Δ). To obtain the equivalent impedance of the proposed

Najmehossadat Nourieh
School of Physics, Engineering and Computer Science, University of Hertfordshire

combination viewed from the IMN output, we must first convert the star to delta. Shown in Figure 3, the impedance values will be simplified using the conversion of star to delta.

Eventually, by analyzing the gained impedances, the final impedance seen from the IMN output is calculated as 1.76+ j1717.62.

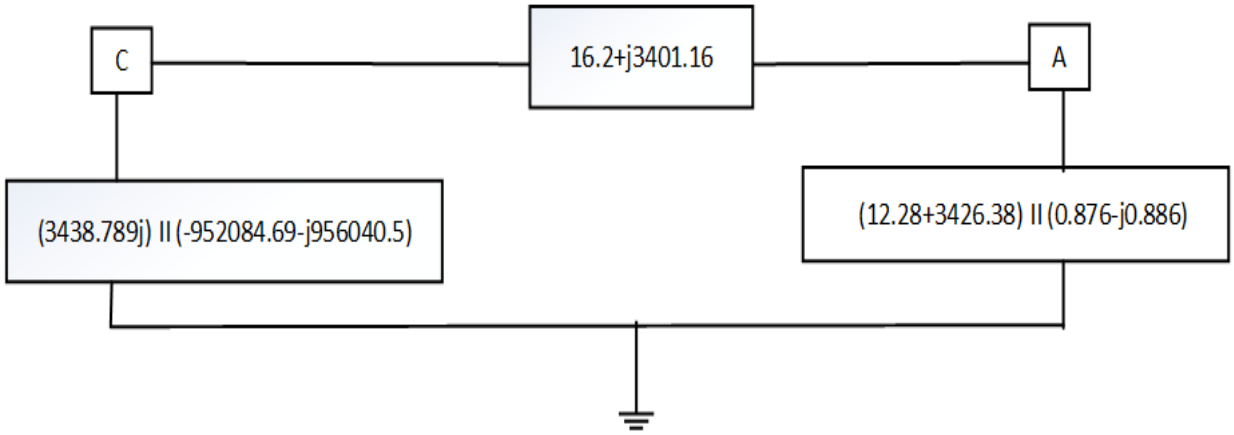

Figure 3. The simplified impedance of the phase shifter and rectifier together

In the following paragraphs, we show a more intuitive approach to impedance matching by using Smith charts. Generally, as a standard, electrical engineers try to match the source/load to either 50Ω or 75Ω.

A Smith Chart is possibly one of the most practical tools to obtain and design the impedance matching network.

As an example, the impedance Smith chart includes four different types of circles that traverse a constant resistance (r), constant susceptance (b), constant conductance (g) or constant reactance (x). Every point on the Smith chart defines an impedance.

First, we calculate this matching circuitry using the methodology explained above. The antenna impedance is equal to Z_{ant} = 50Ω, and the normalized impedance of antenna is z_{ant} =1.0, which is the spot right in the middle of the Smith Chart shown in Fig. 6.13. While Z_{load} = 1.76 + j1717.62, by computing the

Najmehossadat Nourieh
School of Physics, Engineering and Computer Science, University of Hertfordshire

normalized load impedance, we get $z_{load} = 0.035 + j34.352$, So $z^*_{load} = 0.046 - j34.279$. This is what we will end up with, since, if we end up with $z^*_{load} = 0.035 - j34.352$, the +j34.352 and – j34.352 will cancel each other out, and the antenna will be pure resistive to the load (z = 0.045), thus it allows maximum power transfer. This is a properly simple transformation and only two elements are necessary to handle the function: a shunt inductor L_{shunt} and a series capacitor C_{series}.

Since there is a shunt inductor, it is easier to deal with admittance and conductance. The start point here is y = 1 for the normalized impedance of the antenna. Therefore, we have g = 1 and b = 0. A shunt inductor will not change *g*, but will add a value to b. Hence, we traverse the g = 1 constant conductance circle until we meet a point that will help us with the next move. Anticipating that, the next move will be adding a series capacitor, we try to get to a point which has the desired r = 0.035 value. The effect of having a shunt inductor is moving cross the constant g = 1 and ending up at y = 1- j4.543. From this move, we understand that the shunt inductor added the value of –j4.543 to the susceptance, and the corresponding value of inductor will be calculated from $2\pi fL = (1/4.543) * 50$. The value of *L* is $L_{shunt} = 1.922nH$.

Second, we will determine the series capacitor. For this, it is easier to use impedance and resistances. To convert the current impedance we calculated, we can either look at the intersecting impedance point or calculate the formula $z=(1- j4.543)^{-1}$, which gives us z = 0.035 + j0.209. From this point, we try to go to z = 0.035 + j34.352. This traversal keeps r = 0.035 constant and reduces the value of j34.561 from impedance. The value of a capacitor that can realize, can be calculated from $2\pi fC = 1/X_c$ where $X_c = 50/34.561$. By using these equations, the series capacitor is calculated as C= 120pF as shown in Figure 4.

Calculating the shunt inductor and the series capacitor the design of the impedance matching network has been finished and the whole IMN is shown in Figure 4.

Najmehossadat Nourieh
School of Physics, Engineering and Computer Science, University of Hertfordshire

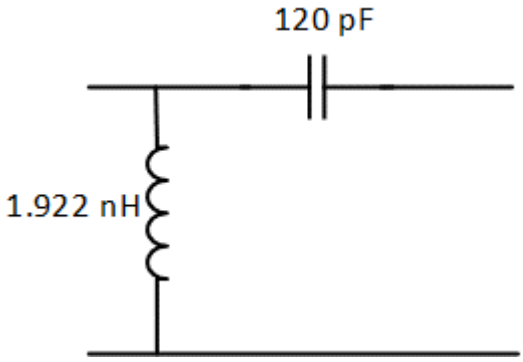

Figure 4. The impedance matching network.

Najmehossadat Nourieh
School of Physics, Engineering and Computer Science, University of Hertfordshire

Appendix 2

```
%Values of the all the components are added.
clear all
 Lr=25e-009;
Cr=1e-009;
C1=0.25e-009;
C2=0.25e-009;
Vs=0.35;
Vo=6;
n=10;
wr=1/(sqrt(Lr*Cr));
fr=wr/(2*pi);
Zr=sqrt(Lr/Cr);
Cs=C1+C2;
a=Cr/Cs;
wa=sqrt(1+a)*wr;
B=n*(Vo/Vs);
I0=Vs/Zr;
 p1=(1.95848e-5-1.89649e-5)*wr;
p3=6.39e-8*wr;
g=sqrt(((1-B)^2)-(2*(1-B)*cos(p1))+(1/a)+1);
pd=acos(B/((2*B)-g));
%Equations of voltage, current and time of seven modes of converter.
%Equations of voltage, current and time of first mode.


I1=(1-B)*sin(p1);
V1=(1-B)*(1-cos(p1));
```


Najmehossadat Nourieh
School of Physics, Engineering and Computer Science, University of Hertfordshire

```
T1=p1/wr;

%Equations of voltage, current and time of second mode.

T2=(sqrt((sin(p1)^2)*((1-B)^2)+((2*(1-B)*cos(p1))/a)-((1+a)/a^2))*(1+a)*sin(p1))+((1-B)*(cos(p1)^2))-
(((1+a)/a)*cos(p1));

I2=((1-B)*sin(p1))*cos(wa*T2)+(((1-B)*cos(p1))/sqrt(1+a))*sin(wa*T2);

V2=(((1-B)*sin(p1))/(sqrt(1+a)))*sin(wa*T2)-(((1-B)*cos(p1))/(1+a))*cos(wa*T2)+(1-B)-(a*(1-
B)*cos(p1))/(1+a);

I2_F=sqrt((sin(p1)^2)*((1-B)^2)+((2*(1-B)*cos(p1))/a)-((1+a)/a^2));

V2_F=(1-B)*(1-cos(p1))+(1/a);

%Equations of voltage, current and time of third mode.

T3=(atan(I2/(V2+B)))/wr;

V3=I2*sin(wr*T3)+(V2+B)*cos(wr*T3)-B;

I3=I2*cos(wr*T3)-(V2+B)*sin(wr*T3);

I3_F=0;

V3_F=sqrt(((1-B)^2)-(2*(1-B)*cos(p1))+(1/a)+1)-B;

%Equations of voltage, current and time of fourth mode.

 T4=pd/wr;

V4=(g-(2*B))*cos(wr*T4)+B;

I4=((2*B)-g)*sin(wr*T4);

I4_F=-sqrt((((2*B)-g)^2)-(B^2));

V4_F=0;

%Equations of voltage, current and time of fifth mode.

T5=p3/wr;

V5=0;

I5=I4+(B*p3);

%Equations of voltage, current and time of sixth mode.

T6=(acos(((I5*(-sqrt((I5^2)-(1+(2*B))/a))*a)+(B*(1+B)))/((B^2)+((I5^2)*a))))/(sqrt(a)*wr);

V6=0;

I6=I5*cos(sqrt(a)*wr*T6)+(B/sqrt(a))*sin(sqrt(a)*wr*T6);
```


Najmehossadat Nourieh
School of Physics, Engineering and Computer Science, University of Hertfordshire

```
I6_F=-sqrt((I5^2)-((1+(2*B))/a));
%Equations of voltage, current and time of seventh mode.
I7_F=0;
V7=0;
T7=(sqrt((I5^2)-((1+(2*B))/a)))/(wr*(B+1));
 disp(' ');
disp('-----------------------------------------------');
disp([' f     = ' num2str(fr/1e3) ' (KHz)          a = ' num2str(a) ' ']);
 disp([' Phi1  = ' num2str(p1*180/pi)  ' (deg)   Phi3 =  ' num2str(p3*180/pi)  ' (deg)']);
disp([' V1 = ' num2str(V1*Vs)   ' (V)   I1 = ' num2str(I1*I0)   ' (A)   T1 = ' num2str(T1*1e6) ' (us)']);
disp([' V2 = ' num2str(V2_F*Vs) ' (V)   I2 = ' num2str(I2_F*I0) ' (A)   T2 = ' num2str(T2*1e6) ' (us)']);
disp([' V3 = ' num2str(V3_F*Vs) ' (V)   I3 = ' num2str(I3_F*I0) ' (A)   T3 = ' num2str(T3*1e6) ' (us)']);
disp([' V4 = ' num2str(V4_F*Vs) ' (V)   I4 = ' num2str(I4_F*I0) ' (A)   T4 = ' num2str(T4*1e6) ' (us)']);
disp([' V5 = ' num2str(V5*Vs) ' (V)   I5 = ' num2str(I5*I0)   ' (A)   T5 = ' num2str(T5*1e6) ' (us)']);
disp([' V6 = ' num2str(V6*Vs) ' (V)   I6 = ' num2str(I6_F*I0) ' (A)   T6 = ' num2str(T6*1e6) ' (us)']);
disp([' V7 = ' num2str(V7*Vs) ' (V)   I7 = ' num2str(I7_F*I0) ' (A)   T7 = ' num2str(T7*1e6) ' (us)']);
disp('***********************************************');
```


Najmehossadat Nourieh
School of Physics, Engineering and Computer Science, University of Hertfordshire

Najmehossadat Nourieh
School of Physics, Engineering and Computer Science, University of Hertfordshire